UNIVERSITY OF OKLAHOMA

GRADUATE COLLEGE

EEG OSCILLATORY ACTIVITIES FROM HUMAN MOTOR BRAIN

A DISSERTATION

SUBMITTED TO THE GRADUATE FACULTY

in partial fulfillment of the requirements for the

Degree of

DOCTOR OF PHILOSOPHY

By

RAN XIAO
Norman, Oklahoma
2015

EEG OSCILLATORY ACTIVITIES FROM HUMAN MOTOR BRAIN

A DISSERTATION APPROVED FOR THE
SCHOOL OF ELECTRICAL AND COMPUTER ENGINEERING

BY

_____
Dr. Lei Ding, Chair

_____
Dr. Thordur Runolfsson

_____
Dr. Choon Yik Tang

_____
Dr. Michael Wenger

_____
Dr. Tian-You Yu

Acknowledgements

Over the past five years, I have received countless support and encouragement from many wonderful individuals. I'd like to express my deepest gratitude to Dr. Lei Ding, who has been a great mentor, colleague and friend to me. His kind guidance has made my Ph.D. research experience a fruitful and pleasant journey. Besides, I would like to thank my advisory committee members, Dr. Thordur Runolfsson, Dr. Choon Yik Tang, Dr. Michael Wenger and Dr. Tian-You Yu for their kind guidance during my graduate research.

Special thanks go to Dr. Thubi H.A. Kolobe, Dr. Andrew H. Fagg and Dr. David P. Miller, who have not only provided me with the precious opportunity in participating in this wonderful collaborative project about infant motor development, but also offered invaluable support and guidance constantly along the way. I also want to thank everyone else in the project, Kimberly Andrew, Elise Baudille, Brandon Boos, Rebecca Browder, Mustafa A. Ghazi, Zac Morris, Michael Nash, Emily North, Johnny O'Keefe, Amanda Porter, Laura Rauh, Tyler Schmiderberg, Joshua B. Southerland, and Leonard W. Wilson, who have provided tremendous help in their areas of expertise.

I'd also like to thank everyone in our research lab. Thank you all for the friendship all these years. Ke Liao, Guofa Shou, Min Zhu, Xiao Qi and Deepika Dasari have provided constructive discussions and suggestions to my research. Chuang Li, Alejandro Patino and Gregory Butron have helped a lot on experimental recordings.

In addition, I want to thank NSF (NSF DIIS Award #1208639 under NRI; NSF CAREER ECCS-0955260) and OCAST (HR09-125S) for funding the projects I've worked in, and University of Oklahoma (OU Research Report), OU Graduate College

(Robberson Conference Presentation Travel Grant; GSS Research and Conference Grants) and School of Electrical and Computer Engineering (ECE Journal Paper Award; ECE Travel Award) for the recognition and support for me to present our results in international conferences.

Finally, I'd like to thank my wife Min Zhu, my parents Shuyan Jing and Yongyin Xiao. It's their unwavering support and encouragement that inspire me all the way through my dissertation research.

Table of Contents

Acknowledgements iv

List of Tables x

List of Figures xi

Abstract xiii

Chapter 1: Introduction 1

Chapter 2: Background 8

2.1 Introduction to EEG 9

2.2 EEG Acquisition System 11

2.3 Oscillatory Activities in EEG 12

2.4 Mu Rhythm from Human Motor Brain 14

2.5 Mu Rhythm in Understanding Motor Development 15

2.6 Mu Rhythm in Developing Assistive Technology 17

Chapter 3: Further the Understanding about Motor Development 20

3.1 Experimental Design 21

3.1.1 Participants 21

3.1.2 Acquisition of EEG 21

3.2 Data Processing 24

3.2.1 EEG Preprocessing 24

3.2.2 Spectral Analysis 26

3.2.3 Spectral Peak Statistics 28

3.2.4 Clustering Analysis for Band Separation 28

3.2.5 Subject Variation from Correlation Analysis 29

3.3 Experimental Results 30
3.3.1 Weekly Spectral Changes 30
3.3.2 Peak Frequency of the Mu Rhythm 31
3.3.3 Spectral Topographies of Individual Frequency Bins 32
3.3.4 Refinement of Frequency Bands 36
3.3.5 Results from Individual-Subject Level 38
3.4 Discussion and Summary 40
3.4.1 Peak Frequencies in Mu Rhythm 40
3.4.2 Band Separation in Infant EEG 41
3.4.3 Cortical Activation of the Mu Rhythm 42
3.4.4 Implication to Early Intervention for CP 42
Chapter 4: EEG Resolutions in Movements of Fine Body Parts 44
4.1 Experimental Design 46
4.1.1 Subject Information and Experimental Protocol 46
4.1.2 Data Acquisition 47
4.2 Data Preparation 49
4.2.1 Preprocessing 49
4.2.2 Extraction of Movement EEG 50
4.3 Spectral Analysis 52
4.3.1 Spectral Features from the Mu Rhythm 52
4.3.2 Spectral Principal Component Analysis 53
4.4 Procedures for Evaluation and Classification 55
4.4.1 Evaluation of Spectral Features 55

4.4.2 Classification Procedures 56
4.4.3 Assessment of Decoding Performance 58
4.5 Feature Evaluation Results 59
4.5.1 Profiles of Mu/Beta Rhythms 59
4.5.2 Profiles of Spectral Structures from PCA 60
4.5.3 Spatial Patterns of Different Features 62
4.6 Detection of Individual Finger Movements 66
4.6.1 Single Features for Classification 66
4.6.2 Combined Features for Classification 68
4.7 Pairwise Decoding of Individual Finger Movements 69
4.7.1 Single Features for Pairwise Classification 69
4.7.2 Decoding Efficacies from Single and Combined PC Features 70
4.7.3 Decoding Performance from Resting Data 72
4.8 Decoding Individual Finger Movements from One Hand 73
4.8.1 Single Features for Classification of Five Fingers 73
4.8.2 Combined Features for Classification of Five Fingers 74
4.9 Discussion and Summary 76
4.9.1 Spectral Structures and Features 76
4.9.2 EEG Resolutions in Decoding Individual Finger Movements 78
4.9.3 Information Independence and Redundancy in Spectral Features 79
4.9.4 Implications to BCI Applications and Neuroprosthesis 80
Chapter 5: Towards Decoding Motor Imageries of Fine Body Parts 82
5.1 Data Acquisition and Analysis 83

5.1.1 Subjects and Materials 83
5.1.2 Experimental Design 84
5.1.3 Data Processing 85
5.1.4 Selection of Feature Channels and Classification 87
5.2 Spectral Structures from Different Motor Imageries 88
5.3 Topography of r^2 Values and Classification Results 89
5.4 Discussion and Summary 91
Chapter 6: Conclusion and Future Directions 94
6.1 Added Resolutions in Capturing Motor Development 94
6.2 Improved Resolutions in Decoding Movements/Motor Imageries 96
6.3 Implications to Interventions for Motor Impairments 97
6.4 Recommendations for Future Research 98
References 101
Appendix 111

List of Tables

Table 4.1 Summary of trial information from all subjects 51

Table 4.2 Summary of Student t-test results for movement detection 67

Table 4.3 Significance test results for pairwise decoding of finger movements..... 71

List of Figures

Figure 2.1 Typical neuron structure 9

Figure 2.2 EEG measurement of neural electrical activities 10

Figure 2.3 EEG acquisition system 12

Figure 2.4 ERD induced by left hand movement 14

Figure 2.5 Diagram of BCI technology 17

Figure 3.1 Participant wearing EEG sensor net 22

Figure 3.2 Netstation for synchronized EEG and video acquisition 23

Figure 3.3 Flowchart of EEG preprocessing procedure 25

Figure 3.4 EEG sensor layout 26

Figure 3.5 Weekly spectral profiles 31

Figure 3.6 Distribution patterns of frequency peaks 32

Figure 3.7 Weekly spectral topographies of individual frequency bins 34

Figure 3.8 Normalized weekly spectral topographies of individual frequency bins 35

Figure 3.9 Band definitions from clustering analysis 37

Figure 3.10 Topographies based on refined frequency bands 38

Figure 3.11 Results from correlation test 39

Figure 4.1 Experimental trial design 46

Figure 4.2 Potential differences generated by finger movements 48

Figure 4.3 Profiles of Mu/Beta rhythms 60

Figure 4.4 Spectral PCs in EEG and ECoG from ten pairs of fingers 61

Figure 4.5 Spectral PCs in EEG of movements from all fingers 62

Figure 4.6 Topographies of different types of features 63

Figure 4.7 Topographies of r^2 values between different task conditions 65

Figure 4.8 Accuracies in detecting finger movements from individual features 66

Figure 4.9 Accuracies in detecting finger movements from combined features..... 68

Figure 4.10 DAs of pairwise decoding from single features..... 70

Figure 4.11 Decoding accuracies from single and combined PC features 72

Figure 4.12 Decoding accuracies using the resting EEG data..... 73

Figure 4.13 Confusion matrices from individual features..... 74

Figure 4.14 Confusion matrices from combined features 75

Figure 5.1 Experimental design..... 84

Figure 5.2 Diagram of data processing..... 85

Figure 5.3 Spectral structures and projection weights..... 88

Figure 5.4 r^2 topographies of six MI pairs..... 90

Figure 5.5 Average decoding accuracy for each MI 91

Abstract

Motor skills are essential in people's daily life in exploring and interacting with the ambient environment. Impairments to motor functions affect the acquisition of motor skills, which not only reduce the quality of life, but also impose heavy economic burdens to sufferers and their families. Oscillatory activities in electroencephalography (EEG), such as the mu rhythm, present functional correlation to motor functions, which provide accessible windows to understand underlying neural mechanism in healthy persons and perform diagnoses in patients with various motor impairments. It is thus of significant importance to further investigate classic and/or identify new motor-related EEG oscillatory activities.

In this dissertation, EEG oscillations from both infants and adults are investigated to uncover motor-related neural information noninvasively from the human brain regarding their developmental changes and movement representations of body parts, respectively. In typical developing infants at 5-7 months of age, knowledge about mu rhythm development is expanded by capturing subtle developmental changes of its characteristics in a fine age resolution, through the development of new spatio-spectral analysis of EEG data recorded longitudinally on a weekly basis. In adults, motor tasks involving fine body parts are studied to investigate EEG resolutions in decoding movements/motor imageries of individual fingers, which have only been addressed in large body parts in literature. Discriminative information in EEG oscillations about motor tasks of fine body parts is revealed through the discovery of a novel type of spectral structures in EEG, which exhibits better sensitivity to movements of fine body parts than the classic mu rhythm. The findings in this dissertation broaden the scope of

neural information in EEG oscillations in relation to motor functions, and contribute to the understanding about human motor functions at various life stages. These results and technologies are promising to be translated to patient studies in the future.

Chapter 1: Introduction

The ability to move freely and interact with the outside world is one of the fundamental skills for humans' activities of daily living. These movements are coordinated and controlled by the human motor system, which allows people to explore ambient environment and gain life experience. Impairments to the motor system from cerebral palsy (CP), spinal cord injuries, stroke, etc. could lead to movement disorders and even severe paralysis. In the United States, CP accounts for the most common physically disabling condition in children, with prevalence at approximately 3.1 to 3.6 out of 1000 children (Christensen et al., 2014). As for paralysis, there are about 5,596,000 Americans suffering from some kind of paralysis, taking up 1.9% of the U.S. population (Christopher Reeve Paralysis Foundation, 2009). People with motor impairments cannot live, work or exercise like healthy individuals, leading to degeneration in quality of life depending on the severity of impairments. At the same time, sufferers of motor impairments usually bear with heavy economic burdens. A survey published in 2009 reported approximately 25% of families with a paralytic have household income lower than $10,000 per year, much lower than the ratio 7% of families in general population (Christopher Reeve Paralysis Foundation, 2009). Thus, it's in urgent need for solutions to ease the hardship of these individuals.

The variety of medical conditions leading to motor impairments can range from congenital diseases of the neural system as early as during infancy to acquired diseases of the neural system or damages to motor actuators (e.g., limbs) at later ages. The former type of conditions, such as CP, has great impact on the formulation of motor functions at the developmental phase, while the later ones, such as spinal cord injury,

stroke, multiple sclerosis and damage or loss of limbs, usually affect a fully grown motor system, resulting in movement disorders or movement difficulties to the sufferers. The aforementioned variety in intrinsic characteristics and affected population of motor impairments suggests different approaches for interventions that could maximize the efforts in promoting motor skills of people with motor impairments.

Cerebral palsy is one of the typical neurological disorders developed at early ages, and it may start during prenatal, perinatal and postnatal stages due to damage or abnormal development of motor brains (Jones et al., 2007). CP sufferers usually sustain poor movement, balance and posture control. Although the condition of CP is not progressive with age, a decrease of spontaneous movements during the first year of life has been found for infants who are later diagnosed with CP (Hadders-Algra, 2001). This could lead to muscle weakness and atrophy at later ages. Aside from the effect on motor skills, recent studies found connections of CP with delayed speech and language (Hustad et al., 2014), as well as cognitive development (Bottcher, 2010). Both brain plasticity theory at the developing phase (Bach-y-Rita, 1990) and neuronal group selection theory (Edelman, 1993; Hadders-Algra, 2000) suggest, with intervention and training at early ages, better modulation and coordination of movements can be achieved for CP sufferers to promote their motor skills. Common interventions, such as physical therapy and occupational therapy, rely heavily on behavioral scores as treatment assessment. In such circumstances, neurophysiological biomarkers for motor development could provide more direct and accurate information for treatment assessment and improvement of intervention design. However, such information is still

scarce, since it requires further understanding about typical motor brain development as a reference.

As for motor impairments developed at later ages, either deficiencies of the nervous system (caused by various neurological disorders) or damages to the motor actuators (damage or loss of limbs), developing advanced assistive technologies is a promising approach to promote movement abilities of people with these motor impairments. Traditional assistive technologies, such as wheelchair, walker and prosthesis, can help them regain some sort of abilities to engage normal life activities. However, most of these technologies require a certain level of motor inputs, making them inaccessible to people with severe motor disabilities. Hence, novel and advanced types of assistive technologies are needed for their assistance. For instance, patients of tetraplegia caused by injuries to high-cervical nerves in spinal cord lose control over all limbs, but their motor brain functions might be intact. In such situations, the technology of brain-computer interface (BCI) might be a viable approach, which aims to identify various activation patterns in brain waves and translates them into control signals for external applications, such as an electrical wheelchair, computer programs and neuroprosthesis (Wolpaw et al., 2002; Birbaumer, 2006; Schwartz et al., 2006; Muller-Putz et al., 2005). In this way, BCI users can directly communicate and interact with the outside world by performing mental tasks, bypassing the damaged motor pathway. Especially, activation patterns from motor tasks gain increasing attention in the field of BCI research, since they provide more proactive and intuitive control paradigms for BCI users, compared to those from passive mental tasks.

As described above, the interventions for motor impairments at different stages all rely on the knowledge about human motor brains. Oscillatory activities in human electroencephalography (EEG) have exhibited functional correlations to certain brain functionalities, indicating the investigation of motor related brain rhythms in EEG oscillations could facilitate the understanding about human motor brain. In infant EEG, characteristics of the mu rhythm, a type of EEG oscillations from the motor cortex, have been investigated to probe motor functions at early stage, due to its close relation to motor development (Smith 1941; Hagne et al., 1973). Studies have found the frequency band of the mu rhythm (6-9 Hz) to be lower than that of adults (8-12 Hz) and its peak frequency shifts to the higher frequency range towards the adult level along maturation (Lindsley, 1939; Hagne et al., 1973; Marshal et al., 2002; Orekhova et al., 2006). Such correlation makes the mu rhythm a promising biomarker for understanding motor development at early ages as well as for intervention assessment. However, most studies are with cross-sectional design and/or months/years apart between adjacent age points, the subtle longitudinal motor development at a finer age resolution has not been well studied. In adults, spectral features from the mu rhythm have demonstrated decoding capability of movements/motor imageries (MI) of large body parts, which can serve as control features for BCI applications (Gu et al., 2009; Zhou et al., 2009b). One challenge for motor-rhythm based BCIs is the limitation of available control features, which largely confines BCI systems to simple applications, such as cursor movements in restricted dimensions on the computer screen (Wilson et al., 2009; Wolpaw and McFarland, 2004). To enlarge the repertoire of control features for BCIs, one possible approach is to decode movements/MIs of finer body parts other than whole hands/limbs,

such as individual fingers, which are most dexterous body parts and account for majority of human interactions with the outside world. However, the feasibility of such decoding tasks has not been sufficiently investigated in EEG.

Both capturing the motor development at finer age resolution and decoding movements/MIs of finer body parts are to expand the knowledge of human motor brain, in an effort to facilitate the development of interventions for motor impairment at different stages. In this dissertation, infant EEG sessions were acquired on a weekly basis using high-density EEG sensor nets that contain information of subtle motor development within fine age ranges. A procedure involving a series of advanced signal processing techniques in both temporal and spatial domains was developed to improve signal quality of infant EEG, before spectral analysis was applied to capture longitudinal changes of the mu rhythm. My experimental results concur previous findings about frequency peak shifting of mu rhythm and complement other developmental studies in depicting more detailed developmental curve of the motor brain. This expands the scanty knowledge about infant motor development, facilitating the development and assessment of interventions to motor impairments at early ages.

In adult EEG, a novel type of spectral structures from spectral principal component analysis (SPCA) was uncovered during experimental tasks of individual finger movements. Three decoding tasks involving individual finger movements of one hand were designed to comprehensively evaluate the decoding efficacy of the newly discovered features. The three tasks are detection of finger movements, pairwise decoding of individual finger movements, and decoding individual finger movements from one hand, by the order of their difficulty levels. My experimental results show

promising decoding performance from the newly discovered spectral structures in EEG in all three tasks, demonstrating the existence of sufficient information in EEG oscillations for movement identification of fine body parts. Furthermore, the spectral structures from SPCA exhibit much better sensitivity to movements of fine body parts, comparing to the classic mu rhythm. The identification of four motor imageries from thumb and fist from both hands was also explored as an extension of movement identification. Similar processing approaches were taken to investigate the feasibility of EEG oscillations in decoding different motor imageries involving individual fingers. The significantly higher accuracies than guessing in all decoding tasks in this dissertation demonstrate the feasibility of discriminating movements/MIs of fine body parts as a promising approach towards complex BCI applications with flexible and intuitive controls for people suffering from motor impairments.

With the promising findings mentioned above, this dissertation expands the knowledge about human motor brains in both motor development at early ages and identification of cortical activation from movements/motor imageries of fine body parts, which might have great implications to developing interventions at different ages, treatment assessment and motor assistance for people with motor impairments.

Here is an outline of the dissertation. Following this introductory chapter, Chapter 2 provides background knowledge related to the dissertation topic, including an introduction to EEG and acquisition system, typical rhythmic activities in EEG oscillations and current knowledge about motor development and movement/motor imagery identification. Chapter 3 covers a study investigating EEG oscillations of high spatial and temporal resolutions to further the understanding about motor development

at early stage. Chapter 4 presents studies about EEG resolutions in identifying movements of fine body parts, including detection of finger movements from resting condition, pairwise decoding of individual finger movements, and decoding individual finger movements from one hand. In Chapter 5, a preliminary study of decoding motor imageries of individual fingers against fists from both hands is introduced, to probe the feasibility of decoding motor imageries of fine body parts from EEG oscillations. Chapter 6 draws a conclusion to the dissertation and opens up the discussion and suggestion to future works.

Chapter 2: Background

Various brain imaging techniques have been developed to capture neural activities of the human brain based on different principles. For instance, functional magnetic resonance imaging (fMRI) measures neural activates by detecting the changes in blood oxygenation associated with brain activities; magnetoencephalography (MEG) implements a very sensitive magnetometer (i.e., superconducting quantum interface device, SQUID) to measure magnetic fields induced by neuroelectrical signals in the human brain; electroencephalography (EEG) and electrocorticography (ECoG) measure electrical signals generated by the human brain by placing electrodes outside of the scalp and at the brain surface, respectively. Among these techniques, EEG setup is easy and inexpensive, making it more accessible to be used in real world than others. And the high temporal resolution of EEG enables the capturing of brain activities at the millisecond level. Furthermore, EEG is noninvasive and safe to users comparing to invasive techniques like ECoG, which requires clinical surgeries to expose the brain surface for electrode placement. Thanks to these merits, EEG is widely adopted in the field of biomedical research to study human brain functionalities.

This chapter aims to provide readers with background information of EEG oscillations in human brain research. The neurophysiological origin of EEG is firstly discussed, together with the EEG acquisition system implemented in this dissertation. Following that is an introduction to typical EEG oscillatory activities, especially the mu rhythm, a unique motor rhythm associated with motor functionalities. Then, current knowledge about motor development and motor assistive technologies is summarized.

2.1 Introduction to EEG

Neurons are basic working units in the human central nervous system (CNS), forming the core components of the brain and spinal cord. There are a large variety of neurons discovered in the human nervous system, such as retinal bipolar neurons, retinal ganglion neurons, cortical pyramidal neurons, and cerebellar Purkinje neurons, just to name a few (Purves et al., 2004). Typical neurons consist of three major components, cell body, axon and dendrites. Their corresponding structures are depicted in Figure 2.1 (Figure shared under GNU Free Documentation License Ver. 1.2., https://en.wikipedia.org/wiki/Neuron#/media/File:Neuron_Hand-tuned.svg). The cell body is the living part of neurons that produces proteins needed by other components. It holds basic organelles of a cell, such as nucleus, Golgi apparatus and endoplasmic reticulum. The dendrites are branch-like structures that collect information from other neurons, and the axon works as a sender to transmit information out of the neuron.

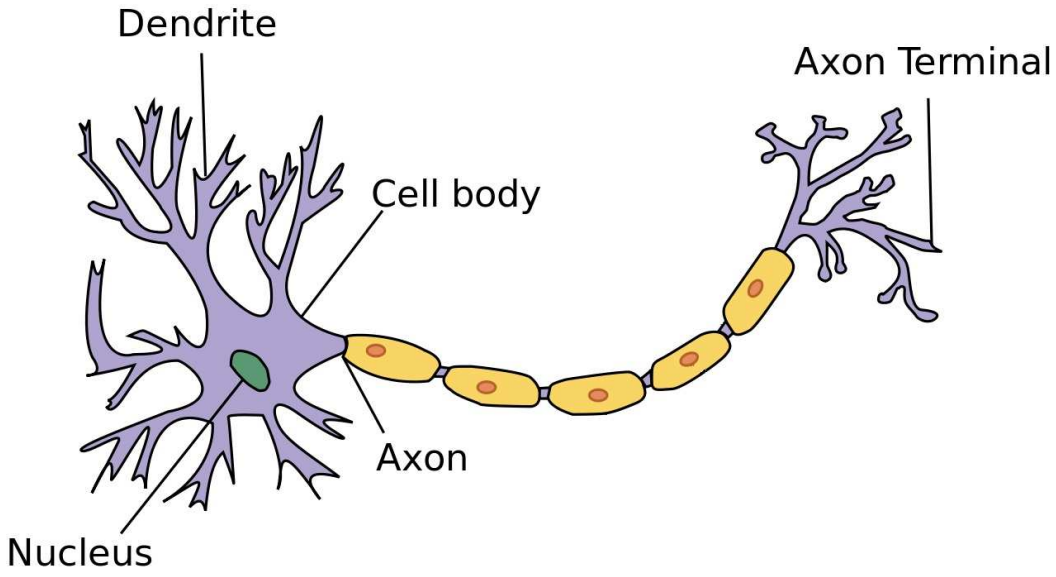

Figure 2.1 Typical neuron structure
Typical neurons consist of three components: cell body, dendrite and axon.

The neurons in the human brain are all electrically excitable cells that communicate to one another via electrical or chemical signals at synapse, where exchange of charged ions takes place. Resulted ionic potentials form the physiological origin of EEG. By placing electrodes at the surface of the scalp, EEG measures aggregated electrical potentials from a large population of underlying neurons, usually in the order of thousands and millions. Among different types of neurons, cortical pyramidal neurons contribute the most to EEG signals due to the orientation of their long apical dendrites that are perpendicular to the cortical surface (Kirschstein and Kohling, 2009). Such a cortical organization of pyramidal neurons enhances the synchrony of electrical signals being picked up by EEG.

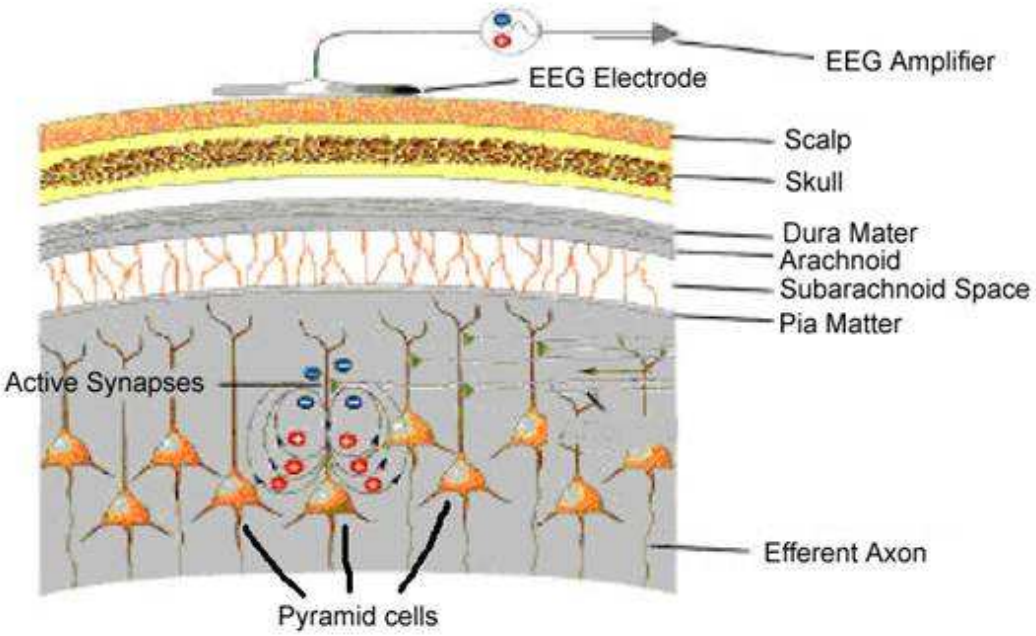

Figure 2.2 EEG measurement of neural electrical activities
Electrical signals produced by cortical pyramidal neurons are picked up by EEG electrodes placed at the scalp.

As illustrated in Figure 2.2 (Figure source: An introduction to EEG. Mind and Brain Laboratory. http://www.psych.nmsu.edu/~jkroger/lab/EEG_Introduction.html),

electrical signals generated by neurons propagate through different layers of brain organisms, such as the cerebrospinal fluid (CSF), skull and scalp, before being measured by EEG electrodes placed outside of the scalp. Due to the anisotropic conductivity of these organisms, especially the CSF (Wendel et al., 2008) and skull (van den Broek et al., 1998), neural electrical signals are smeared and attenuated at the scalp level, resulting in tiny magnitudes of signals integrated from multiple sources of underlying neural mechanisms.

2.2 EEG Acquisition System

Advancement in biomedical devices grants researchers access to EEG amplifiers with high input impedance to capture tiny cortical signals from the brain with fidelity, as well as high spatial and temporal resolutions. Figure 2.3 (a) shows the EEG acquisition system (Net Amps 300, Electrical Geodesic Inc., OR, USA) used in the studies of this dissertation. From left to right are three core components of the EEG system, including an EEG sensor net, an amplifier (Net Amps 300) and a data acquisition computer. The 128-channel high-density EEG sensor net covers more cortical regions than 32- or 64-channel ones used by many other studies, providing EEG with a relatively high spatial resolution. The Net Amps 300 amplifier has an input impedance of 200 MΩ compared to below 100 MΩ from most other commercially available amplifiers, and is capable of sampling up to 20,000 Hz on all channels simultaneously. The added resolutions in temporal and spatial domains provide rich information to study the human brain through scalp EEG recordings. Figure 2.3 (b) presents an example of a subject wearing the EEG sensor net performing an

experimental task in an electromagnetically shielded chamber room. Such an experimental setting can minimize electrical and/or magnetic interferences from ambient environments in order to acquire EEG with high signal-to-noise ratio (SNR).

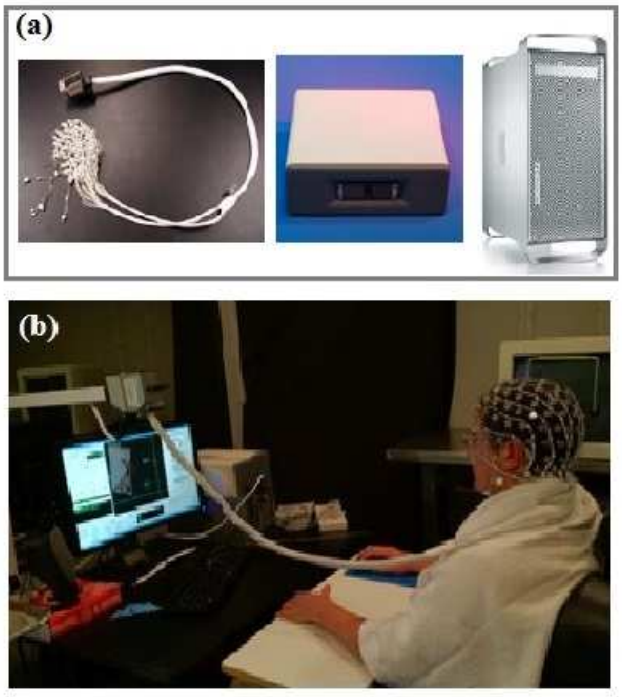

Figure 2.3 EEG acquisition system
(a) Core components of an EGI EEG system, including a sensor net, an amplifier and a data acquisition computer. (b) EEG acquisition in a shielded chamber room.

2.3 Oscillatory Activities in EEG

Ever since Berger's first recording of human EEG in 1920s, EEG oscillations have drawn attentions of researchers for decades due to their close correlations with brain functionalities. Various EEG rhythms, neural oscillations within different frequency bands, have been discovered and investigated to expand the knowledge about the human brain. Posterior alpha rhythm is one of the most prominent EEG rhythms in human EEG, reflecting neural oscillations approximately between 8 and 12 Hz. It is most obvious at the occipital cortex during wakeful relaxation with eyes closed, and its

amplitudes are attenuated with eyes open (Kirschfeld, 2005). Posterior alpha rhythm is associated with the idle state of visual functions and its fluctuation reflects functional changes in the visual cortex related to visual detection (Vanni et al., 1997; Ergenoglu, et al., 2004), sleep (McKinney et al., 2011), attention level (Kim et al., 2013) and drowsiness (Lin et al., 2005). Theta rhythm accounts for another EEG rhythmic activity, represented by 4-7 Hz of EEG oscillations. Theta rhythm has exhibited location-specific functional correlations. While theta rhythm at the frontal cortex is found to associate with memory processing of the brain (Urgen et al., 2013), it correlates with function of spatial navigation in the parietal cortex (Snider et al., 2013).

Besides band-specific rhythmic activities in EEG oscillations, recent studies reveal spatial and temporal couplings of rhythmic activities from different frequency bands (Pfurtscheller et al., 1997, Miller et al., 2009b, Canolty et al., 2006). In the motor brain, nonlinear couplings among harmonic frequency components between mu and beta rhythms and between low and high beta rhythms have been reported (Pfurtscheller et al., 1997, 1999). Coupling between high gamma power and theta oscillation has also been observed in cognitive processes of the human brain studied using ECoG signals (Canolty et al., 2006). One clinical study further indicates the coexistence of slow shift and high frequency oscillation during seizures in epileptic patients (Imamura et al., 2011). A recent study (Miller et al., 2009b) reported power increase over a broadband spectrum (up to 200 Hz) in ECoG data from a finger tapping task. These studies demonstrate that well-defined spectral structures over multiple frequency bands might exist in brain signals and their changes may contain rich information that is not available in the analysis of rhythmic activities at individual frequency bands.

2.4 Mu Rhythm from Human Motor Brain

In the human motor brain, the mu rhythm is a unique EEG rhythm at the alpha band (8-12 Hz) (Pfurscheller and Lopes da Silva, 1999; Pfurtscheller et al., 2006; Yuan and He, 2014). It shares similar frequency band with the posterior alpha rhythm, but they present functional and topographical differences from each other (Marshall and Meltzoff, 2011; Niedermeyer, 1997). Unlike posterior alpha rhythm, the mu rhythm is minimally affected by light illumination or eye open/close (Kuhlman, 1978). Instead, the attenuation of mu rhythm activities can be observed during preparation/execution of voluntary movements or motor imageries at the contralateral side of motor cortex, accompanied by a harmonic decrease in beta band (13-30 Hz), known as event-related desynchronization (ERD) (Pfurscheller and Lopes da Silva, 1999).

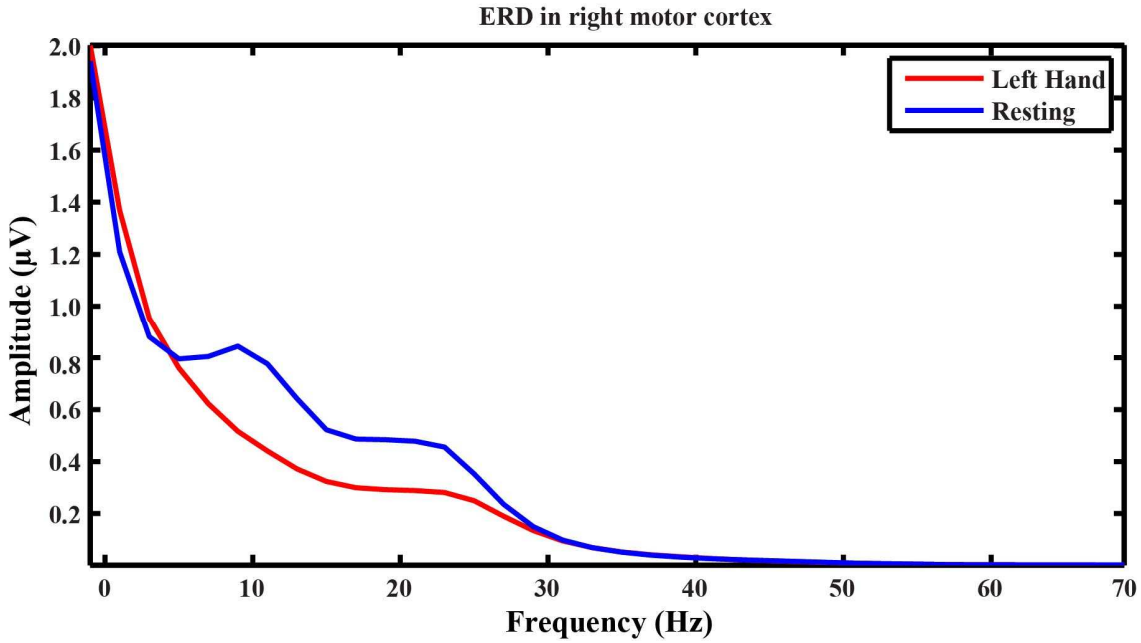

Figure 2.4 ERD induced by left hand movement

Figure 2.4 presents an example of ERD pattern induced by left hand movements from the resting condition on an EEG channel at the right motor cortex. It shows that

power decreases can be observed in both alpha (8-12 Hz) and beta (13-30 Hz) bands, when comparing the condition of left hand movements (red curve) to the resting condition (blue curve). The ERD is usually followed by a power rebound in the mu rhythmic after cessation of movements, known as event-related synchronization (ERS) (Pfurscheller and Lopes da Silva, 1999). ERD/ERS patterns of the mu rhythm are believed to reflect sensorimotor activation and deactivation (Neuper et al., 2006).

2.5 Mu Rhythm in Understanding Motor Development

The mu rhythm has been extensively studied to understand the human motor brain, due to its functional correlation to motor functions (Pfurscheller and Lopes da Silva, 1999; Berchicci et al., 2011). On the one hand, the characteristics of mu rhythm are investigated in infant EEG to probe the motor development at early stage. Early studies found the range of alpha band in infant EEG to be lower than that of adults (Smith, 1938; Lindsley, 1939), with 6-9 Hz generally accepted as the alpha band due to its functional resemblance to the adult alpha rhythms (i.e., 8-12 Hz). Similar to adults, there are two distinct alpha rhythms in infant EEG. One of them originated from posterior cortical sites resembles the posterior alpha rhythm in adults, and the other alpha rhythm originated from the central cortical site is analogous to the adult mu rhythm. Stroganove et al. (1999) found that the former rhythm presents increased activities during darkness comparing to attention with illumination, while activities of the latter rhythm are suppressed during darkness, demonstrating their different functional correlates.

Numerous studies have been carried out to investigate the mu rhythm in infancy in an effort to understand the motor development at early stage. As early as 1939, Smith reported the transition of EEG oscillations of 7 Hz at 4 months of age to 8.5 Hz at 18 months of age over sensorimotor system (Smith, 1939). Hagne et al. (1973) found the emergence of the mu rhythm peak at 6 months of age and the shift of mu peak frequency from 6 Hz at 6 months to 7 Hz at 12 months of age. Marshal et al. (2002) did not find the mu peak at 5 months of age, but identified the emergence of 7-8 Hz mu rhythm peak at 10 months of age, shifting towards 8 Hz at 14 and 24 months of age. Orekhova et al. (2006) found mu ranges from 6.4-8.4 Hz for infants about 10 months of age, to 8.4-10.4 Hz for 5-year-old children. Berchicci et al. (2011) reported the shift of mu rhythm peaks from 2.75 Hz at as early as 3 months to 8.25 Hz at 11 months of age with magnetoencephalographic recordings (MEG).

Aforementioned studies have enriched the knowledge about the mu rhythm during infancy, whereas some disagreements about emergence of the mu rhythm and mu peak frequencies at specific ages are presented, impeding the full comprehension of the mu rhythm and its indicative role in infant motor development. Considering the time span of these studies, evolvement of techniques of EEG recording and signal processing over the years might have some impacts on the interpretation. Early studies (Smith, 1939) were carried out when EEG data were acquired and plotted on EEG chart paper, while later studies took advantage of computers, with which EEG could be digitally stored and advanced digital signal processing algorithms could be applied (Marshal et al., 2002, Orekhova et al., 2006). Most of studies about motor development recruit different subjects at each age point, like other cross-sectional studies, lacking the

information of cause and effect about motor development. Moreover, durations between two age points are usually months apart, while developmental changes of the human motor brain in a finer time resolution are not well captured yet. All these factors indicate results from more studies are needed to reach conclusive evaluation.

2.6 Mu Rhythm in Developing Assistive Technology

Aside from capturing motor developmental changes in infancy, the changes of mu rhythm activities are used to identify movements or motor imageries of different body parts, in an effort to develop advanced assistive technologies for people with severe motor disabilities. For people suffering from severe motor disabilities, the BCI technology provides alternative channels to perform necessary motor functions in daily

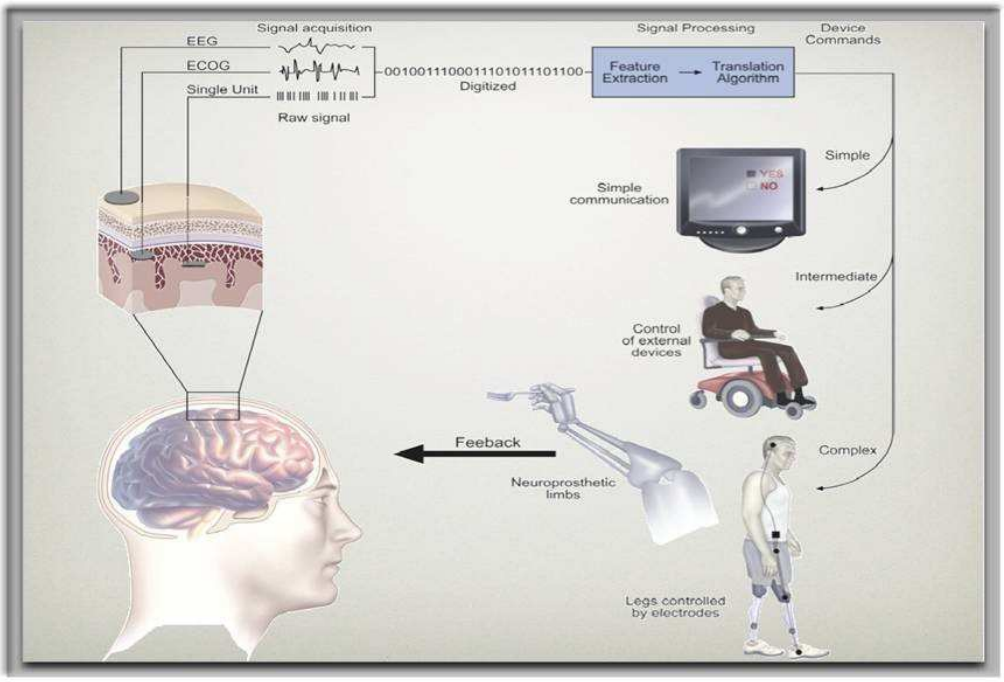

Figure 2.5 Diagram of BCI technology

life, bypassing damaged peripheral nerves and muscles (Wolpaw et al., 2002; Birbaumer, 2006; Schwartz et al., 2006). BCI decodes neurophysiological signals from brain activities and translate human intentions into commands to control external devices or computer applications, as illustrated in Figure 2.5 (Adapted from Leuthardt et al., 2006).

Among various brain signals used in BCI, including EEG (Bradberry et al., 2010; Wolpaw and McFarland, 2004), ECoG (Miller et al., 2010; Pistohl et al., 2012), fMRI (Sitaram et al., 2007; Yoo et al., 2004), MEG (Bradberry et al., 2009), EEG-based BCI research is gaining popularity over other measurement techniques. This is due to some intrinsic merits of EEG recording technique, such as direct reflections of the electrical responses of the human brain, cost efficiency and noninvasiveness, as described in details in the first paragraph of Chapter 2.

In EEG oscillations, aside from the change of mu rhythm activities from the motor cortex during movement/motor imagery of certain body parts (Wolpaw and McFarland, 2004), there are also other brain patterns identified and extracted as control features for BCI, such as P300 wave from the parietal lobe (Farwell and Donchin, 1988) and steady-state visually evoked potentials (SSVEP) from the occipital lobe (Bin et al., 2009). Comparing to other features, the mu rhythm-based features are able to provide self-initiated stimulus-free control paradigm for BCI users, which fit better for applications involving movement controls. However, mu rhythm-based BCIs suffer from limited degrees of freedom (DOF), i.e., the small number of reliable control signals available, which significantly constrain the complexity of BCI applications. During the past decade, movements/motor imageries of large body parts have been

investigated in EEG-based BCIs, including wrists (Gu et al., 2009), upper limbs (Doud et al., 2011), elbows and shoulders (Zhou et al., 2009b), legs (Pfurtscheller et al., 2006), and tongue (Morash et al., 2008). However, the movements of fine body structures, such as individual fingers from one hand, have not been well studied in EEG-based BCI, while they are the most dexterous part of our body and play an irreplaceable role in our daily activities. The successful decoding of fine body parts would greatly advance the mu rhythm-based noninvasive BCIs with rich control dimensions.

In the following studies of this dissertation, one goal is to investigate the subtle changes of mu rhythm in infancy in fine age range with EEG recordings of high spatial and temporal resolutions, in an effort to further the understanding about human motor development at early stage. Another goal is to investigate resolutions of EEG oscillations in decoding movement/motor imageries of fine body. The unified goal of this dissertation is to uncover new information in EEG oscillations from human motor brain, which not only furthers the understanding about human motor functions but also could implicate to effective interventions for people with motor impairments at different stages.

Chapter 3: Further the Understanding about Motor Development

Studies in developmental neuroscience suggest the important role of understanding motor development through neuroimaging techniques for early diagnosis and intervention of motor neurological disorders developed before maturation of the human motor brain (Hadders-Algra, 2014). Until now, very little information is available to accurately assess the effect of early interventions on motor development. Age-related changes in characteristics of the mu rhythm in infant EEG provide a potential biomarker for such purposes. However, due to practical difficulties in recruiting infant subjects and acquiring EEG from infants, studies about the infant mu rhythm are still scarce in comparison to adults. Most of previous studies either focus on one single age group or are cross-sectional with different subjects for each age point (Orekhova et al., 2006; Stroganova et al., 1999), lacking cause and effect information about motor development that is only available in longitudinal studies. Many of these studies cover a long age span, with months apart between adjacent age points (Marshall et al., 2002), while subtle changes of the mu rhythm within fine age resolutions have not been investigated. Furthermore, some discrepancies about emergence of the mu rhythm peak and peak frequencies at specific ages are presented from different studies. All these factors impede the further comprehension of infant motor development, and more efforts and knowledge are urgently needed.

In this chapter, a longitudinal study investigating mu rhythm development in infant EEG is reported, with EEG recordings of high temporal and spatial resolutions. EEG data were acquired on a weekly basis from infants during their 5 to 7 months of age from high-density EEG sensor net, enabling the close observation of subtle changes

in the mu rhythm along this period. Spectral analysis was performed to examine the developmental changes of the mu rhythm in both spectral and spatial domains. Furthermore, a clustering analysis was adopted to refine the separation of frequency bands in infant EEG at different age points. The findings concur and complement previous studies in capturing the development of rhythmic activities during infancy that would facilitate development and assessment of interventions for motor impairments at early ages. Some results in this chapter have been reported in Xiao et al., 2015.

3.1 Experimental Design

3.1.1 Participants

Ten infant subjects participated in the study, with informed consents obtained from their parents before experiments. Data from two subjects were excluded from the study, due to the facts that one baby was diagnosed as atypical developing condition from post-experiment evaluation and another one exceeded the age range of the study after gestation adjustment. The resting eight subjects were healthy infants (4 males, 4 females), with their gestation adjusted age ranging from 17 to 23 weeks (Mean age: 20.5 weeks; SD: 1.85 weeks) during their first EEG recordings. The study was reviewed and approved by the local institutional review board at the University of Oklahoma Health Sciences Center.

3.1.2 Acquisition of EEG

EEG data were acquired with EGI Geodesic EEG System 300 (Electrical Geodesics, Inc., Eugene, OR), including Net Amps 300 amplifier and 124-channel HydroCel Geodesic Sensor Net (HCGSN 130) for infants. EEG sensor nets with three

different sizes (40-42 cm, 42-43 cm and 43-44 cm) were adopted to accommodate infant subjects of different head circumferences. During experimental recordings, infants wearing EEG sensor nets sat on their parents' laps, and parents were instructed to avoid rocking or moving the infants and to keep infants' heads in upright position. Figure 3.1 illustrates an infant participant wears an EEG sensor net during an experimental recording. A baby rattle phone app was presented to infants, out of their reaching range (approximately 1 meter away), to keep them calm and still during EEG recording. EEG signals were recorded at a sampling frequency of 1 kHz for 5 minutes of resting data in each experimental session.

Figure 3.1 Participant wearing EEG sensor net

Aside from EEG, videos were recorded simultaneously during each session, synchronized to EEG signals through EGI's Netstation software, as shown in Figure 3.2. Participants were asked to attend weekly EEG recordings until reaching 8 months of age or being able to crawl. Only sessions recorded when infants were between 5 and 7 months of ages were selected for further analysis. Sessions with excessive motion artifacts, identified by visual inspection of EEG and video recordings, were also removed. There were in general 10 EEG sessions left from each participant after these data selection criteria, except one participant with 5 sessions (the participant presented crawling ability at as early as the beginning of 7 months of age).

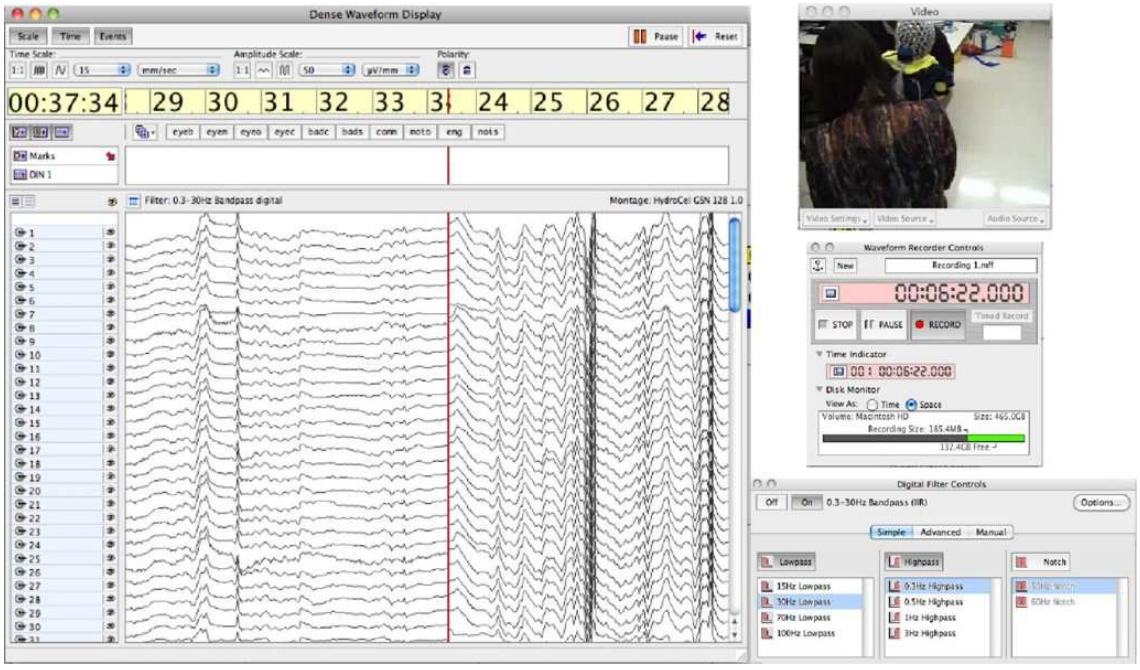

Figure 3.2 Netstation for synchronized EEG and video acquisition

3.2 Data Processing

3.2.1 EEG Preprocessing

A preprocessing procedure involving multiple signal processing techniques was developed to enhance the signal quality of EEG. A flowchart of preprocessing steps is depicted in Figure 3.3. EEG from all sessions firstly went through a 0.3-30 Hz band-pass digital filter with infinite impulse response (IIR), to remove DC offsets and interferences from unwanted high-frequency components, such as muscle activities. Secondly, EEG data from channels near boundaries of sensor nets (marked as red in Figure 3.4), including those near the neck, ears and eyes, were disregarded. These channels were found to be easily affected by head, face and eye movements, and susceptible to motion artifacts. That left 70 channels (marked as green in Figure 3.4) in the center for further analysis. Thirdly, sections of EEG, with either abnormally large amplitudes during visual inspection of EEG waveforms or the presence of abrupt voluntary movements from participants identified through video recordings, were marked and removed. There were in general 2 minutes of EEG left for each session after the bad section rejection. Fourthly, channel statistics was implemented to determine channels to be rejected. Specifically, the kurtosis value, which is the fourth cumulant of data, was calculated for each channel. Kurtosis measured the peakedness of a distribution, and EEG data from channels with kurtosis values larger than 5 standard deviation of the mean were removed and interpolated by mean EEG amplitudes of surrounding channels. Fifthly, a common average reference (CAR) filter was applied to the temporal EEG. The CAR is a spatial filter to further increase the signal-to-noise ratio, by removing cross-channel mean from each EEG channel at each sample point.

Lastly, a blind source decomposition technique, independent component analysis (ICA), was implemented to isolate neuronally generated EEG sources from artifactual ones (Delorme et al., 2012). The temporal EEG data were decomposed into 30 independent components (IC), and ones associated with common EEG artifacts, such as eye movements, electrical activities generated by heart, muscular activities, etc., were removed to improve the quality of EEG signals. Some functions involved in the data preprocessing procedures were accomplished using the EEGLAB toolbox, developed by Swartz Center for Computational Neuroscience in the University of California San Diego (Delorme and Makeig, 2004).

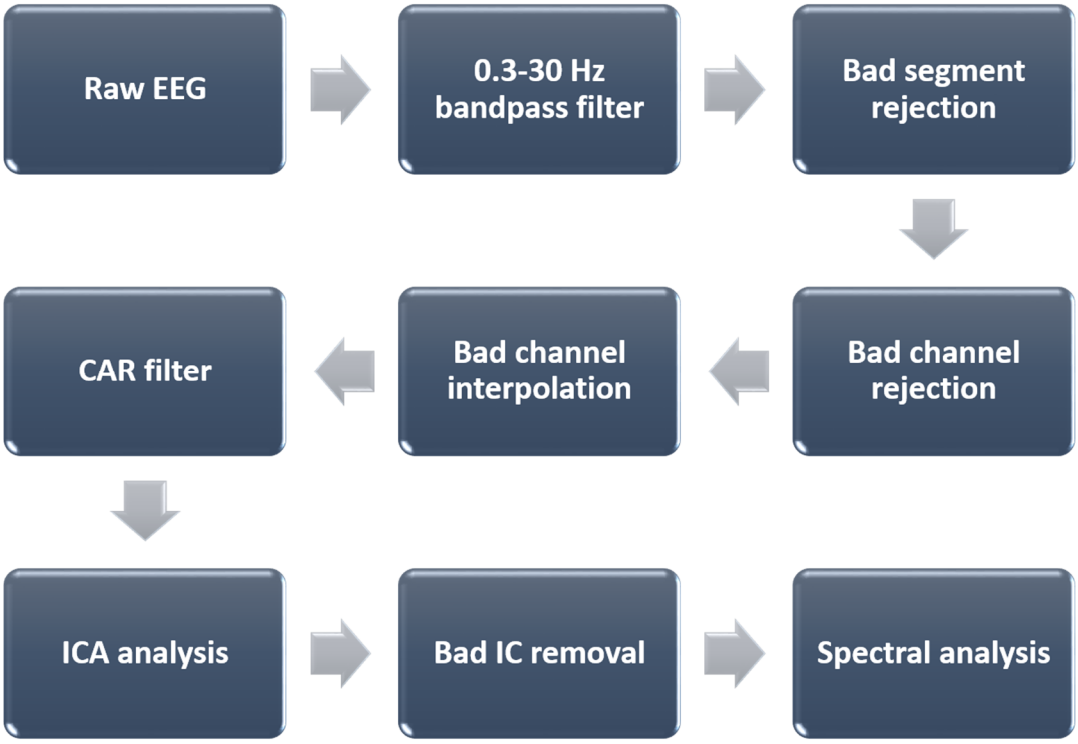

Figure 3.3 Flowchart of EEG preprocessing procedure

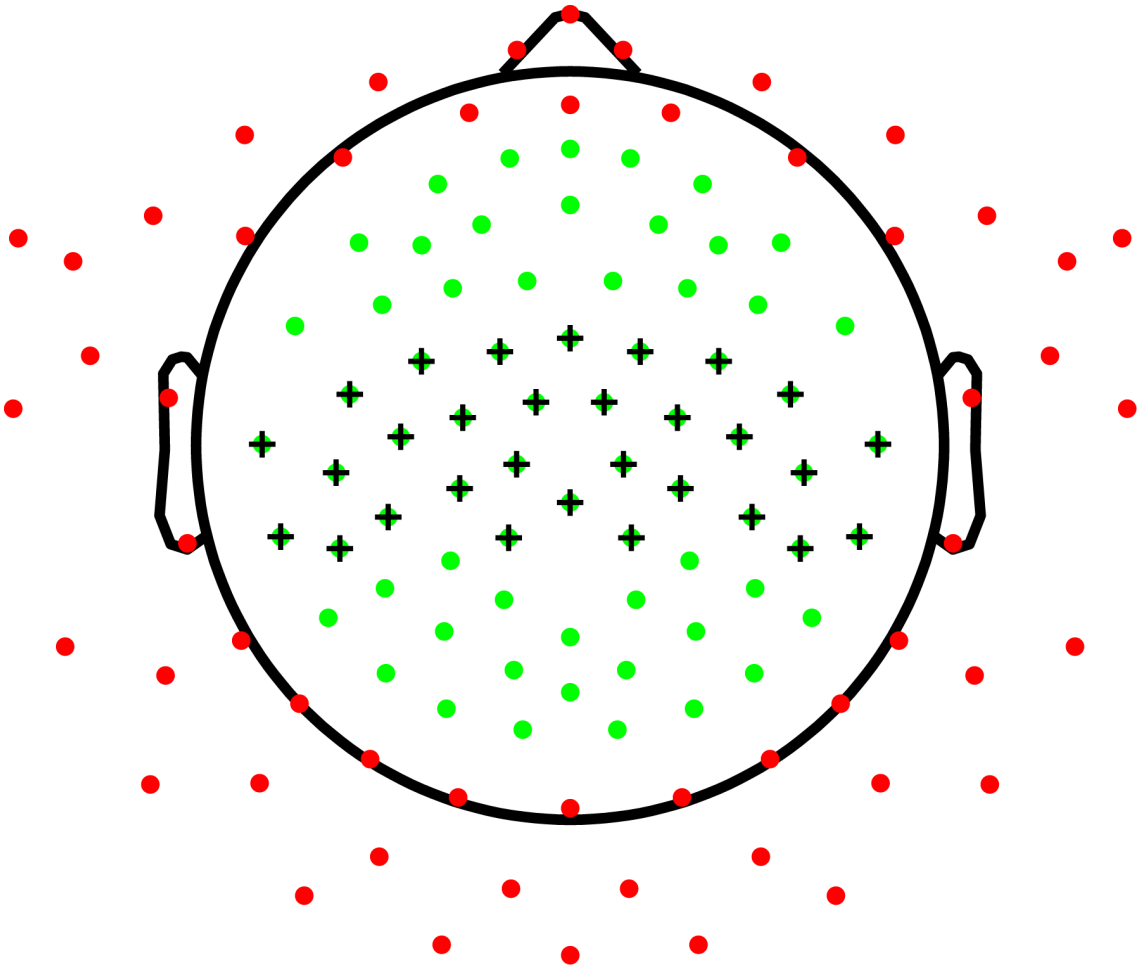

Figure 3.4 EEG sensor layout

3.2.2 Spectral Analysis

For each EEG channel, power spectral densities (PSD) were estimated based on Welch's method (Welch, 1967). It estimated the spectral powers for each 3-second epoch in the temporal EEG waveform using Hanning window with 50% overlaps between two adjacent epochs. This resulted in a frequency resolution of 1/3 Hz for PSDs, and mean PSDs of all epochs were calculated to obtain averaged estimations. The "pwelch" function from Matlab software (R2014a, MathWorks Inc., Natick, MA) was used for the PSD calculation.

To compensate the scale changes due to the fluctuations of EEG across different subjects and recording sessions (Marton et al., 2014), relative power densities were computed upon PSD estimations, using

$$R_f = P_f / \sum_{1}^{30} P, \qquad f = 1, 1\frac{1}{3}, 1\frac{2}{3}, 2, \ldots, 30 \text{ Hz} \tag{3.1}$$

where R_f and P_f are relative and absolute power density for each frequency bin f, respectively. Relative power densities for frequency bins between 1 and 30 Hz are calculated by the ratio of absolute power density at individual frequency bins against the sum of power over the whole studied frequency band (1-30 Hz). An average across 30 channels (marked by black crosses in Figure 3.4) covering the central cortex, i.e., the motor cortex, were computed to evaluate spectral profiles of EEG powers with respect to motor development.

The relative power densities on each channel were registered to their corresponding geodesic locations on the scalp to generate longitudinal topographies for each frequency bin. The power-law decaying property of EEG spectrum makes it hard to compare topographies across different frequency bins. Hence, relative PSDs from all channels at each epoch were normalized to z scores by

$$Z_f = \frac{R_f - \mu_{R_f}}{\sigma_{R_f}}, \qquad f = 1, 1\frac{1}{3}, 1\frac{2}{3}, 2, \ldots, 30 \text{ Hz} \tag{3.2}$$

where Z_f is the z score at the frequency bin f after normalization. μ_{R_f} and σ_{R_f} are the mean and standard deviation of relative power density at the frequency bin f across all channels, respectively.

3.2.3 Spectral Peak Statistics

To examine the shifting pattern of peak frequency of the mu rhythm along maturation, the spectral peak distribution across different frequency bins was constructed. For each channel at the motor cortex, a simple 5-point peak selection algorithm was applied to the relative PSDs in the range of 2-9 Hz, as below

$$N_{f(i)} = \begin{cases} 1, & \begin{array}{l} if\ R_{f(i-2)} < R_{f(i-1)} < R_{f(i)} \\ and\ R_{f(i)} > R_{f(i+1)} > R_{f(i+2)}, \quad i = 4,\ldots,25 \end{array} \\ 0, & otherwise \end{cases} \tag{3.3}$$

where N_f indicates if there exists a peak at the frequency bin f for $f = 1, 1\frac{1}{3}, 1\frac{2}{3}, 2, \ldots, 30$ Hz . For each monthly age point, a histogram of peak frequency distribution was generated by adding the number of peaks at each frequency bin from all motor channels and sessions. To balance the different numbers of sessions at different monthly age points, the peak frequency distribution from each monthly age point was normalized by dividing the corresponding number of sessions at that age point. The total number of peaks within the empirical infant alpha band (6-9 Hz) was also calculated for each monthly age point to evaluate developmental changes of the mu rhythm.

3.2.4 Clustering Analysis for Band Separation

EEG recorded from high-density sensor nets enables the observation of scalp representation of spectral information from each frequency bin in high spatial resolution. Due to the spatial specificity of EEG rhythmic activities from different frequency bands and the empirical separation of three frequency bands below 9 Hz in infant EEG (Saby and Marshall, 2012), clustering analysis was conducted to assign each

frequency bin to one of the three frequency bands, i.e., delta, theta and alpha, based on their spatial patterns to refine the definition of frequency bands in the range of 2-9 Hz.

The k-means clustering method was adopted for the clustering analysis, which assigns observations to different clusters by minimizing point-to-centroid distances, fulfilled by the Matlab function k-means (Arthor and Vassilvitskii, 2007). The process of clustering analysis can be summarized as following. Firstly, three centroids representing spatial patterns of three frequency bands were randomly initiated. Secondly, each frequency bin was assigned to one of the three bands by the minimal Euclidean distance between their vectors of spatial patterns. Thirdly, the three centroids were updated by the mean spatial patterns of frequency bins from each cluster. Lastly, the last two steps were repeated until the minimal sum of total Euclidean distances from all clusters was achieved. The cluster analysis was performed on EEG data averaged from sessions of same weekly age point across all subjects and those averaged from same monthly age point, to evaluate frequency band separation in different temporal resolutions.

3.2.5 Subject Variation from Correlation Analysis

To assess effectiveness of band separation after clustering using data from the group level, a correlation analysis was performed at the individual-subject level. Monthly scalp representations from refined frequency bands based on results of the clustering analysis were firstly generated as templates (9 templates from 3 monthly age and 3 frequency bands). Then, correlations between spatial patterns of data from all sessions and all frequency bins in individual subjects and spatial patterns of the nine

templates were calculated to investigate consistency of these templates from the clustering analysis with data from individual sessions and subjects.

3.3 Experimental Results

3.3.1 Weekly Spectral Changes

Figure 3.5 provides an up-close observation of changes in relative power densities at the motor cortex along weekly age points in the 1/3 Hz resolution. Each curve represents an average spectral density from sessions of the same weekly age point. By comparing spectral powers of individual frequency bins, it shows spectral profiles of EEG follow a power-law decaying pattern, i.e., spectral powers as a reciprocal of frequency (Miller et al., 2009a), as early as 20 weeks of age. It can be observed that spectral changes across different weekly age points mainly take place at the frequency range below 9 Hz, while spectral changes in the higher frequency range in infant EEG are few. Furthermore, in the frequency range of 2-9 Hz, large variations of spectral powers along the weekly age points take place in various sections, which corroborates the development of EEG rhythms in frequency bands during infancy. In general, three frequency bands can be approximately obtained in the frequency range of 2-9 Hz by observing these spectral profiles, that is delta (2-3 Hz), theta (3-6 Hz) and alpha (6-9 Hz) bands.

Among these frequency bands, the delta band presents dominating powers among the three, followed by theta and alpha bands. While both delta and theta band powers do not present consistent changing trend, with magnitudes fluctuating along weekly age points, a clear age-related peak formulation can be observed from 20 weeks

until reaching maximal peak at 31 weeks of age in the alpha band. Furthermore, the peak frequency of the alpha band presents a shifting pattern towards the high frequency range.

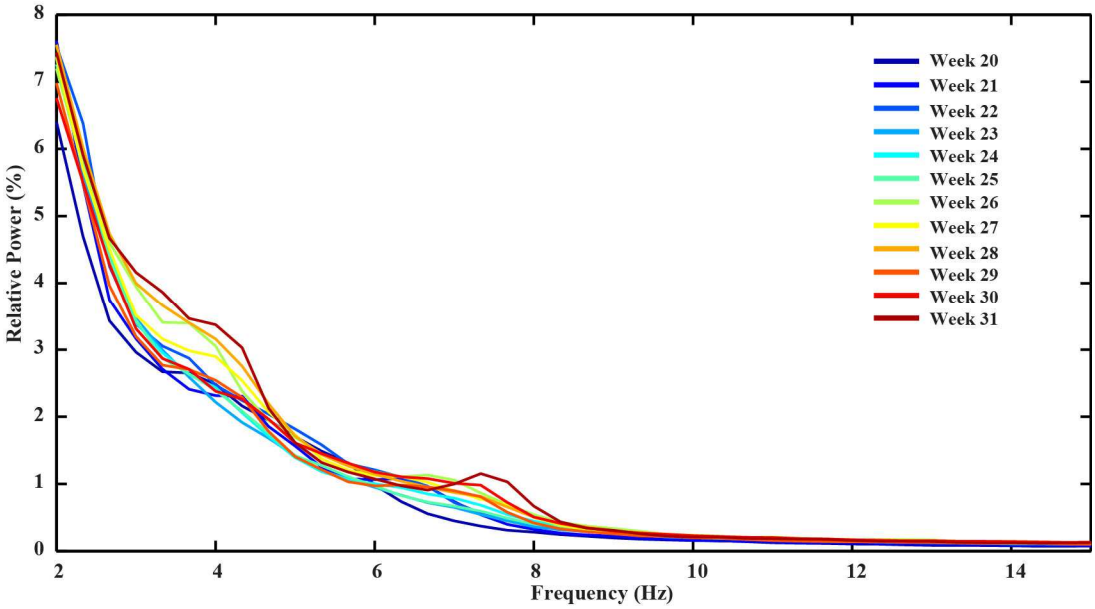

Figure 3.5 Weekly spectral profiles

3.3.2 Peak Frequency of the Mu Rhythm

Besides the age-related changes of spectral profiles, peak frequency distributions at different age points provide another angle to evaluate mu rhythm development. Figure 3.6(a) presents normalized peak distributions along different monthly age points. Three subplots in the figure represent frequency peak distributions between 2 and 9 Hz for 5, 6 and 7 months of age, respectively. For all age points, peak frequencies are mostly located in the range of theta and alpha bands, with few peaks in the delta band. It also shows clear separation between theta and alpha bands for all monthly distributions. When looking the shifting patterns of frequency peaks in the alpha band, it reveals the modal peak frequency of the mu rhythm shifts from about 6.67 Hz at 5 months of age to

7.33 Hz at 7 months of age. When considering the total number of frequency peaks within the alpha band, it demonstrates an increasing pattern from 5 to 7 months of age, as shown in Figure 3.6(b).

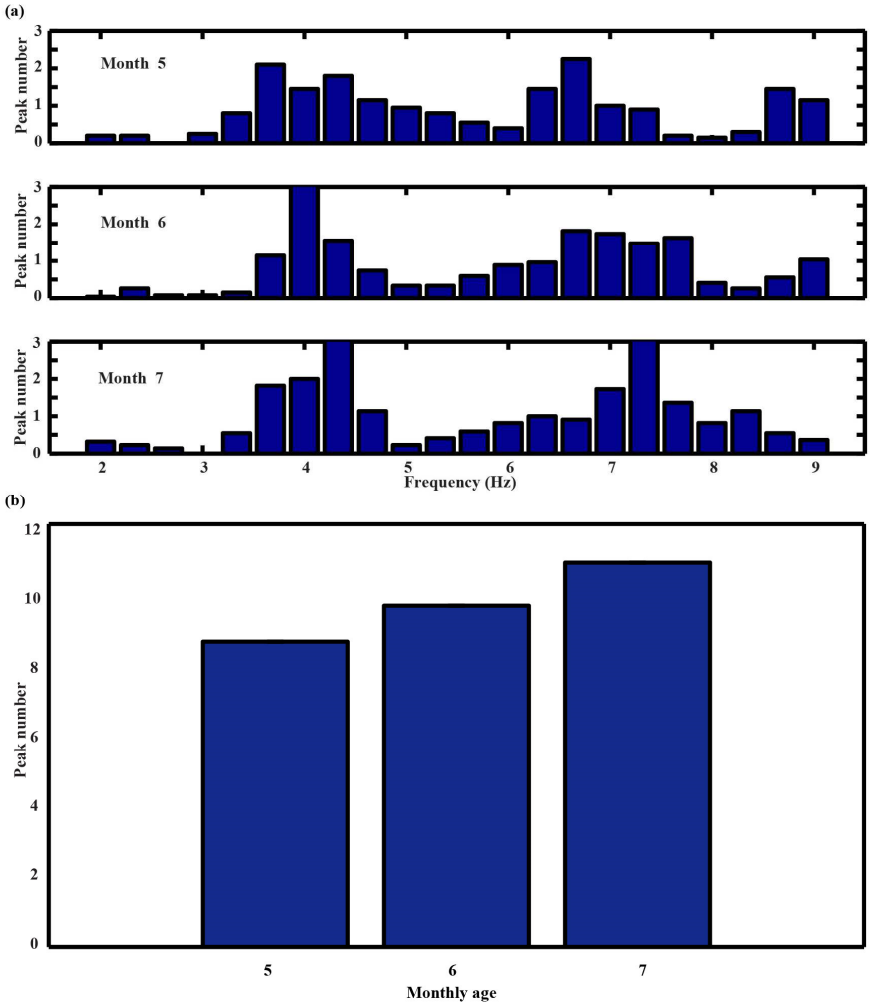

Figure 3.6 Distribution patterns of frequency peaks
(a) Frequency peak distributions for different monthly age points (b) Number of peaks in the alpha band for different monthly age points.

3.3.3 Spectral Topographies of Individual Frequency Bins

Figure 3.7 depicts the spatial patterns of relative PSDs from each frequency bin along weekly age points. Each row in the figure shows spectral topographies of one weekly age point and the columns show spectral topographies of different frequency

bins. It presents distinct spatial patterns among distant frequency bins, while reveals a certain level of similarities in adjacent frequency bins. When comparing spatial patterns of individual frequency bins along weekly age points, smaller variations across different age points can be observed than across different frequency bins, while they are more interesting to observe for the developmental study of the motor cortex. The power-law decaying pattern of EEG spectrum obscures the comparison of spatial patterns of different individual frequency bins, due to the large magnitude differences among different frequency ranges.

The spatial normalization across all EEG channels provides one way to set their scalp representations to the equal footing. Figure 3.8 presents the spatially normalized spectral topographies from different frequency bins along the weekly age points. It reveals distinct scalp distributions at different frequency bins, which can be approximately generalized into three classes. The first class mainly resides in the low frequency range below or around 3 Hz (within the delta band), with large cortical activations focusing on the frontal lobe. From about 3 to 6 Hz, similar to the empirical theta band, spectral topographies present large cortical activations near the posterior sites, which partially extend to the lateral central sites. In the empirical alpha band (6-9 Hz), major activations mostly fall in the central areas covering both lateral and medial motor cortices and part of premotor cortices. Only small variations can be observed when comparing spatial patterns of the same frequency bin across different weekly age points.

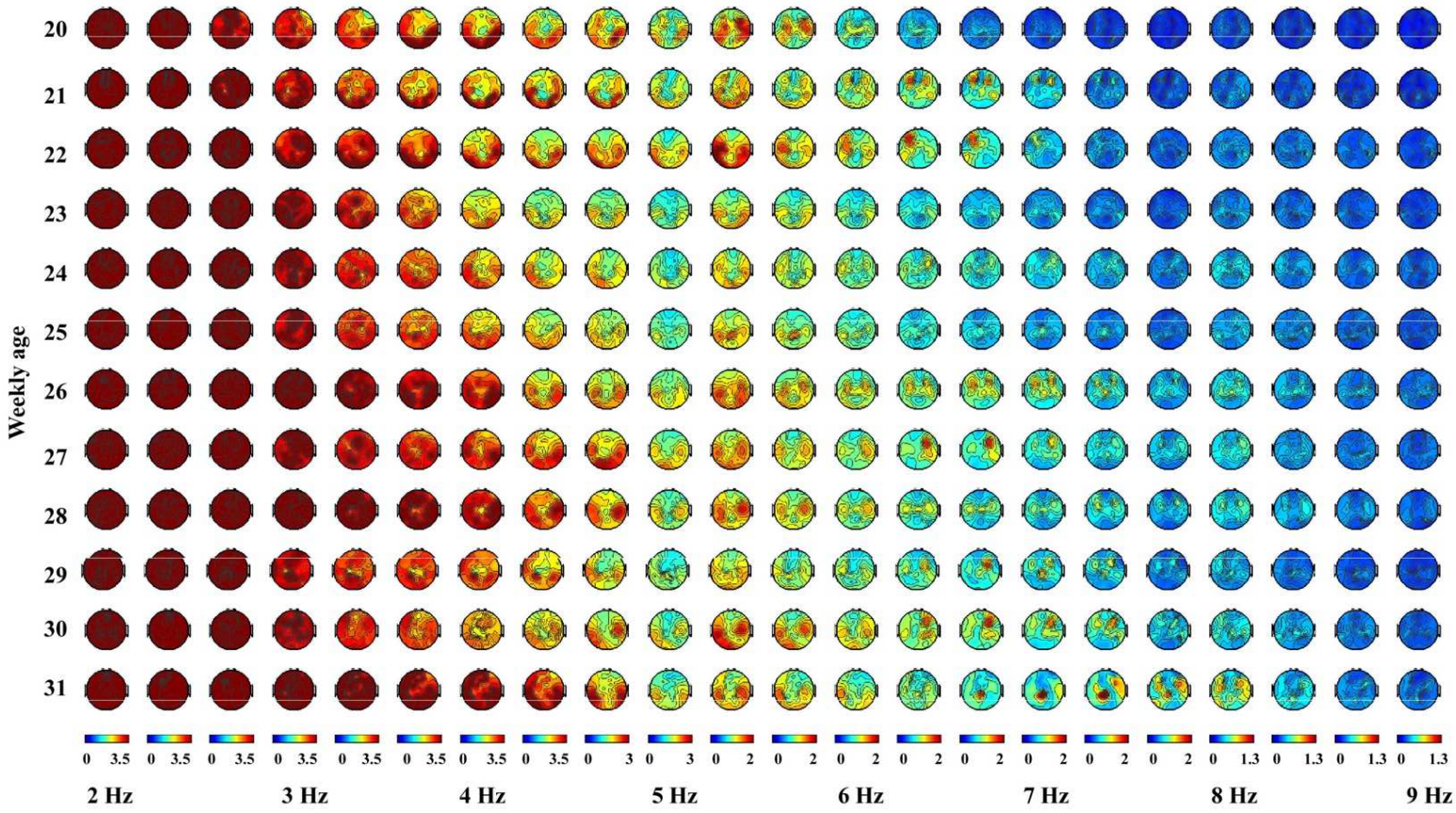

Figure 3.7 Weekly spectral topographies of individual frequency bins

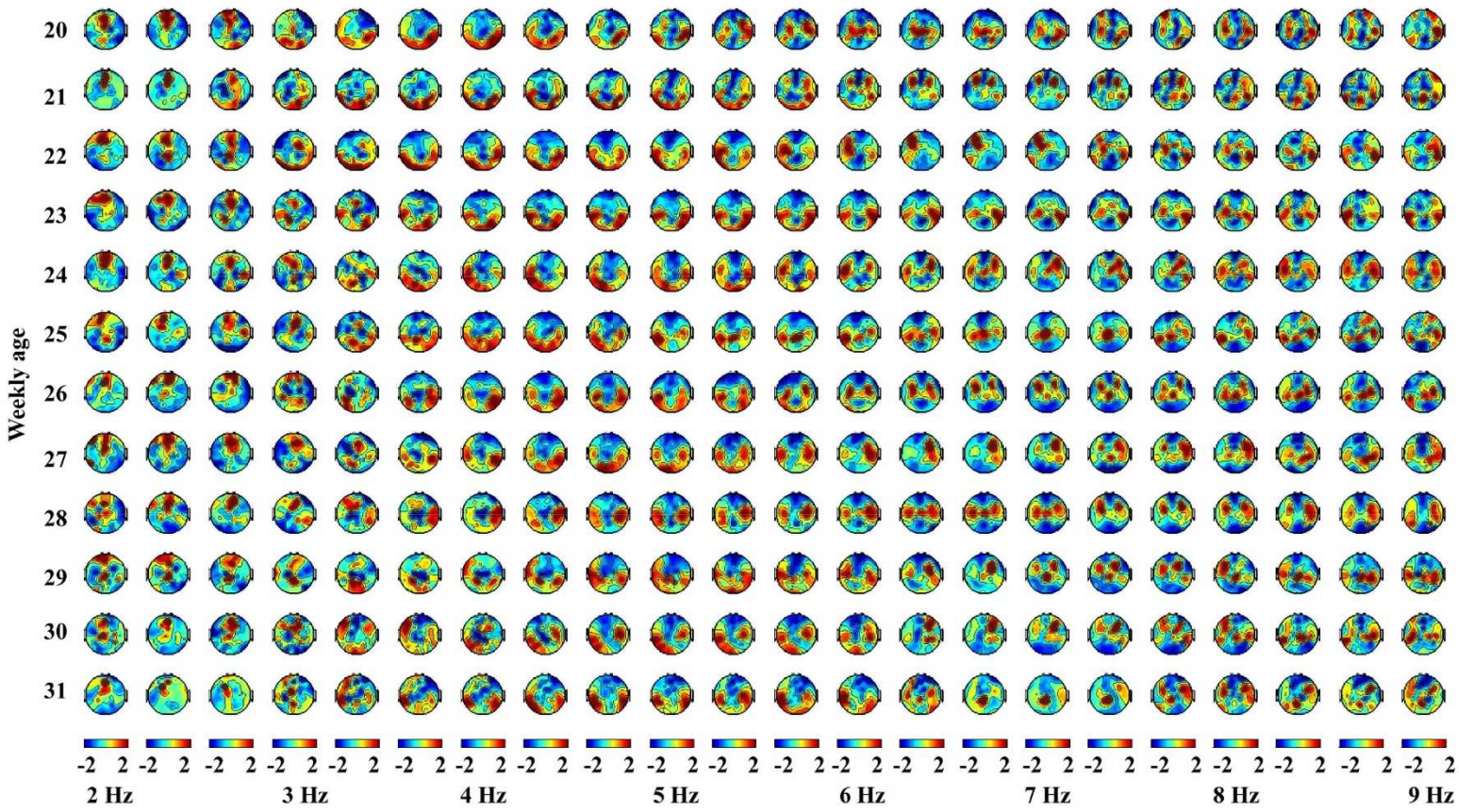

Figure 3.8 Normalized weekly spectral topographies of individual frequency bins

3.3.4 Refinement of Frequency Bands

Weekly spectral profiles and spectral topographies from the individual frequency bins demonstrate the existence of three frequency bands, while their separations are coarsely estimated and can be further refined by the clustering analysis. Figure 3.9(a) presents the clustering results from the weekly resolution. It reveals three clusters mainly gather within three frequency bands, i.e., the delta band (2-3 Hz), the theta band (3-6 Hz) and the alpha band (6-9 Hz), which are mostly in line with previous observations from their spectral and spatial profiles (Figure 3.5 and 3.8), with only a few sessions in the alpha band assigned to other clusters. It further shows the lower boundary of the alpha band shifts toward a high frequency range along weekly age points, although there are some fluctuations during the shifting process.

While weekly evaluation provides detailed information to probe developmental changes of motor brains, it is also impacted by fluctuations due to variations in both EEG data and developmental changes. Figure 3.9(b) presents the clustering results from EEG sessions grouped by different monthly age points, aiming to capture the general developmental trend. Each row represents clustering results from data averaged at the resolution of month, with each column for different frequency bins. It reveals not only self-contained clusters, but also age-related changing patterns of boundaries between different frequency bands. Particularly, the lower boundary of the alpha band is 5.67 Hz at month 5, 6 Hz at month 6 and 6.33 Hz at month 7, demonstrating the pattern of alpha band power shifts towards a higher frequency.

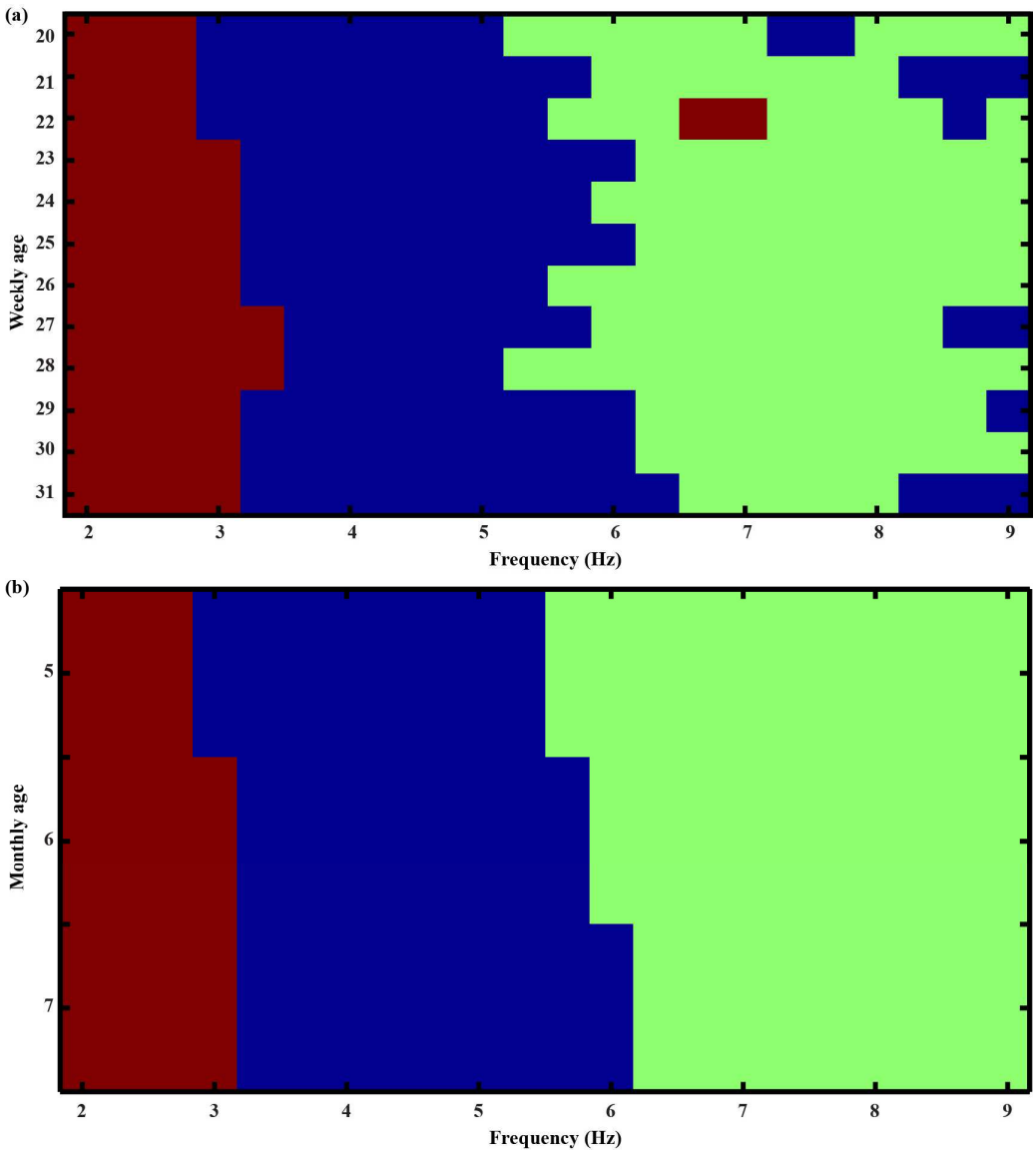

Figure 3.9 Band definitions from clustering analysis

The spatial patterns of different frequency bands along monthly age points are then evaluated based on the refined frequency bands from the clustering analysis on EEG of the monthly resolution, as shown in Figure 3.10. Rows of the figure depict spectral topographies of delta, theta and alpha bands from top down, and columns are for different monthly age points. It demonstrates distinct cortical activations from different frequency bands. Delta activities mainly take place at the medial frontal lobe

and present a slight decreasing pattern along maturation. Theta activities show similar spatial patterns over the cortex along maturation, all located in the posterior regions and the lateral central lobe. Alpha band activities are located in in central cortices for all three monthly age points. Particularly, similar activations for lateral central cortices are observed for three monthly age points, whereas the proportion of alpha band activities at the medial central cortical sites to other brain regions present an increasing pattern along maturation.

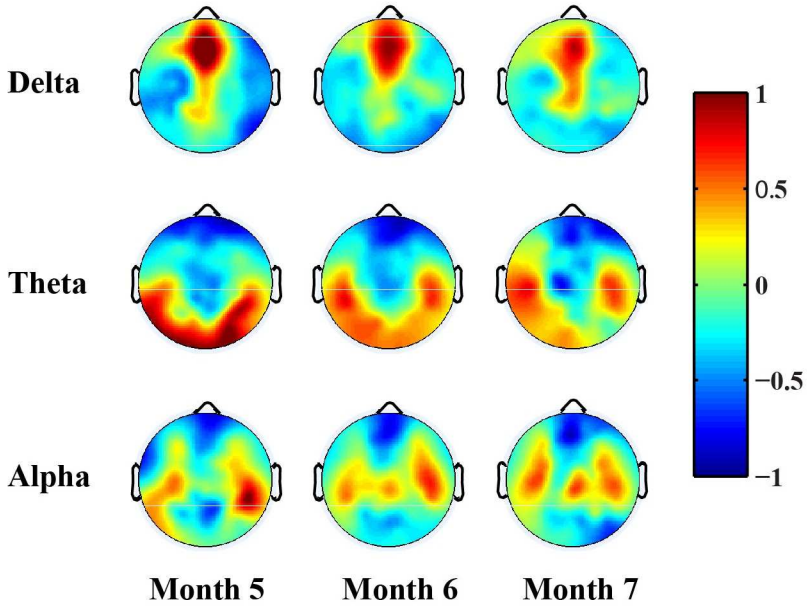

Figure 3.10 Topographies based on refined frequency bands

3.3.5 Results from Individual-Subject Level

Figure 3.11 shows correlations of the spectral topography of each session from all subjects at different frequency bins with the nine topographic templates. For all plots in the figure, rows represent sessions from all subjects in a chronical order, with columns for individual frequency bins. The subplots in the first row of the figure present correlation maps to the delta band topographies of monthly age points.

Frequency bins present large correlations at the range of delta band, and consistent patterns can be observed from sessions of all subjects. The second row of the figure presents correlation maps to the monthly theta band topographies. Similar to delta band, most bins in theta band present large correlations, which are consistent across sessions from different subjects. The same phenomena can be observed for the alpha band, with largest correlations in the range of alpha band and consistency across individual subjects, as shown in the third row of the figure.

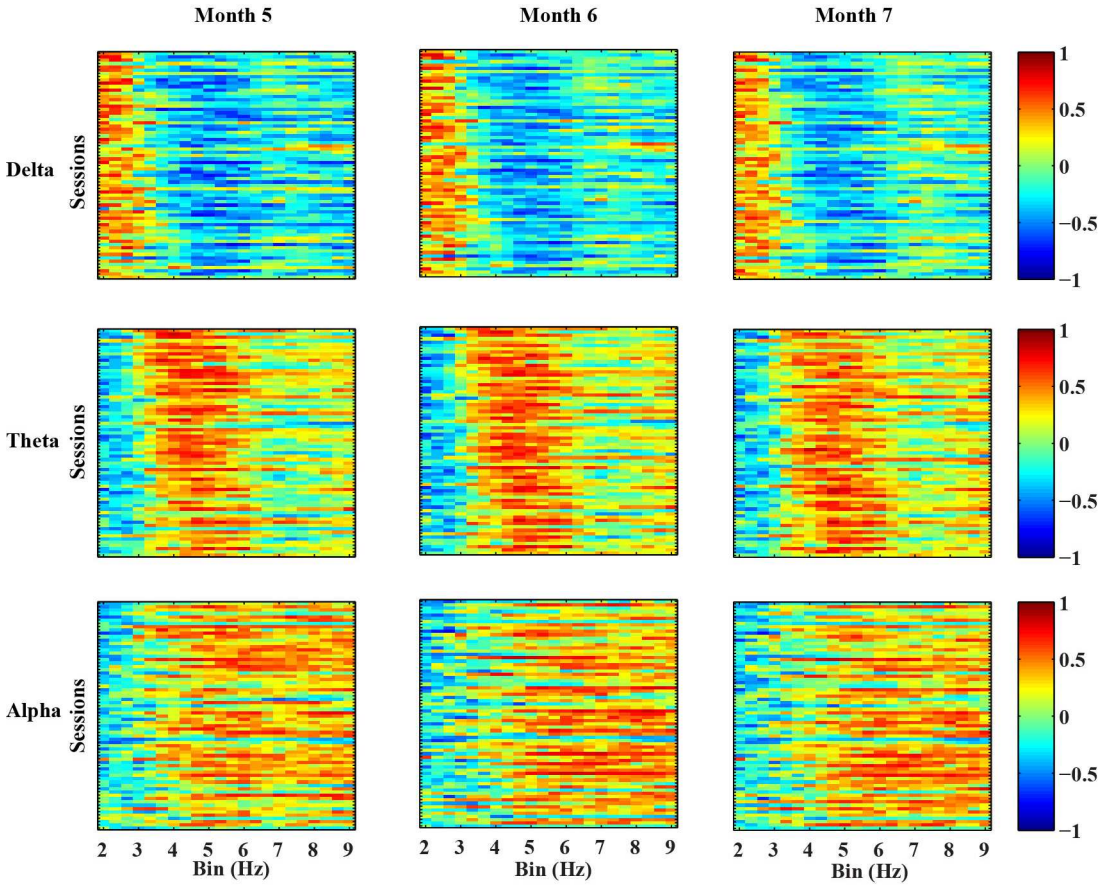

Figure 3.11 Results from correlation test

3.4 Discussion and Summary

3.4.1 Peak Frequencies in Mu Rhythm

Peak frequencies in the alpha band have always been the focal point in infant mu rhythm studies, since they provide a reference for development of the mu rhythm, which in turn shed light on the maturation of human motor brain. However, variations from experimental designs, subject groups and data processing techniques in different studies, result in discrepancies in formulation and shifting patterns of peak frequencies in the mu rhythm. Results of many studies indicate emergence of the mu rhythm peak at certain monthly age, although the time of emergence is still inconclusive. For example, Marshal et al. (2002) reported emergence of the mu rhythm peak at 10 months of age with the peak frequency at 7 or 8 Hz, which moves to 8 Hz at 24 months and 9 Hz at 4 years of age, while no similar peaks are found at 5 months of age. In agreement, Stroganova et al. (1999) reported the identified mu peak frequency increases from about 7 Hz at 8 months to 7.42 Hz at 11 months. Hagne et al. (1973) demonstrated emergence of the mu peak frequency at 6 Hz at 6 months of age, with no similar peaks at 4 months of age, while it is 7 Hz at as early as 4 months of age in Smith (1941). More significantly, one MEG study argues the existence of the mu rhythm peak as early as 11 weeks of age at 2.75 Hz, which is overlapped with activities in theta band and shifting towards the alpha band along chronological age (Berchicci et al., 2011). Such a divergence about peak frequencies of the mu rhythm requires evaluations of more studies to reach conclusion.

The longitudinal weekly EEG recordings in the present study reveal a gradually growing process of a bump shape in spectral profiles in the alpha range, from no-bump

patterns in 20 weeks to a clear bump in 24 weeks, which keeps developing until 31 weeks of age (Figure 3.5). Such a process suggests the emergence of mu rhythm peak takes place around 5 or 6 months of age, and provides insights about its formulation. Number of frequency peaks in the alpha band from 5 to 7 monthly presents fewest counts in 5 months of all three groups, providing collaborative evidence that the formulation of mu rhythm peaks has already started since 5 months of age (Figure 3.6(b)). In term of the pattern of peak shift, both weekly spectral profiles (Figure 3.5) and monthly peak distributions (Figure 3.6(a)) demonstrate the shift of peak frequency towards a higher frequency range from 5 to 7 months of age, which consolidates observations from previous studies with subjects of different age ranges (Marshal et al., 2002; Stroganova et al., 1999). Moreover, results in the present study show that the emergence of peak frequency as presented in the weekly spectral profiles (Figure 3.5) is not accompanied with the transition of peaks from the theta to alpha band (Figure 3.6(a)), favoring the emergence theory of mu rhythm independent of theta band activities, which is different from the previous MEG study (Berchicci et al., 2011).

3.4.2 Band Separation in Infant EEG

While most previous studies evaluate the development of mu rhythm within the frequency range of 6-9 Hz (Marshall et al., 2011, 2013; Saby et al., 2012) or its close variant 6-8 Hz (Paulus et al., 2012; Fox et al., 2001; Davidson and Fox, 1989), the variation of alpha band range along maturation has not been well investigated yet. The high spatial and spectral resolutions of EEG recordings in the present study enables the grouping of 1/3 Hz frequency bins into bands by observing and comparing their spectral topographies from each monthly age through the clustering analysis. The clustering

results show that the alpha band range does change along maturation, with lower boundary shifting from 5.67 Hz at 5 months, 6 Hz at 6 months, to 6.33 Hz at 7 months of age (Figure 3.9(b)). It suggests age-related changes of alpha band range should be taken into account when capturing the developmental change of mu rhythm.

3.4.3 Cortical Activation of the Mu Rhythm

With refined frequency bands and the high-spatial resolution in EEG recordings, spectral topographies for infant delta, theta and alpha bands are revealed for the first time, to the best of my knowledge (Figure 3.10). And the band separations and cortical activations are stable with consistency across sessions of individual subjects (Figure 3.11). Distinct spectral topographies are presented for different frequency bands, suggesting different neural correlates behind these rhythmic activities. The findings also back up the practice of using band power analysis in the study of infant EEG (Saby and Marshall, 2012). Brain regions presenting large alpha activations that mainly fall into central cortices provides collaborative evidence for the association between the mu rhythm and motor brain development reported in early studies (Smith 1941; Hagne et al., 1973). In addition, spectral topographies of the mu rhythm along monthly age points reveal spatial specificity in the changing modalities among different sites in the motor cortices (third row in Figure 3.10), indicating asynchronous development of different cortical regions in motor brains during infancy.

3.4.4 Implication to Early Intervention for CP

CP accounts for one of the most common neuropediatric disorders, which describes a group of disorders in movement and posture development (Rosenbaum et al., 2007). Although CP is non-progressive along age, studies have found early

interventions, such as physical therapy, occupational therapy and recently developed robotic assistance, present positive effect on the motor development (Blauw-Hospers and Hadders-Algra, 2005; Kolobe et al., 2013; Miller et al., 2015). However, little evidence has been provided from the neurodevelopmental domain. Results from the present study enrich the scanty data about the development of the human motor brain at the time exactly before infants develop their first locomotive movement skills, i.e. crawling. This provides a promising biomarker for the assessment of effectiveness of different interventions and could also potentially serve as guidance for improving early interventions to promote motor skills for CP sufferers.

In summary, the longitudinal study about development of the mu rhythm in infant EEG is presented in this chapter. The findings concur with previous studies about the existence of spatially and functionally distinct frequency bands in infant EEG and the association of mu rhythm in the alpha band at central cortices with motor brain development. The added information from high spatial and temporal EEG recordings enables the evaluation of formulation and shifting patterns of frequency peaks, especially spectral topographies of infant mu rhythm in this age range for the first time. All these findings further the understanding about typical development of the human motor brain, which might have great implication to the early diagnosis, intervention and treatment assessment for neurological diseases developed at early ages.

Chapter 4: EEG Resolutions in Movements of Fine Body Parts

While expanding the knowledge of motor development has great implication to early interventions for motor impairments at early stages as discussed in the last chapter, medical conditions, such as neurological diseases, injuries to spinal cords and damaged or missing limbs, have impacts on the already developed human motor system, requiring a different type of intervention. The mu-rhythm based BCI technology is a promising approach, which detects spectral changes in the mu rhythm induced by movements of different body parts as control outputs for external applications. Features from the mu rhythm have demonstrated decoding efficacy for movements of large body parts, such as whole hands and limbs (Wolpaw and McFarland, 2004). But less can be revealed in them about movements of different fine body parts that activate adjacent brain regions, such as individual fingers from one hand. Several studies have reported spatial and temporal couplings of rhythmic activities between alpha and beta frequency bands during movements and motor imageries, suggesting the existence of well-defined spectral structures across multiple frequency bands (Pfurtscheller et al., 1997, Miller et al., 2009b, Canolty et al., 2006). Furthermore, a recent study has presented a type of broadband spectral structures in invasive ECoG contain discriminative information about different finger movements (Miller et al., 2009b). All these studies point to the possible existence of spectral structures in EEG other than the mu rhythm that might contain discriminative information about movements of fine body parts.

In this chapter, studies about decoding movements of fine body parts using EEG are described. For the first time, procedures of spectral principal component analysis

(SPCA) are applied on EEG acquired during individual finger movements, to identify cross-frequency spectral structures in EEG. The newly identified spectral structures were examined in their spatial and cross-condition changing patterns. After that, they were implemented in three decoding tasks, including detection of finger movements from resting, pairwise decoding of individual finger movements and decoding individual finger movements (all five fingers) from one hand, all in comparison to the classic mu rhythm and its harmonic rhythm in the beta band. These new features reveal some similar, but more different spatial and spectral patterns as compared with classic mu/beta rhythms. Decoding results further indicate that these new features (91%) can detect finger movements much better than classic mu/beta rhythms (75.6%). More importantly, these new features reveal discriminative information about movements of different fingers (fine body-part movements), which is not available in classic mu/beta rhythms. The capability in decoding fingers (potentially hand gestures in the future) from EEG will contribute significantly to the development of noninvasive BCIs with intuitive and flexible control. The results in this chapter have been published in the following peer-reviewed journals, detection of finger movements from resting in Frontiers in Neuroscience (Xiao and Ding, 2015); pairwise decoding of finger movements is published in PLOS ONE (Liao^{CO} and Xiao^{CO} et al., 2014); decoding all individual finger movements from one hand in Computational and Mathematical Methods in Medicine (Xiao and Ding, 2013) and Frontiers in Neuroscience (Xiao and Ding, 2015).

4.1 Experimental Design

4.1.1 Subject Information and Experimental Protocol

Eleven healthy and right-handed subjects (1 female and 10 males, mean age: 26.4 years old, range: 22–32 years old) participated in the studies. All of them provided written informed consents prior to taking up the experiments. The studies were approved by the Institutional Review Board of the University of Oklahoma. None of these subjects had prior training on the experimental procedures in present studies. Due to poor data quality, data from one subject were excluded from further analysis.

EEG experiments were carried out in a dim-lighted and electrically shielded chamber room to reduce environmental noises. Subjects were seated in a comfortable armchair, with their arms supported in a supine position. During the experiments, subjects either rested or performed repetitive movements of individual fingers from one hand according to visually presented cues. The stimuli were presented using the E-Prime software (Psychology Software Tools, Inc., Pittsburgh, PA, USA).

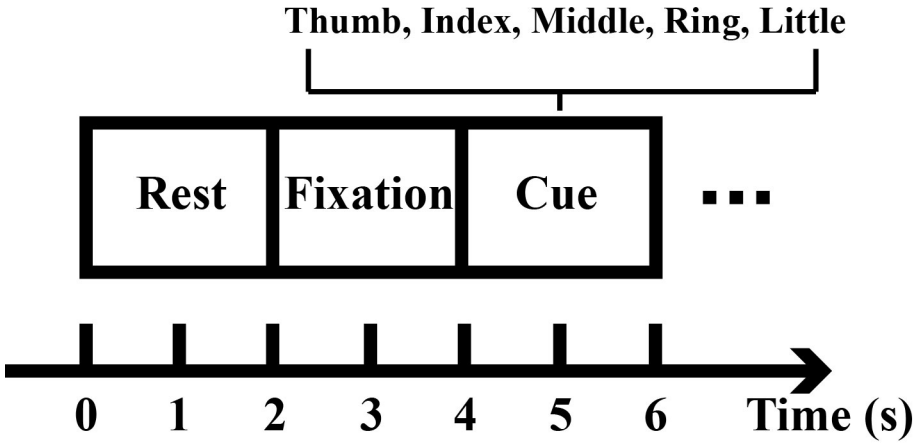

Figure 4.1 Experimental trial design
Events in each trial: a two-second blank window, a two-second fixation, and a two-second cue for finger movements.

The design of experimental trials was illustrated in Figure 4.1. At the beginning of each trial, a two-second blank window on the computer screen allowed subjects to prepare for the upcoming trial. Subjects were instructed to relax, blink, or swallow only during this period. A fixation cross was then presented for another two seconds as a resting condition, during which subjects were required to look at the fixation cross without any physical movements. After that, one of five words (i.e., thumb, index, middle, ring, little) as a cue was displayed for two seconds, which instructed subjects to continuously perform full flexion and extension of the cued finger (usually twice in one trial). There were 80 trials for each finger in most subjects, resulting in total 400 trials for all five fingers, except one subject who reported difficulties in finishing all trials, ending up with 60 trials for each finger.

4.1.2 Data Acquisition

During experiments, EEG signals were recorded from a 128-electrode EEG system (Geodesic EEG System 300, Electrical Geodesic Inc., OR, USA), sampled at either 250 Hz (in the first 6 subjects) or 1000 Hz (in the remaining 5 subjects) and referenced to a non-data channel at the vertex.

At the same time, movements of individual fingers generated potential differences, which were measured by five bipolar electrodes placed on both sides of each finger at the same sampling rate as in EEG (Figure 4.2). Real-time videos on the moving hands were recorded, for the purpose of removing trials from further analysis when subjects moved wrong fingers.

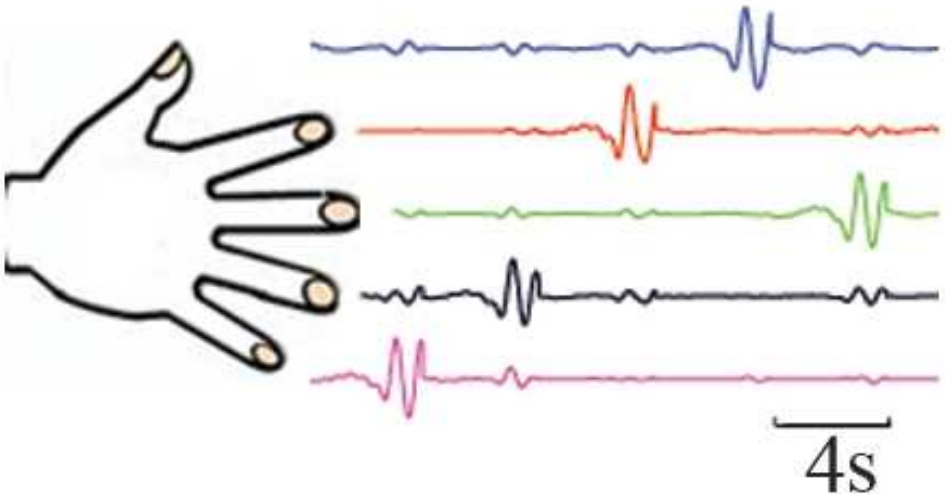

Figure 4.2 Potential differences generated by finger movements

To evaluate extracted features from EEG as compared to spectral structures in ECoG, ECoG data from the BCI Competition IV (Schalk et al., 2007) were analyzed following the same approaches in EEG analysis. The data were recorded from three epileptic patients using implanted 62-, 48- and 64-electrode grids, respectively, when they performed similar individual finger movements as in the present EEG studies. Briefly, subjects were cued to move one of five fingers from the hand contralateral to implanted grids, with each cue lasting two seconds and followed by a two-second resting period. The visual cues were presented using BCI2000 (Schalk et al., 2004). During each cue, subjects typically moved the corresponding finger 3 to 5 times. ECoG signals were recorded for 10 minutes, digitized at 1000 Hz, and bandpass filtered (0.15–200 Hz). Kinematic data during finger movements were simultaneously recorded using a data glove (Fifth Dimension Technologies, Irvine, CA).

4.2 Data Preparation

4.2.1 Preprocessing

Datasets recorded at the sampling rate of 1000 Hz were firstly downsampled to 250 Hz to be consistent with other datasets. The first two-second EEG data in each six-second trial were removed from further analysis, since the period was designed for subjects to engage unavoidable movements, such as blink or swallowing. The remaining data were then high-pass filtered at 0.3 Hz using an elliptic infinite impulse response (IIR) filter from the EEGLAB toolbox (Delorme and Makeig, 2004) with both forward and reverse filtering to minimize phase distortions. A 60 Hz notch filter with a transition band of 0.3 Hz was further applied to remove power-line noise. To remove common physiological artifacts, independent component analysis (ICA) (Hyvärinen and Oja, 2000) from the EEGLAB toolbox was performed, implemented with the Infomax algorithm (Bell and Sejnowski, 1995). EEG artifacts, such as generic discontinuities, electrooculogram (EOG), electrocardiogram (ECG), and electromyogram (EMG), were then identified and rejected using the ADJUST toolbox (Mognon et al., 2011) and visual inspections. Total 64 independent components (ICs) were reconstructed and about 10 to 20 artifact-related ICs were rejected in each subject.

For ECoG data, the 60 Hz power line noise and its harmonic components were removed using a notch filter with 0.8 Hz transition band (elliptic IIR filter from EEGLAB). Channels that contain unusually large values (greater than 10^5 μV) were rejected as bad channels, resulting 61, 46 and 63 channels of ECoG data for each subject, respectively.

Both EEG and ECoG data were re-referenced using a common average

reference (CAR) spatial filter before further analysis, which could enhance SNR (McFarland et al., 1997):

$$X_n(t) = X_n^o(t) - \frac{1}{N}\sum_{i=1}^{N} X_i^o(t) \qquad n = 1, 2, \cdots, N \tag{4.1}$$

where $X_n^0(\mathrm{t})$ and $X_n(\mathrm{t})$ are EEG or ECoG signals on channel *n* and at time *t* before and after CAR, and *N* is the total number of channels. It was calculated by subtracting EEG potential $X_n^0(\mathrm{t})$ at channel *n* and sample point *t* to the average potential of total *N* channels at that sample point.

4.2.2 Extraction of Movement EEG

Since subjects usually performed finger movements twice in each movement segment, i.e., two seconds, the potential differences from each pair of bipolar electrodes were band-pass filtered ranging from 0.5 to 2 Hz to capture major kinematic information of 1 Hz. It was observed that movement peaks happened when a finger was fully flexed, and those peaks were identified using the following criteria. Firstly, the amplitudes at the prospective peaks were at least 200 microvolt (μV). Secondly, these movement peaks occurred 400 milliseconds (ms) after stimulus onsets, since the reaction time from visual stimulus to movement onset was about 180 ms (Welford, 1980) and the time reaching the peak from movement onset was usually longer than 200 ms. Thirdly, movement peaks in the last 500 ms of each trial were not used because their corresponding EEG data might be contaminated by the following trial. Lastly, movement peaks were at least 200 ms apart from each other and, if there were multiple peaks within 400 ms time window, the peak with the maximal strength was selected. Trials in which subjects made wrong movements were removed. Numbers of detected

finger movements and their distributions among individual fingers were listed in Table 4.1.

Table 4.1 Summary of trial information from all subjects

	Trials	Movements	Thumb	Index	Middle	Ring	Little
Subject 1	400	409	93	79	80	78	79
Subject 2	400	485	87	97	117	97	87
Subject 3	300	380	74	59	84	81	82
Subject 4	400	435	83	77	86	80	109
Subject 5	400	396	68	105	88	71	64
Subject 6	400	396	80	79	80	79	78
Subject 7	400	394	79	77	80	79	79
Subject 8	400	394	80	80	79	75	80
Subject 9	400	395	80	80	75	80	80
Subject 10	400	394	80	79	80	75	80
Average	390	407.8	80.4	81.2	84.9	79.5	81.8

Then, EEG data centered at corresponding finger movement peaks in all trials were extracted with the length of one second and categorized into different fingers. In accordance with data for movements, their corresponding resting data were also selected as one-second segments, which were located in the middle of fixation, i.e., 2.5 -

3.5s of each 6-second epoch. Movement data and resting data, together with the corresponding labels that indicate the fingers moved, were then combined for later processing. For ECoG data, the similar procedure for the detection of finger movements was performed. Position data from the data glove was in the range of [-5, 10] (with arbitrary unit). Finger movement peaks were identified using two criteria: above the threshold of 2 and peaks at least 200 ms apart and the one with maximal strength selected if there are multiple peaks within 400 ms. ECoG data within one-second window corresponding to each movement peak were then extracted as movement trials.

4.3 Spectral Analysis

4.3.1 Spectral Features from the Mu Rhythm

To extract spectral features from the mu rhythm, the power spectral densities (PSDs) of data on each channel were calculated. Data from a short-time window T centered at movement peaks and resting conditions were used, where refers to time windows for different fingers, and refers to time windows of corresponding resting conditions of different fingers. PSDs were then calculated using a windowed Fourier transform (Miller et al., 2009b):

$$P_n(f,\tau_q)=\frac{1}{T}\left|\sum_{t=-\frac{T}{2}}^{\frac{T}{2}-1} X_n(\tau_q+t)\cdot H(t)\cdot\exp\left(i\frac{2\pi}{T}(f-1)t\right)\right|^2 \quad f=1,2,\cdots,N_f \quad \tau_q=1,2,\cdots,N_q \quad (4.2)$$

where $P_n(f,\tau_q)$ is the PSD at frequency f and time τ_q on channel n, N_q is the number of movements (including corresponding resting conditions). The Hanning window $H(t)=\left(1+\cos\left(2\pi t/T\right)\right)/2$ was used with the window length T of one second. The upper-

bound frequency N_f was 70 or 125 Hz in EEG data and 200 Hz in ECoG data, depending on the different studies.

Since adult mu rhythm reflects EEG oscillations in the alpha band and it elicits harmonic activities in beta band (Pfurscheller and Lopes da Silva, 1999), the spectral powers at both 8-12 Hz (i.e., alpha band) and 13-30 Hz (i.e., beta band) were selected as movement-related features to evaluate their efficacies in the three decoding tasks involving individual finger movements.

4.3.2 Spectral Principal Component Analysis

To further reveal movement-related changes in EEG, the principal component analysis (PCA) (Glaser and Ruchkin, 1976) was applied to PSD data from both movement trials and resting trials in order to identify movement-related spectral structures. Depending on decoding tasks, combinations of data from different conditions were chosen to reveal spectral structures associated with the specific tasks. For detection of finger movements and decoding individual finger movements from one hand, all finger movement conditions and their corresponding resting conditions were grouped together for the following calculations. For pairwise decoding of finger movements, since there were ten pairs of combinations from five finger, PSD data from each pair of conditions (i.e., fingers) to be compared and their corresponding resting data were grouped for the PCA analysis using the following procedures.

Grouped PSD data were firstly element-wise normalized to the ensemble average spectrum at each frequency and then the logarithm was taken:

$$\tilde{P}_n\left(f,\tau_q\right)=\ln\left(P_n\left(f,\tau_q\right)\right)-\ln\left(\frac{1}{N_q}\cdot\sum_{p=1}^{N_q}P_n\left(f,\tau_p\right)\right) \tag{4.3}$$

where $\tilde{P}_n\left(f,\tau_q\right)$ is the log-normalized PSD at frequency f and time τ_q on channel n. The purpose of normalization was to evaluate increased or decreased changes in specific spectral structures that would be identified with PCA as discussed below. And the logarithm operation was to treat increased changes (ranging from zero to infinity after logarithm) and decreased changes (ranging from negative infinity to zero after logarithm) equally (Miller et al., 2009b).

The PCA method (Glaser and Runchkin, 1976) was then applied to seek the most representative spectral structures in PSD data $\tilde{P}_n\left(f,\tau_q\right)$, which calculates the eigenvalues λ and eigenvectors v of the covariance matrix $C\left(f,\tilde{f}\right)$ of $\tilde{P}_n\left(f,\tau_q\right)$ among different frequencies

$$C\left(f,f'\right)=\sum_{\tau_q}\tilde{P}_n(f,\tau_q)\cdot\tilde{P}_n(f',\tau_q) \qquad f,f'=1,2,\cdots,N_f \tag{4.4}$$

where f and f' are frequencies and τ_q are task conditions from different decoding tasks. The covariance matrix reveals the correlation between power spectra of every two frequency bins. Its eigenvectors v_k $\left(k=1,2,\cdots,N_f\right)$ (principal component, PC) define a set of spectral structures in PSD data and their contributions to the variance of PSD data are reflected in corresponding eigenvalues λ_k. The PCs are rearranged according to eigenvalues in a descending order, which forms a set of orthogonal basis in the frequency domain denoted as $V(f,k)=(v_1,v_2,\cdots,v_{N_f})$. The projection of PSD data from each trial onto the new basis $V(f,k)$ can then be calculated as

$$W_n(k,\tau_q)=V^T(f,k)\cdot\tilde{P}_n(f,\tau_q) \qquad k=1,2,\cdots,N_f \tag{4.5}$$

where $W_n(k, \tau_q)$ are the weights of PSD on n^{th} channel from movement (and resting) data of τ_q projected onto the k^{th} PC. Projection weights were grouped according to conditions (resting data were also separated according to finger moved after it) and compared to illustrate difference of movement-related changes in spectral structures from different finger movements.

4.4 Procedures for Evaluation and Classification

4.4.1 Evaluation of Spectral Features

The evaluation of new spectral structures in EEG consisted of two parts: qualitative inspection of their characteristic spectral profiles and spatial patterns, and quantitative assessment of their efficacies in the three decoding tasks, i.e., detection of finger movements from resting, pairwise decoding fingers movements and decoding individual finger movements from one hand. These evaluations were performed in comparison to classic mu/beta rhythms, and detailed below.

Firstly, spectral profiles of different features were observed and compared. Then, topographies of spectral features associated with the first three PCs (accounted for most data variance) were compared with topographies of mu/beta rhythms via visual inspections in conditions of resting and movements of different fingers. The topographies of mu/beta rhythms were obtained by mapping averaged spectral powers within each frequency band on the scalp.

Secondly, cross-condition changes (i.e. resting vs. movement and movements of different fingers) in spatial patterns of mu, beta, and three new spectral features were quantitatively evaluated by calculating coefficient of determination (r^2 values):

$$r = \frac{\sqrt{n_1 \cdot n_2}}{n_1 + n_2} \cdot \frac{mean(w_1) - mean(w_2)}{std(w_1 \bigcup w_2)}, \quad r^2 = r \cdot r \tag{4.6}$$

where n_1 and n_2 are numbers of segments for two conditions to be compared. w_1 and w_2 are the feature vectors of each condition, which are data defining spatial patterns of features. They are projection weights on spectral PCs at channels for the three new spectral features, and PSDs in the alpha and beta bands at channels for the mu/beta spectral features. The $std(w_1 \bigcup w_2)$ calculates the standard deviation of data pooled together from two conditions. The calculation of r^2 values was performed between two conditions of same features at channels and, therefore, topographies of differences for different features and conditions were generated.

Lastly, two types of spectral features (i.e., projection weights on the first three PCs and alpha/beta band powers) were evaluated in three decoding tasks involving individual finger movements. In the first task, movements of five fingers were grouped as the movement condition to be decoded from the resting condition. The second and third tasks were to decode each pair of fingers and all five fingers from one hand, respectively. Furthermore, to study the independence and redundancy of information in different features in detecting movements and decoding different finger movements, various combinations of spectral features (e.g. three PCs; alpha+beta; and alpha+beta+three PCs) were also investigated.

4.4.2 Classification Procedures

Classification procedures for evaluation of spectral features through the three decoding tasks discussed above are described here. Since most EEG features exhibited localized spatial patterns (e.g. mu/beta rhythms over the motor cortex), spectral features

from subsets of all EEG channels were used as input features to classifiers to avoid negative impacts from irrelevant channels. For the classic mu/beta rhythms features, channel C3 (a representative channel at left motor cortex) and its neighbouring channels were chosen as feature channels (for right hand movements). For features from the PCs, channels were selected based on r^2 values between two compared conditions. In general, channels were ranked by their corresponding r^2 values, and then the first 10 channels were chosen as feature channels. If more than two conditions to be compared, i.e. five fingers, the union of selected channels for all finger pairs was used. For cases using combined features, the union of selected channels for each feature was used.

The linear support vector machine (SVM) (Vapnik, 1998, 1999) with radial basis function (RBF), implemented in a MATLAB package, i.e. LIBSVM (Chang and Lin, 2011), was chosen for classification. Briefly, the method maps input feature data into a high dimensional space and seeks an optimal separating hyper plane that has maximal margins between the two classes of data samples. The penalty parameter and gamma value in RBF kernel were determined by a grid-search approach (Hsu et al., 2010). The decoding features (projection weights on PCs, and mu/beta PSDs) were linearly scaled into the range [-1, +1] to avoid numeric range dominance of one feature over others. A binary SVM classifier was applied in detecting movements from resting and pairwise decoding of finger movements, and the one-versus-one scheme followed by a majority voting was used to solve the multiclass classification problem (Hsu and Lin, 2002) in decoding five fingers.

4.4.3 Assessment of Decoding Performance

Decoding accuracy (DA) was defined as the number of correctly classified movements divided by the total number of movements (Han et al., 2012). To get an unbiased estimation of decoding accuracy, trials of individual movements were randomly permuted before going through the five-fold cross validation. The five-fold cross validation procedure separated the data into two parts, i.e. 80% data for training and 20% data for testing, and each subset was used for testing once. Different features selected for the classification analysis were obtained from the training data only, which made sure that no data in the testing set were involved in building classifiers. The whole process was repeated multiple times (20 times for pairwise finger decoding; 30 times for other tasks), based on which the mean and variance of decoding accuracies were calculated.

The significance of achieved classification accuracy was also compared with respect to guessing level (50% for two-class problem; 20% for five-class problem). One-sample Student's t-test was performed to evaluate whether decoding accuracy was significantly higher than the guessing level of the decoding task. And paired Student's t-test was performed to compare decoding accuracies from different spectral features. As a further exploration, the empirical guessing level p for pairwise decoding of finger movements was calculated using a permutation test. During the test, the class labels were randomly permuted 500 times and the same classification procedure was performed on obtained dataset in each permutation as on the original dataset. The decoding accuracies from all permutations were then averaged to obtain the empirical guessing level and Student t-test was used to test the significance between comparisons.

In a two-class classification problem, the probability (p) and its associated confidence intervals were given as (Muller-Putz et al., 2008)

$$p \pm \sqrt{\frac{p \cdot (1-p)}{m+4}} \cdot Z_{1-\frac{\alpha}{2}} \tag{4.7}$$

where m is the number of total movements from two conditions compared, $Z_{1-\frac{\alpha}{2}}$ is the $1-\frac{\alpha}{2}$ quantile of standard normal distribution, and α is the significance level, such as 0.05. The decoding performance of a classifier is considered to be statistically significant from the guessing level if it is beyond the confidence intervals of empirical guessing level with a significance level α.

4.5 Feature Evaluation Results

4.5.1 Profiles of Mu/Beta Rhythms

Figure 4.3 presents the spectral profiles of mu/beta rhythms. Since all subjects moved fingers from the right hand, which elicited power changes at the left motor cortex, i.e., the contralateral side of brain (McFarland et al., 2000), spectral powers averaged over all segments belonging to one condition from a representative channel C3 on the left motor cortex were chosen to display. The selected channel was marked by the red dot on the scalp map. It shows that all finger movements elicit power decreases in both alpha band (enclosed by 1st and 2nd vertical lines) and beta band (enclosed by 2nd and 3rd vertical lines) compared to the resting (denoted by the cyan curve), while spectral powers in the alpha band present much larger decrease. However, no major differences in spectral powers among different finger movement conditions can be readily identified in both frequency bands. These observations suggest features of

spectral powers from individual frequency bands may detect finger movements from resting, but may not suffice discrimination of different movements of fine body parts, i.e., individual finger movements.

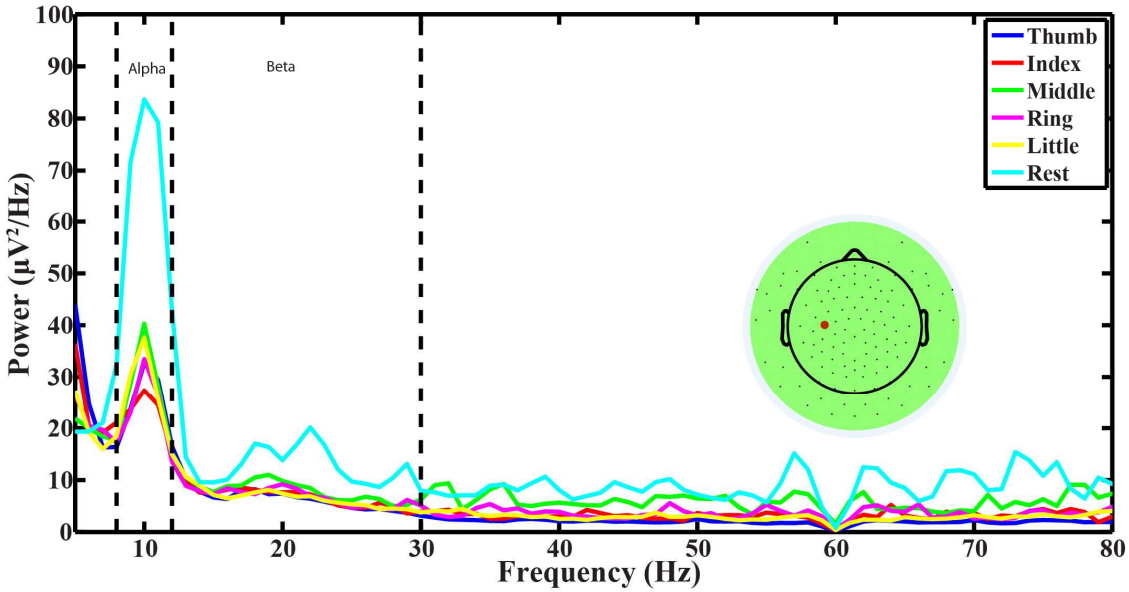

Figure 4.3 Profiles of Mu/Beta rhythms

4.5.2 Profiles of Spectral Structures from PCA

Figure 4.4 illustrates the first and second PCs of EEG and ECoG data from all finger pairs (i.e., ten) in all subjects (i.e., 10 for EEG and 3 for ECoG) along frequency domain. Figure 4.4(a) shows that, for EEG, the first PCs are of non-zero value (around 0.1) over the whole frequency band (up to 125 Hz), which is consistent over all comparisons of different finger movements, over distributed EEG channels and over all subjects. Moreover, these first PCs are of the same signs and closer to each other than they are to zero. The second PCs indicate peaks within the alpha band (8-12 Hz) and beta band (around 20-25 Hz) while the high frequency component (> 40 Hz) is near zero. These phenomena are similar to the results obtained from ECoG data (Figure

4.4(b)), in which the first PCs have the same positively signed magnitudes (around 0.07) over the whole frequency band (up to 200 Hz) over all comparisons of finger pairs and all subjects and the second PCs have elevated deflections away from zero within alpha/beta frequency bands as well. However, it is worth to note that the first PCs in EEG present a slightly increasing pattern in the low frequency range as compared to the ones in ECoG.

As discussed in the ECoG study (Miller et al., 2009b), the first PC with non-zero magnitudes captures the broadband frequency change during finger movements, while the second PC reflects the power-decreasing rhythms in low frequency bands, consistent with event-related desynchronization (ERD) due to movements (Pfurtscheller and Aranibar, 1977). These results indicate that movement-related spectral structures reported in previous ECoG studies (Miller et al., 2009b) are also available and can be identified in EEG data.

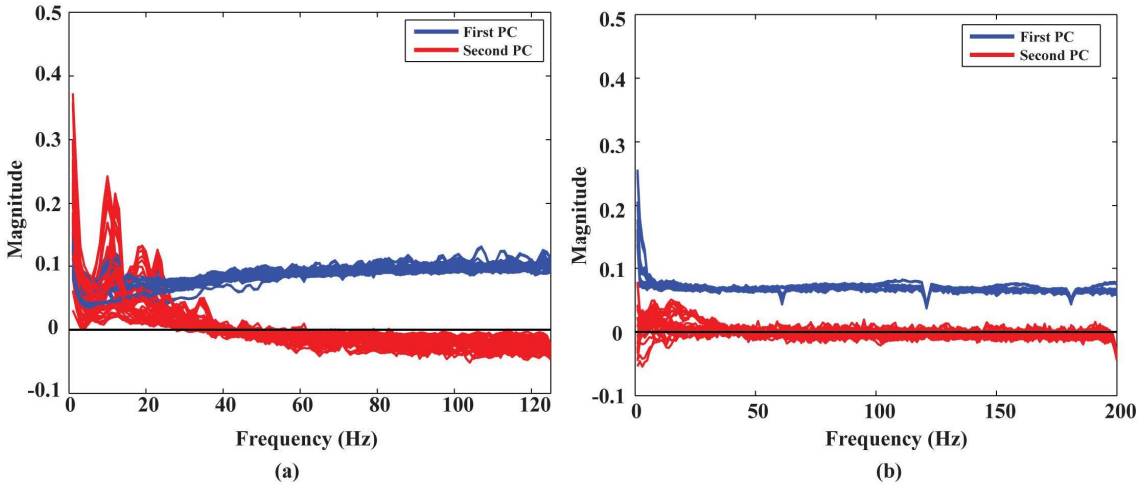

Figure 4.4 Spectral PCs in EEG and ECoG from ten pairs of fingers
Each curve is the averaged 1st or 2nd principal components across channels in motor cortex, from each pair of fingers and subject. (a) EEG data (1 - 125 Hz). (b) ECoG data (1 - 200 Hz).

Figure 4.5 depicts the profiles of first three PCs from EEG data of movements

from all fingers, with each curve representing spectral structure derived from one subject in all plots. It's noted the profiles of first two PCs are in line with those from finger pairs in Figure 4.4(a). All curves in each PC present similar patterns, suggesting the consistency of these spectral structures across subjects, while different PCs show distinct profiles along the whole frequency range. The 1st PC (blue curves) is generally flat with positive elevations across the whole frequency range, which reveals a broadband phenomenon. The 2nd PC (red curves) presents spectral peaks at both alpha and beta bands while exhibits values close to zero for other frequency bands. The 3rd PC (green curves) presents main peaks at the alpha band.

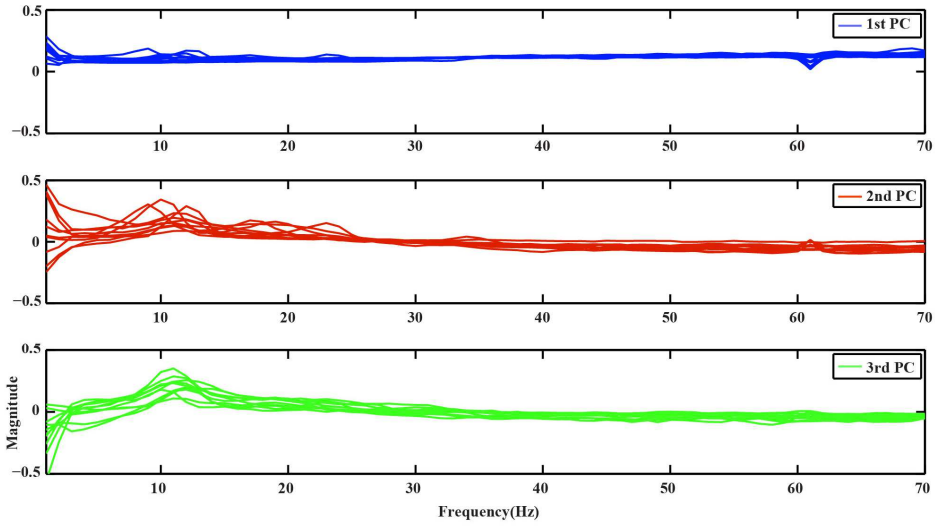

Figure 4.5 Spectral PCs in EEG of movements from all fingers.
Blue, Red, and Green curves represent profiles of the 1st, 2nd and 3rd PCs, respectively.

4.5.3 Spatial Patterns of Different Features

Distinct spatial patterns are observed in the distributions of projection weights on PCs, as shown in Figure 4.6(a). The first row shows the averaged topographies of projection weights over all subjects on the 1st PC from different fingers. Bilateral

clusters of large projection weights (e.g. around -10) are observed over the primary motor (M1) and premotor cortices, which extend more toward anterior areas of the brain. And smaller projection weights (e.g. around -4) form an outstanding cluster in the posterior parietal area. These brain areas, especially the parietal area, also indicate differences when comparing projection weights from movements and resting. Major clusters of projection weights on the 2nd PC are mainly over the central area (the second row in Figure 4.6(a)), including M1 and supplementary motor area (SMA), which also show significant difference between finger movements and resting (with sign changes).

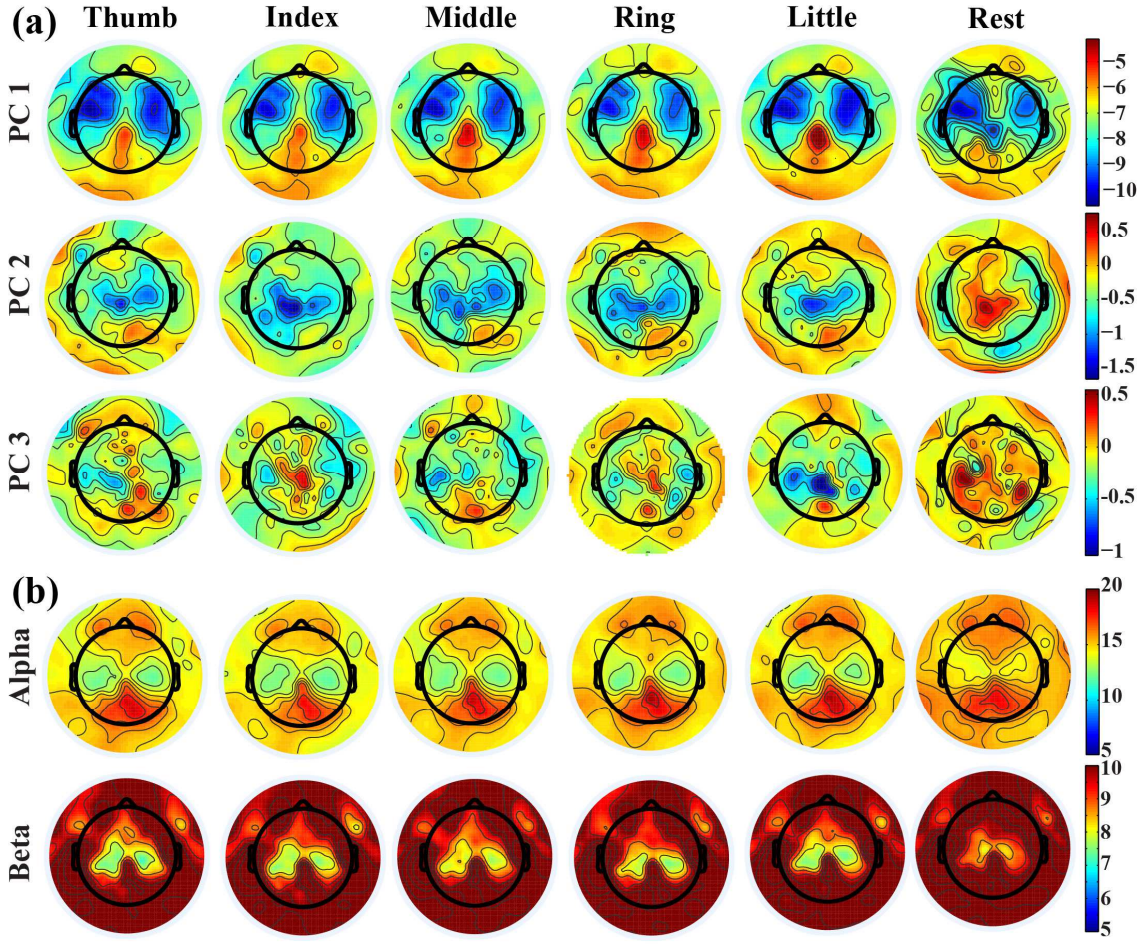

Figure 4.6 Topographies of different types of features
(a) Topographies of projection weights on different PCs for conditions of different finger movements and resting. (b) Topographies of PSDs in alpha and beta bands

Unlike the first two PCs, the 3rd PC indicates scattered patterns in distributions of projection weights, while some relatively weak patterns can still be observed over the central and parietal areas when movement conditions are compared with resting.

Alpha/beta band powers (Figure 4.6(b)) show decreasing patterns during movements as compared with resting over bilateral M1, which is consistent with previous studies (Pfurscheller, 1989, Magnani et al., 1998, Szurhaj et al., 2001) and similar to bilateral patterns over M1 in both the 1st and 2nd PCs. Mu/beta powers (especially mu power) also indicate a clustered pattern over the central parietal area, similar to what is observed in the 1st PC, while its changes between movements and resting are not as large as in the 1st PC (see Figure 4.5 also). It is noted that, while some similarities are observed between the PCs and mu/beta powers, many differences are also suggested when whole patterns of individual features are compared one to another.

Figure 4.7 shows exemplary scalp maps of r^2 values, which provide quantitative metrics for cross-condition differences in individual features. Broader differences over M1, SMA, premotor, and parietal areas from three PCs are observed in the comparison between movements and resting, while more focused differences over SMA, parietal, and some left M1 areas are shown in the comparison of different finger movements. It is observed that some areas that indicate large projection weights (e.g. bilateral premotor and anterior areas in the 1st PC) show almost no changes across different fingers. It is also suggested that much more differences between different conditions are revealed from three new spectral features than mu/beta features. In particular, both mu and beta powers show almost no difference for movements of different fingers.

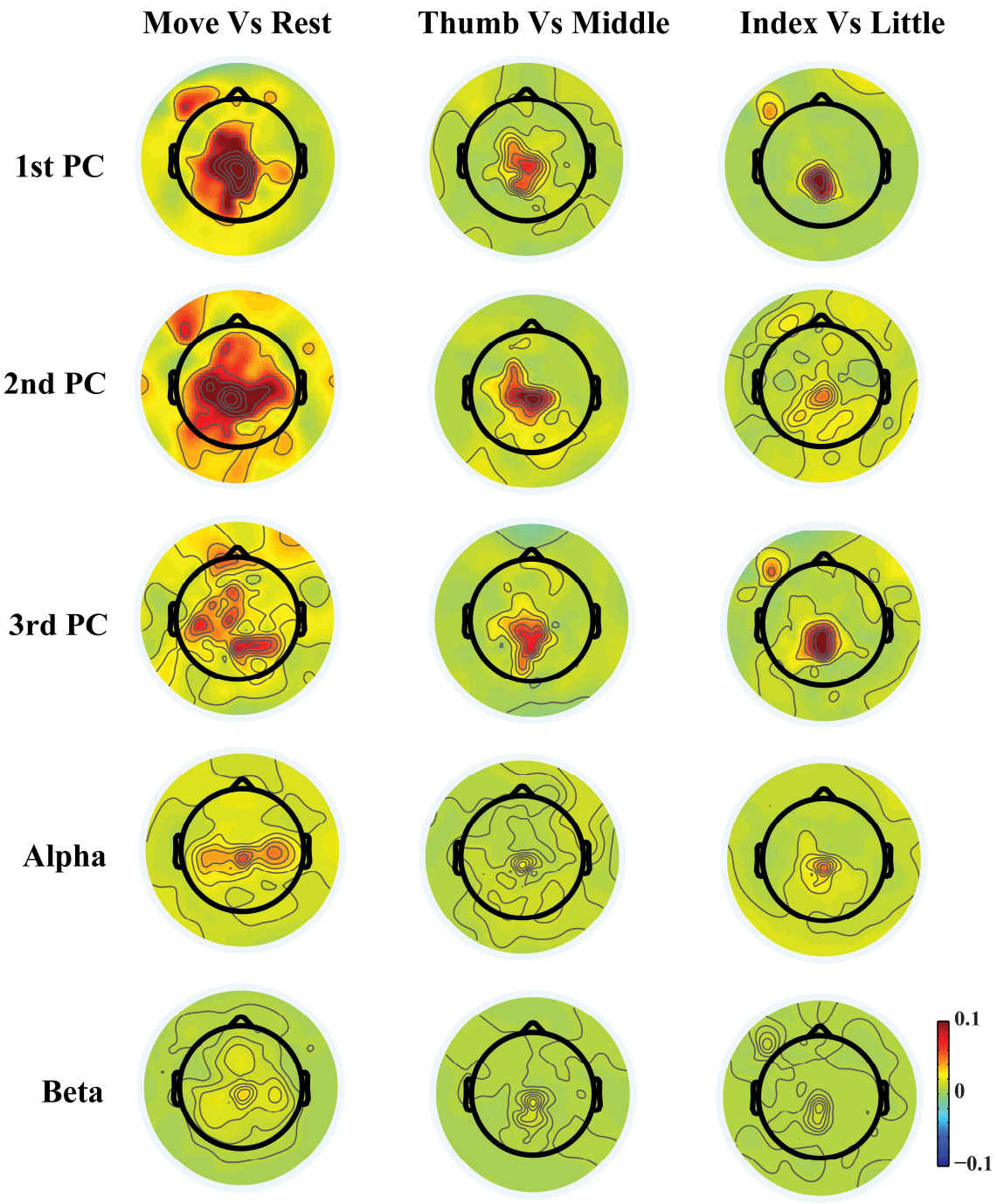

Figure 4.7 Topographies of r^2 values between different task conditions
1st column: movements and resting; 2nd column: movements of thumb and middle; 3rd column: movements of index and little.

4.6 Detection of Individual Finger Movements

4.6.1 Single Features for Classification

Figure 4.8 presents the accuracy in decoding movements from resting using mu, beta, and spectral features from PCs. It indicates that all features individually yield significantly higher detection accuracy than the guessing level ($p<0.05$), suggesting the existence of spectral changes in EEG associated with movements. The mean decoding accuracy achieved by the spectral feature from the 1st PC is 86.8%, followed by the 2nd PC at 76.9% and the 3rd PC at 72.2%, indicating that all three PCs contain discriminative information of finger movements from resting. Spectral powers on the alpha (70.8%) and beta bands (70.6%) yield lower decoding accuracy than all individual PCs, and significantly lower than the 1st PC ($p<0.05$, Table 4.2).

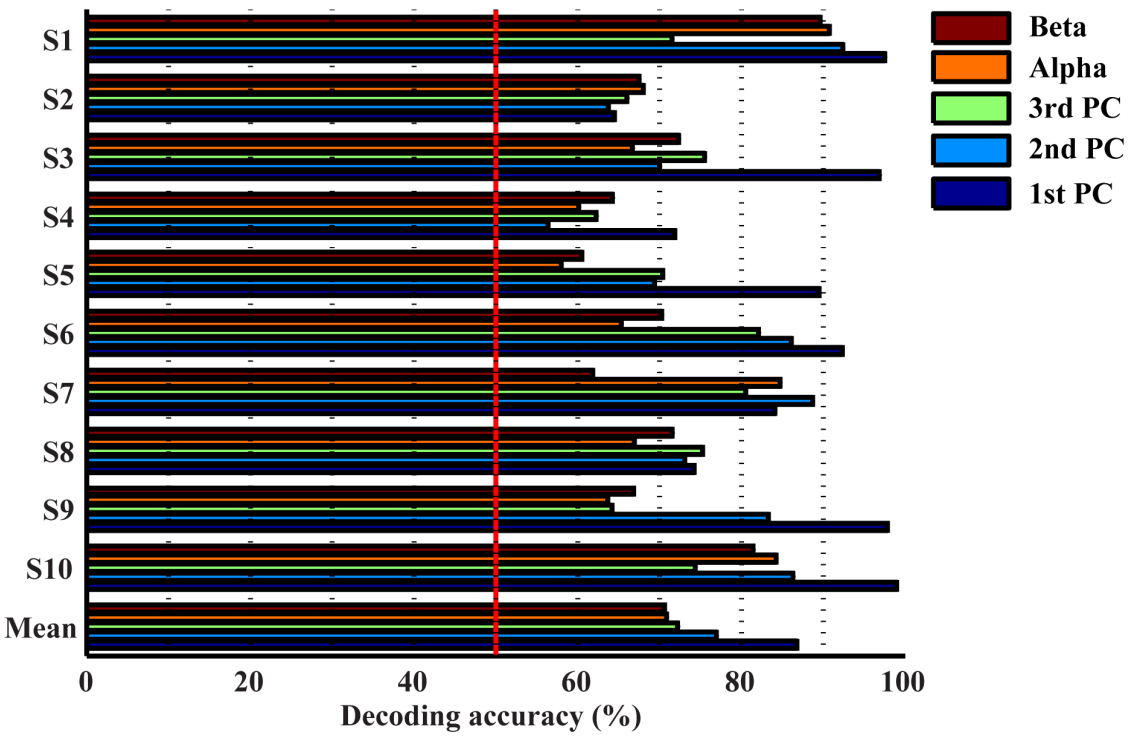

Figure 4.8 Accuracies in detecting finger movements from individual features

Table 4.2 Summary of Student t-test results for movement detection

	1st PC	2nd PC	3rd PC	2 PCs	3 PCs	Alpha (A)	Beta (B)	A+B	A+3PCs	B+3PCs	AB+3PCs
1st PC	NA	**-0.0111**	**-0.0043**	**0.0193**	**0.0084**	**-0.0055**	**-0.0017**	**-0.0125**	**0.0206**	**0.0166**	**0.0212**
2nd PC	**0.0111**	NA	-0.1643	**0.0004**	**0.0002**	-0.0539	-0.0954	-0.5643	**0.0001**	**0.0001**	**0.0001**
3rd PC	**0.0043**	0.1643	NA	**0.0003**	**0.0001**	-0.7009	-0.6402	0.2042	**0.0000**	**0.0000**	**0.0000**
2 PCs	**-0.0193**	**-0.0004**	**-0.0003**	NA	**0.0619**	**-0.0011**	**-0.0006**	**-0.0017**	0.2609	0.2487	0.2236
3 PCs	**-0.0084**	**-0.0002**	**-0.0001**	-0.0619	NA	**-0.0006**	**-0.0002**	**-0.0006**	0.8308	0.5863	0.5667
Alpha (A)	**0.0055**	0.0539	0.7009	**0.0011**	**0.0006**	NA	-0.9324	**0.0036**	**0.0003**	**0.0002**	**0.0002**
Beta (B)	**0.0017**	0.0954	0.6402	**0.0006**	**0.0002**	0.9324	NA	**0.0247**	**0.0001**	**0.0001**	**0.0001**
A+B	**0.0125**	0.5643	-0.2042	**0.0017**	**0.0006**	**-0.0036**	**-0.0247**	NA	**0.0002**	**0.0001**	**0.0001**
A+3PCs	**-0.0206**	**-0.0001**	**-0.0000**	-0.2609	-0.8308	**-0.0003**	**-0.0001**	**-0.0002**	NA	0.5669	0.5020
B+3PCs	**-0.0166**	**-0.0001**	**-0.0000**	-0.2487	-0.5863	**-0.0002**	**-0.0001**	**-0.0001**	-0.5669	NA	0.9870
AB+3PCs	**-0.0212**	**-0.0001**	**-0.0000**	-0.2236	-0.5667	**-0.0002**	**-0.0001**	**-0.0001**	-0.5020	-0.9870	NA

Each entry present p value from statistical test between two features. The bold and underlined entries indicate significant difference ($p<0.05$). Negative entries indicate low decoding accuracy using the feature from column than the one from row.

4.6.2 Combined Features for Classification

The top three bars in Figure 4.9 present the decoding accuracy using combined features from only one category of spectral features (projection weights on spectral PCs or PSDs). It is observed that 2 or 3 spectral PCs together produce significantly higher decoding accuracy, i.e. 90% and 91% respectively, than individual PCs ($p<0.05$ for the 1st PC and $p<0.0005$ for the 2nd and 3rd PCs, Table 4.2). Similar phenomenon is also observed for the combined alpha and beta bands feature, in which the decoding accuracy (i.e. 75.6%) is significantly higher than the feature only from either alpha or beta band alone ($p<0.05$, Table 4.2). Moreover, the combined features from the spectral PCs as the input feature for classification show much higher accuracy than the

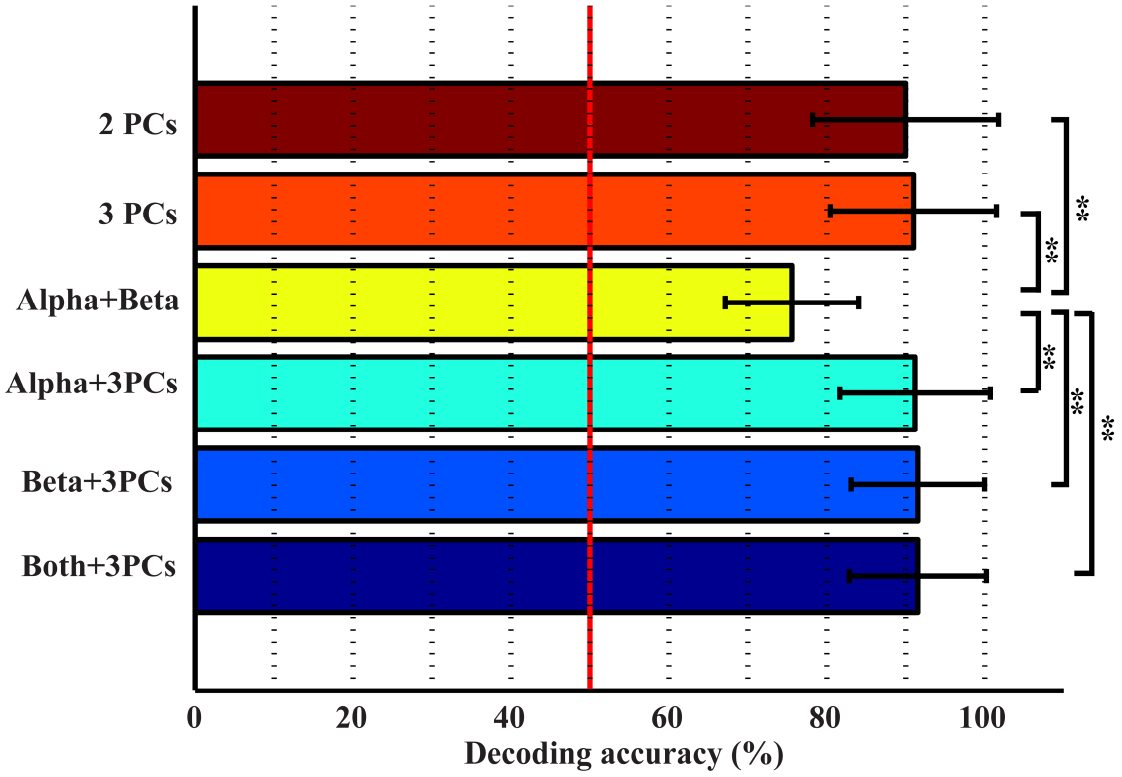

Figure 4.9 Accuracies in detecting finger movements from combined features
Results of paired Student's t-test between each two combinations of features is reflected in the figure. ** denotes $p<0.01$.

combined PSD features ($p<0.001$, Table 4.2). On the other hand, when features from different categories are combined (spectral PCs and PSDs), only slight improvements in decoding accuracy are observed (91.5% by combining total five features), which are not significantly different from ones obtained through the use of combined spectral PCs (i.e. 91% for combined 3 PCs).

4.7 Pairwise Decoding of Individual Finger Movements

4.7.1 Single Features for Pairwise Classification

Figure 4.10 shows the mean decoding accuracies and corresponding standard deviations averaged across all subjects, from single features. It indicates that DAs from ten comparisons using the broadband feature (i.e., projection weights on the first PC) are all higher than 70%, with the lowest DA of 71.43% in index vs. middle and the highest DA of 82.41% in ring vs. little. The average DA across all pairs of fingers and subjects is 77.11%, which is significantly higher than the empirical guessing level 51.26% (the red horizontal dashed line) in one-sample t-test ($p<0.05$). The average DAs achieved by spectral features in the two frequency bands are 58.55% (alpha) and 57.86% (beta), respectively, and all reach significant level against the empirical guessing level ($p<0.05$). Among these features, the difference between alpha and beta band is not significant ($p>0.05$). Furthermore, the broadband feature has significantly higher DAs than the feature from any of these individual frequency bands ($p<0.05$).

The significance of decoding performance for each pair of fingers using EEG data is listed in Table 4.3. With the significance level α as 0.05, most of decoding accuracies for all subjects and all finger pairs were above the upper bound of 95%

confidence interval of guessing, except four pairs out of one hundred (underlined ones in Table 4.3). These results demonstrate that almost all decoding accuracies of ten finger pairs from all subjects are significantly better than the guessing level.

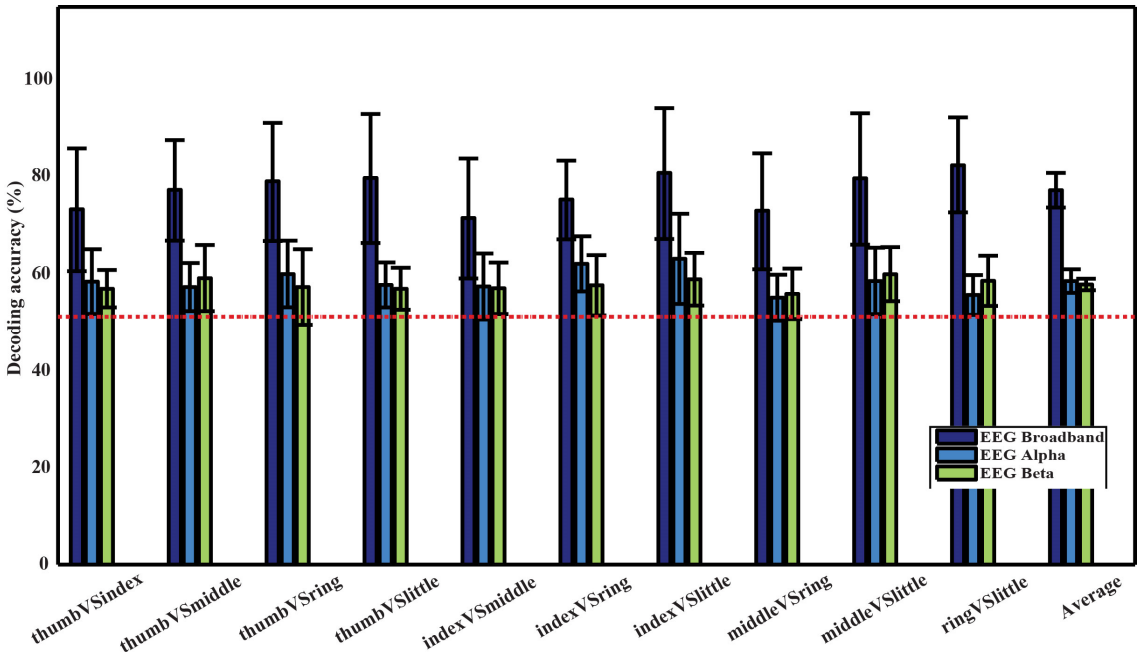

Figure 4.10 DAs of pairwise decoding from single features
The red dashed line indicates the empirical guessing level of 51.26% and the vertical lines indicate standard deviations.

4.7.2 Decoding Efficacies from Single and Combined PC Features

Figure 4.11 illustrates the average decoding accuracies in ten pairs of fingers from EEG signals using projection weights on single (from first to fifth) or multiple (from first two to first five) PC(s) as input features for classification. As far as single PC is concerned, the first PC produces higher DAs than other single PCs, while the differences are not significant against the second and third PCs ($p = 0.22$ and 0.17, respectively). In most cases, the decoding accuracy of each pair of fingers decreases from the first PC to the fifth PC, indicating that the spectral structure in the first PC is more relevant to movements performed by fingers than other PCs.

Table 4.3 Significance test results for pairwise decoding of finger movements

	Subj. 1	Subj. 2	Subj. 3	Subj. 4	Subj. 5	Subj. 6	Subj. 7	Subj. 8	Subj. 9	Subj.10	Mean	Std.
thumb vs. index	68.89/58.15	67.36/56.55	75.12/60.20	66.77/56.92	63.06/65.03	56.65/56.49	71.50/56.61	56.88/56.29	99.16/55.40	87.29/56.68	71.27	13.25
thumb vs. middle	69.82/57.56	70.62/60.76	75.73/57.90	67.61/56.40	76.40/60.61	66.72/56.40	73.65/56.82	57.48/56.56	98.77/56.81	86.56/56.79	74.34	11.43
thumb vs. ring	83.21/58.53	71.11/56.93	87.57/57.32	70.03/56.80	72.00/57.53	74.32/56.93	58.20/56.51	67.58/56.43	99.09/56.83	92.39/57.12	77.55	12.60
thumb vs. little	93.33/58.32	63.03/56.12	76.63/57.76	82.86/59.95	78.00/57.88	95.87/56.27	75.50/56.30	59.13/56.68	94.06/56.51	63.25/56.37	78.16	13.51
index vs. middle	62.97/56.56	72.74/58.02	89.74/63.79	57.53/57.51	67.37/58.40	62.00/56.30	55.13/56.92	65.13/56.13	62.61/56.76	96.29/56.34	69.15	13.57
index vs. ring	77.03/56.82	69.95/55.57	87.22/63.10	63.84/56.64	70.86/63.51	63.40/56.43	64.67/56.52	71.29/56.80	81.25/56.51	85.33/57.00	73.48	8.81
index vs. little	94.50/56.59	78.14/56.56	80.04/63.29	92.39/61.72	76.12/67.24	95.70/56.62	57.97/56.52	58.22/56.15	83.06/56.68	80.23/56.44	79.64	13.32
middle vs. ring	64.23/56.83	63.14/57.93	94.91/55.95	64.67/56.71	81.87/58.81	55.16/56.47	69.26/56.17	62.03/56.28	71.97/57.08	84.23/56.98	71.15	12.24
middle vs. little	91.87/56.50	68.23/61.16	71.19/56.31	94.13/58.79	75.86/62.55	96.97/57.38	55.71/56.68	62.32/56.30	76.39/57.23	86.78/56.45	77.94	14.07
ring vs. little	91.47/56.57	71.92/57.14	90.34/56.74	86.95/60.43	70.62/57.96	97.77/56.99	72.90/56.50	67.97/57.11	70.44/56.51	81.74/57.26	80.21	10.78

Each entry in the table is averaged decoding accuracy / upper bound of (1-α) confidence level, α =0.05. The last two columns of the table show the means and standard deviations of decoding accuracies of each pair of fingers across all subjects. Values underlined are not significantly higher than the guessing level.

When multiple PCs are concerned, it suggests higher DAs than single PCs with the statistical significance ($p < 0.05$). The highest DA can usually be achieved when projection weights on first three PCs are used as input features for classification. It further indicates that three pairs of fingers (thumb vs. little, ring vs. little, and thumb vs. index) achieve the highest DAs using the first three PCs, and others have their highest DAs using the first two, four, or five PCs. None of them gets the highest DA from single PCs.

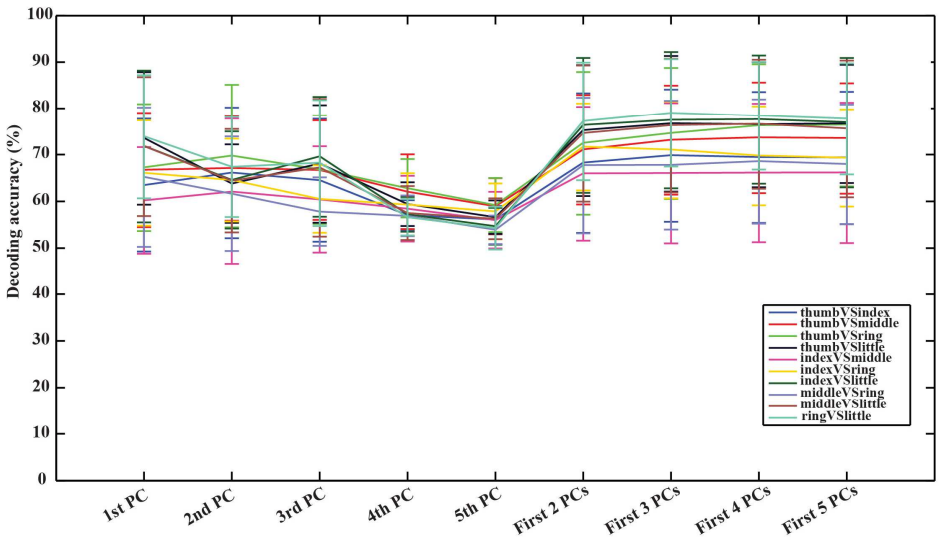

Figure 4.11 Decoding accuracies from single and combined PC features

4.7.3 Decoding Performance from Resting Data

To further verify that it was movement-related changes in EEG data that contributed to the decoding accuracies in Figure 4.10, the same classification procedures were performed on data from resting conditions prior to individual finger movements (they were categorized to different fingers according to movements performed after). Figure 4.12 shows that DAs for all pairs of fingers are at the guessing level, in the range from 47.24% (index vs. little) to 50.55% (middle vs. ring).

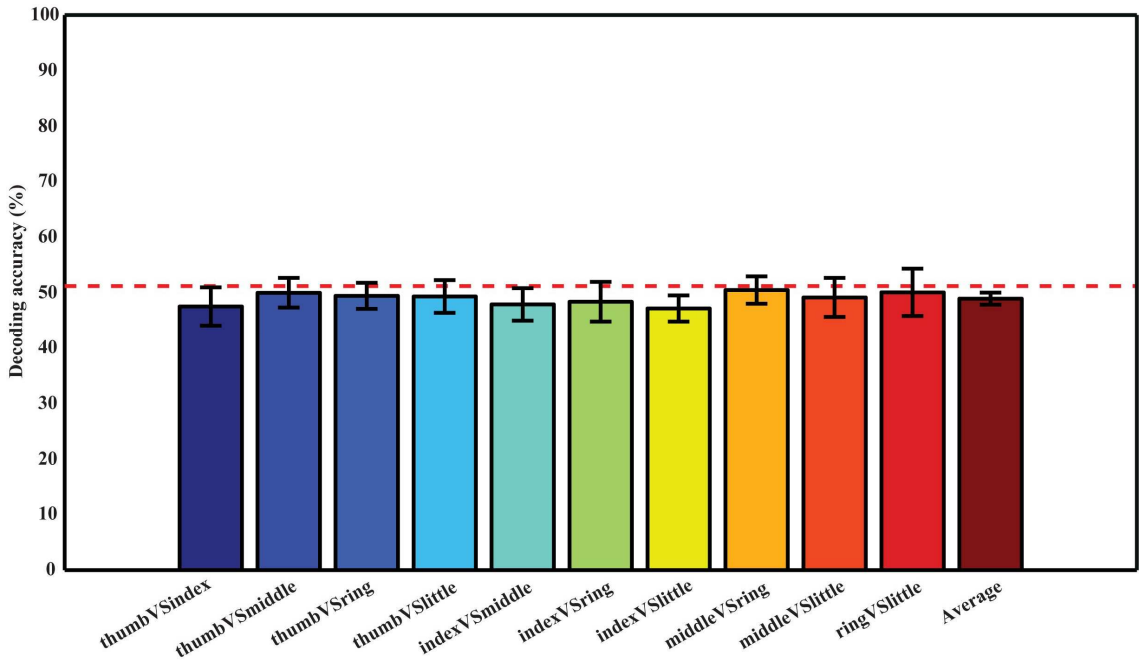

Figure 4.12 Decoding accuracies using the resting EEG data
The red dashed line indicates the empirical guessing level of 51.26% and the vertical lines indicate standard deviations.

4.8 Decoding Individual Finger Movements from One Hand

4.8.1 Single Features for Classification of Five Fingers

In Figure 4.13, confusion matrices of five fingers movements from projection weights of single PCs or PSDs of single frequency bands are illustrated. The rows of these matrices stand for predicted condition labels, while the columns represent actual condition labels. For features from individual PCs, similar performances are achieved in all individual PCs and actually moved fingers were dominantly and correctly identified in the confusion matrices (diagonal elements with larger values than off-diagonal elements). Furthermore, the misclassifications are spread almost evenly in four fingers other than the actual one (off-diagonal elements with similar low values). Considering different fingers, thumb and little seem usually better classified than other fingers. For features from alpha and beta bands, only thumb is classified with relatively high

accuracies, while the decoding accuracies of other fingers are close to the guessing level (i.e. 20%). Moreover, other four fingers are all confused to thumb, which might be the reason for thumb having high decoding accuracy. Spectral features from PCs show obvious better performance than features from mu/beta PSDs (best mean decoding accuracy in each category: 33.1% vs. 23.4%).

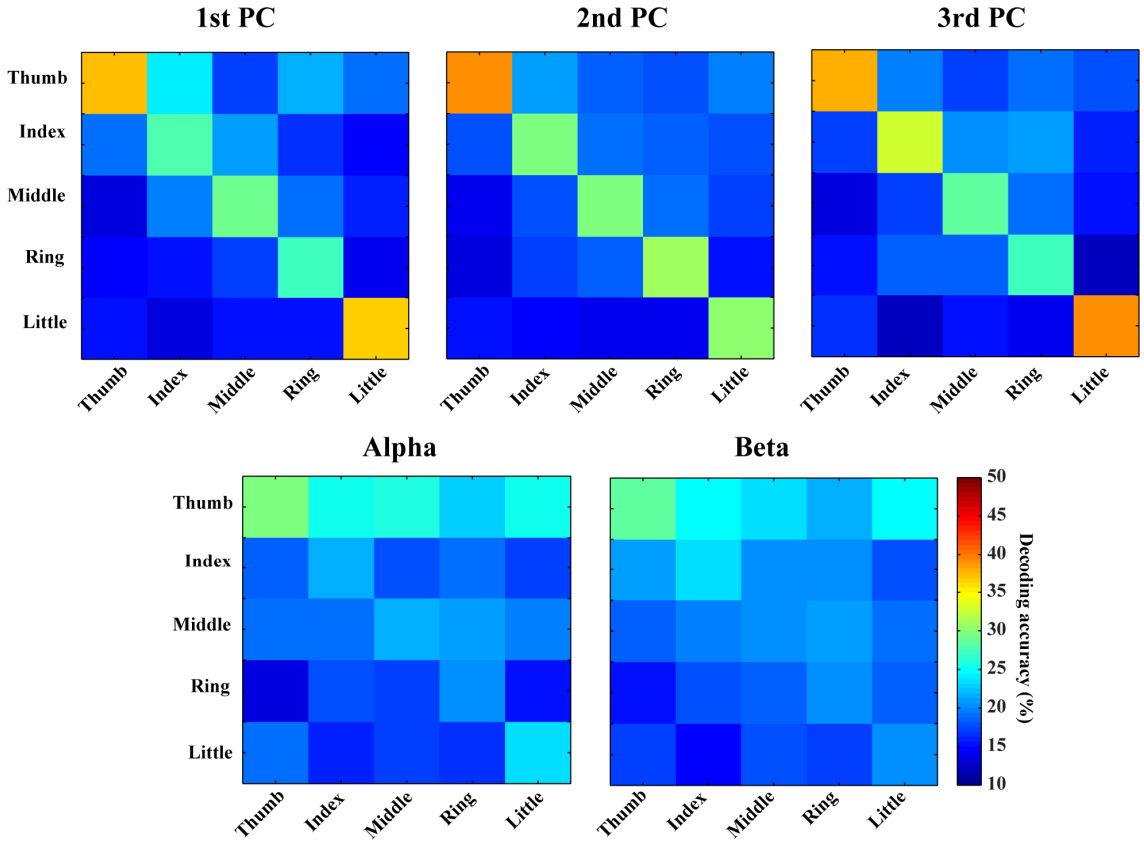

Figure 4.13 Confusion matrices from individual features
Each row indicates predicted labels and each column indicates true labels.

4.8.2 Combined Features for Classification of Five Fingers

Combinations of spectral features from PCs yield better decoding performance than spectral features from individual PCs (best mean decoding accuracy: 39.7%), while combination of features from mu/beta PSDs does not indicate obvious improvement (best mean decoding accuracy: 23.3%). As shown in Figure 4.14 (the first row), values

of diagonal elements in the confusion matrices from three PCs are further increased, which leads to less confusion among fingers (inferring actual labels are better classified). Similarly, better decoding performances are achieved in thumb and little than other three fingers. On the other hand, the combination of mu/beta PSDs still confuses all five fingers to thumb. The combinations of features from two categories actually show slightly more confusion among fingers than the combination of three PCs (38.1% vs. 39.7%), as shown in Figure 4.14 (the bottom row).

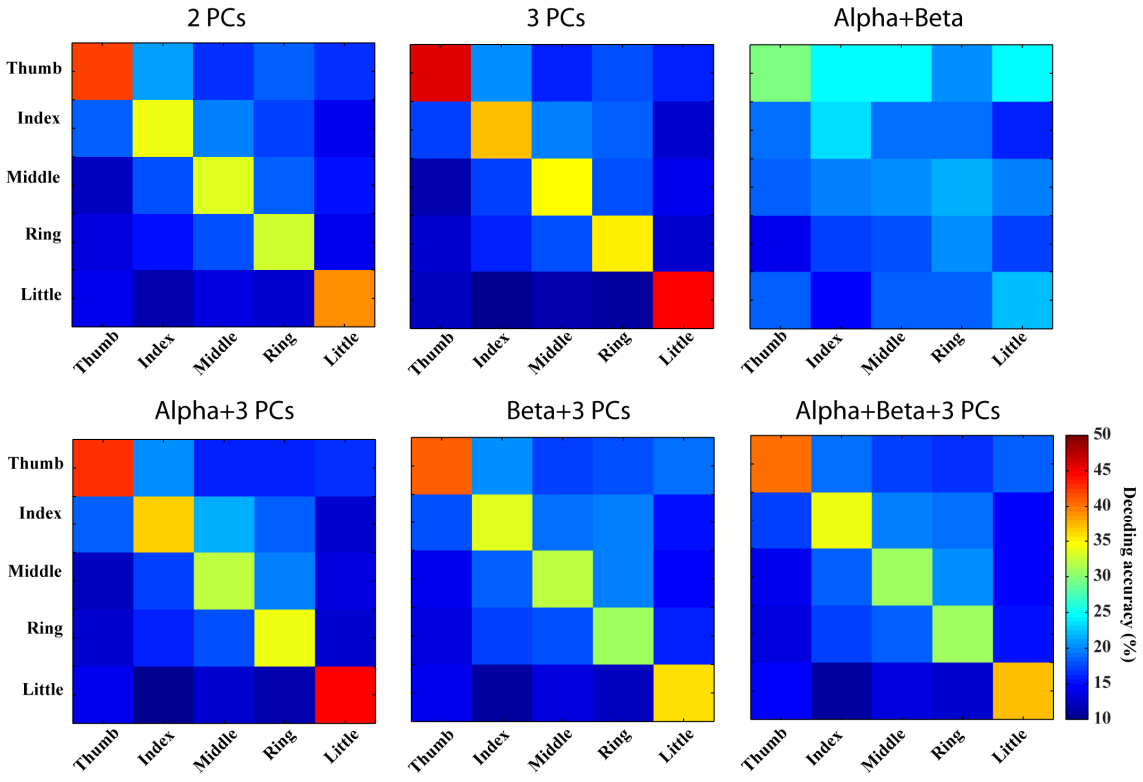

Figure 4.14 Confusion matrices from combined features
Each row indicates predicted labels and each column indicates true labels. Top row: decoding results from combinations within each category of features. Bottom row: decoding results from combinations across different categories.

4.9 Discussion and Summary

In the chapter, spectral structures in noninvasive EEG were investigated during motor tasks of individual finger movements. Three spectral structures were extracted through a PCA analysis from EEG data, which suggested coupled spectral components over wide (e.g. 1st PC) and/or multiple frequency bands (e.g. 2nd PC). The spatial patterns of these newly identified spectral structures were examined and compared to classic mu/beta rhythms. The resolution of these new spectral features in detecting movements from resting and decoding individual finger movements (two fingers or all five fingers from one hand) was further studied in a classification scheme. The experimental results demonstrate that these new spectral structures from the PCA analysis indicate consistent and specific motor-related spatial patterns in different conditions and subjects. Furthermore, spectral features derived from these new spectral structures are able to reveal discriminative information in noninvasive EEG that is related to fine body-part movements, i.e. fingers, beyond large body-part movements (such as hand and shoulder) that can be decoded using classic motor rhythms (i.e. mu and beta rhythms).

4.9.1 Spectral Structures and Features

The spectral structures in EEG decomposed by the PCA analysis present different profiles along frequency axis, yet consistency can be found across all channels, conditions, and subjects (Figure 4.5). These observations are in line with the findings from ECoG studies (Miller et al., 2009b), demonstrating the existence of cross-frequency spectral structures in human EEG measured at both the brain and scalp surfaces (Figure 4.4). Particularly, the first spectral structure (1st PC) suggests a

broadband non-rhythmic spectral pattern, which is different from other two spectral structures. The other two (2^{nd} and 3^{rd} PCs) indicate dominant spectral powers at alpha and beta bands, which might resemble rhythmic activities from classic motor rhythms in mu and beta bands (Pfurtscheller and Lopes da Silva, 1999), while other aspects of these two spectral structures, i.e. spatial pattern and resolution in decoding movements, suggest similarity and difference at the same time.

The spatial patterns of these new spectral structures over the channel domain (Figure 4.6) and their spatial difference patterns between different conditions (e.g. movement vs. resting) (Figure 4.7) suggest that their activity and activity changes are related to motor brain functions, covering the premotor cortex for movement planning (Hoshi and Tanji, 2000), M1 for movement execution (Stippich et al., 2002) and the posterior parietal cortex (PPC) for integrating sensory and motor information (Fogassi and Luppino, 2005). Their capability in decoding movements (see section below) adds further evidences in linking these new patterns/features to motor brain functions. However, it is unknown, so far, about neural mechanisms behind these spectral structures, especially the broadband non-rhythmic one, while neural mechanisms of rhythmic brain activities have been well investigated (Pfurtscheller and Lopes da Silva, 1999, Urgen et al., 2013). Of course, the rhythmic nature of the 2nd and 3rd PCs (across multiple frequency bands) and their spatial similarity at certain levels to classic mu/beta rhythms might suggest common underlying neural sources among them, while these new spectral structures from the PCA analysis might reveal more coupling and coordinating patterns across different rhythmic activities that cannot be revealed by classic frequency band analysis.

4.9.2 EEG Resolutions in Decoding Individual Finger Movements

EEG resolutions in fine body-part movements have not been sufficiently studied, due to the challenges of limited spatial resolution and SNR in EEG signals (Hassanien and Azar, 2014). Several studies explored the resolution of EEG in decoding finger movements from different hands with accuracies ranging from 70% to 90% (Lehtonen et al., 2008, Li et al., 2004). However, to our knowledge, very few studies have been conducted to decode movements of finger from one hand using EEG. Our present results suggest that features from spectral PC structures can detect finger movements from resting condition with the accuracy up to 86.77% (1st PC), which is significantly better than the accuracy achieved with classic mu/beta rhythms (about 70%).

An average decoding accuracy of 77.11% was achieved in distinguishing movements performed by all pairs of different fingers from one hand in ten subjects. Decoding performance was stable across different pairs of fingers (std: 3.72%, Figure 4.10). When examining decoding accuracies of each pair of fingers across different subjects, average decoding accuracies were all above the guessing level with the similar level of variations (Table 4.2). Resting data prior to movements do not contain information to accurately decode movements (Figure 4.12), indicating EEG spectral changes identified in comparisons between different movements and between movements and resting are indeed induced by movements. The DAs of all finger pairs using EEG are significantly higher than the guessing level ($p<0.05$), demonstrating the feasibility of using such features in discriminating individual finger movements from one hand.

For decoding individual finger movements (all five fingers from one hand), our confusion matrix analysis further indicates that movements of individual fingers from one hand can be dominantly labeled to correct fingers (outstanding diagonal elements in confusion matrices) using new spectral features from single-trial EEG data, while all fingers are confused to thumb when classic mu/beta rhythmic features are used. It is also important to note that dominantly correct labeling using new spectral features for all fingers is achieved upon the fact that various fingers, especially those close to each other and in the middle, show behavior dependences during movements (Hager-Ross and Schieber, 2000). Thumb is the most independent finger in behaving, which is consistent with our results that thumb is the one with the least confusion (Figure 4.13 and 4.14). These facts indicate that some confusion is from inherent characteristics of the human motor system. The discriminative information obtained from the PCA analysis on EEG regarding different fingers from one hand suggests that noninvasive EEG can be used to study fine body-part movements beyond large body-part movements that have been well studied using classic rhythmic brain activity (Neuper and Pfurtscheller, 1996, Hashimotor and Ushiba, 2013).

4.9.3 Information Independence and Redundancy in Spectral Features

Various combinations of spectral features (from new spectral structures and mu/beta rhythms) were studied to probe information independence/redundancy within and cross feature categories. Combinations of PCs can increase the decoding accuracy of movements from resting up to 91%, which is significantly higher than individual PCs ($p<0.05$). This is also comparable to a recent ECoG study achieving an average of 94% classification rate in detecting any finger movements from resting (Chestek et al.,

2013), considering ECoG offers much better signal quality than EEG (Ball et al., 2009). In term of finger decoding, confusion matrices are less confused with more single-trial EEG data correctly labeled (Figure 4.14). For mu/beta rhythms, combination of alpha and beta PSDs also significantly improves accuracy in detecting movements from resting over individual frequency band PSDs ($p<0.05$). However, their combination is not able to improve the performance of labeling different fingers, which is reasonable since both lack discriminative information in distinguishing fingers when used alone. These results suggest that different features within each category exhibit independent information in discriminating movements, to which they are sensitive.

Results from cross-category combinations of features, however, suggest no significant improvements in detecting movements from resting (Figure 4.9), which might suggest that most discriminative information about movements from resting revealed in mu/beta rhythms are also revealed in PCs. Since mu/beta rhythms present little efficacy in decoding fingers, it is expected that cross-category combinations of PCs with mu/beta features would not lead to improvement of finger decoding performance. On the contrary, slight degeneration is observed (Figure 4.14), which might be attributed to the non-specific nature of mu/beta features to fingers that smoothes out other finger-specific features in the spectral PC structures.

4.9.4 Implications to BCI Applications and Neuroprosthesis

Motor rhythm-based BCIs have the merit of providing asynchronous control on a single-trial basis (Pfurtscheller et al., 2005, Leeb et al., 2007), while most of other popular BCI schemes require repetition of trials for accurate control, such as P300 (Sellers et al., 2006, Mak et al., 2011) and SSVEP (Wang et al., 2008, Bin et al., 2009).

However, limited control signals generated from decoding large body parts using classic motor rhythms largely confine the complexity of noninvasive BCI techniques. Until now, such BCIs are only applied to simple applications, such as cursor movements on the computer screen (Wolpaw and McFarland, 2004, Wilson et al., 2009). In the present studies, new spectral features present promising movement detection capability and sensitivity to movements of fine body parts, i.e. fingers. With the potential to decode gestures in the future, these new features could provide an alternative mean to overcome the restriction. To be used in neuroprosthesis, they could not only increase the degree-of-freedom of control signals, but also contribute to a more naïve mapping from EEG to robotic fingers. Further, robust detection of movements from resting can create an idle control state, which is crucial in designing online applications for both BCI and neuroprosthesis (Blankerz et al., 2002). It is, however, important to note the decoding performance has yet to reach the level of practical usage. My studies in this chapter only demonstrated the feasibility in decoding movements of fine body parts using noninvasive EEG recordings. Its practical usage in the future is expected to be dependent on significantly refined detection of usable signals and significantly improved classification accuracy.

Chapter 5: Towards Decoding Motor Imageries of Fine Body Parts

In the last chapter, studies about detection of finger movements from the resting condition and decoding different individual finger movements were introduced, and the experimental results demonstrated EEG's resolution about fine body movements. For people who have already lost moving ability or amputees with missing limbs, real movements for training BCIs are no longer an option, but motor imageries can be obtained through proper training. Given that both movements and motor imageries induce spectral changes in the mu rhythm and they evoke similar cortical activations in literature (Miller et al., 2010), it is meaningful to further investigate feasibility of EEG in decoding motor imageries (MI) of fine body parts. However, unlike movements that are naïve to healthy subjects, motor imageries require extensive training before subjects are used to the tasks. Thus, I investigated the feasibility of discriminating four different motor imagery (MI) types including thumb and fist from each hand using EEG, as a first step in this preliminary study, leaving MIs of all fingers from one hand as future works.

In this chapter, the spectral PCA procedures in decoding finger movements were implemented in extracting spectral and spatial features related to different MIs involving finger movements. Extracted features were evaluated using a linear discriminant analysis (LDA) classifier, resulting in an average decoding accuracy about 50%, which is significantly higher than the guess level (25% for 4-class classification problem) and the 95% confidence level of guess. The preliminary results demonstrate the great potential of extracting features from different MIs to generate control signals with more degrees of freedom (DOF) for non-invasive brain-computer interface

applications. In addition, for movement related applications, especially for neuroprosthesis, the present study may facilitate the development of a non-invasive BCI, which is highly intuitive and based on users' spontaneous intentions. The results in the chapter were published in Xiao et al., 2012.

5.1 Data Acquisition and Analysis

5.1.1 Subjects and Materials

Three subjects volunteered to participate in the study (all males, aged 30 ± 2 and right-handed). Two of them had experience in MI-based BCIs, who participated in research of one-dimensional cursor tasks (Wolpaw and McFarland, 2004). The third subject was naïve to any BCI paradigms. All of them provided informed consents. The study was approved by the Institutional Review Board of the University of Oklahoma.

Experiments were conducted in a shielded chamber room under a dim light. Subjects were seated in a comfortable armchair with their arms semi-rested. EEG data were recorded using the same EEG acquisition system as the studies in Chapter 4, including EGI's Geodesic EEG System 300 (GES 300) and a 128-electrode HydroCel Geodesic Sensor Net (Electrical Geodesic Inc., OR, USA). Signals were digitized at 1000 Hz, referenced to an inactive electrode Cz at the vertex. During recording, subjects were instructed to sit still and avoid movements to reduce motion artifacts. BCI2000, a general-purpose system for BCI research (Schalk et al., 2004), was used to present stimuli to subjects through a LCD monitor. It also streamed EEG data to computers for storage, as well as corresponding event markers and time stamps. During recordings, no source filters were applied to raw EEG signals.

5.1.2 Experimental Design

Stimuli were presented in a sequence of left thumb movement (LTM), MI of left thumb (LT), left fist movement (LFM), MI of left fist (LF), right thumb movement (RTM), MI of right thumb (RT), right fist movement (RFM), MI of right fist (RF), and fixation (Figure 5.1). Real-movement cues were included in the design to facilitate subjects' adaption to motor imagination, because two subjects reported having difficulties following MI cues alone during training sessions. Each condition lasted 3 seconds, followed by 2 seconds of blank screen for necessary blinks or swallowing. The whole sequence was repeated 40 times in one session, resulting in 40 trials for each condition and 360 trials in total. In each condition, subjects were instructed to perform either real movements or kinesthetic MI indicated by cues. Trials related to fixations were counted as resting conditions. During this period, subjects sit still and stared at the fixation cross on screen. Only trials related to MIs of thumb and fist and trials from resting conditions were used for subsequent processing. The first subject completed 7 experimental sessions, and other two subjects completed 3 sessions each.

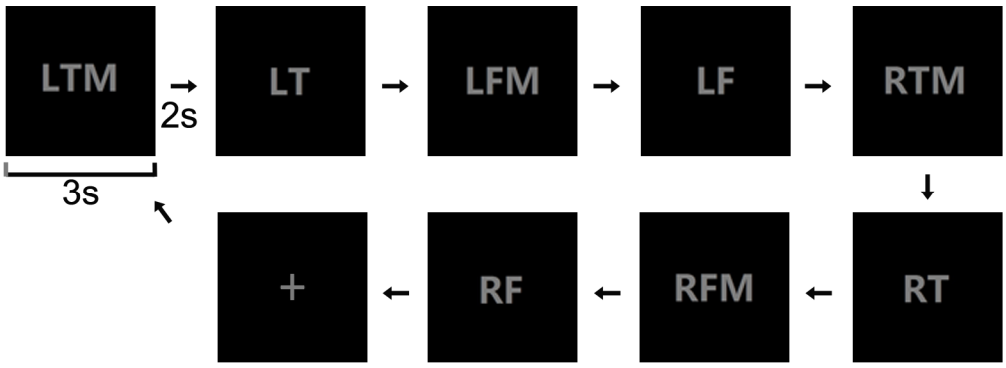

Figure 5.1 Experimental design
Each sequence of stimulus starts from LTM and ends with fixation. Each stimulus lasted for 3 seconds and inter-stimulus interval was 2 seconds.

5.1.3 Data Processing

The data processing procedures are outlined in Figure 5.2. EEGLAB (Delorme and Makeig, 2004) was used for preprocessing the acquired EEG data. EEG raw data recorded were first down-sampled to 256 Hz to reduce computational load. Then EEG data from each channel were re-referenced to the common average reference (CAR) obtained across all channels to increase signal-to-noise ratio (SNR) (McFarland et al., 1997). Bad channels were rejected using Kurtosis method in EEGLAB and interpolated using averaged data from surrounding channels. A band-pass filter (0.03 Hz ~ 70 Hz) and a notch filter (60 Hz) were applied to remove DC offset and reduce influences from power lines. Three-second epoch data corresponding to the length of trials were extracted and categorized according to conditions. Data from trials of four MIs and resting condition were used for subsequent processing.

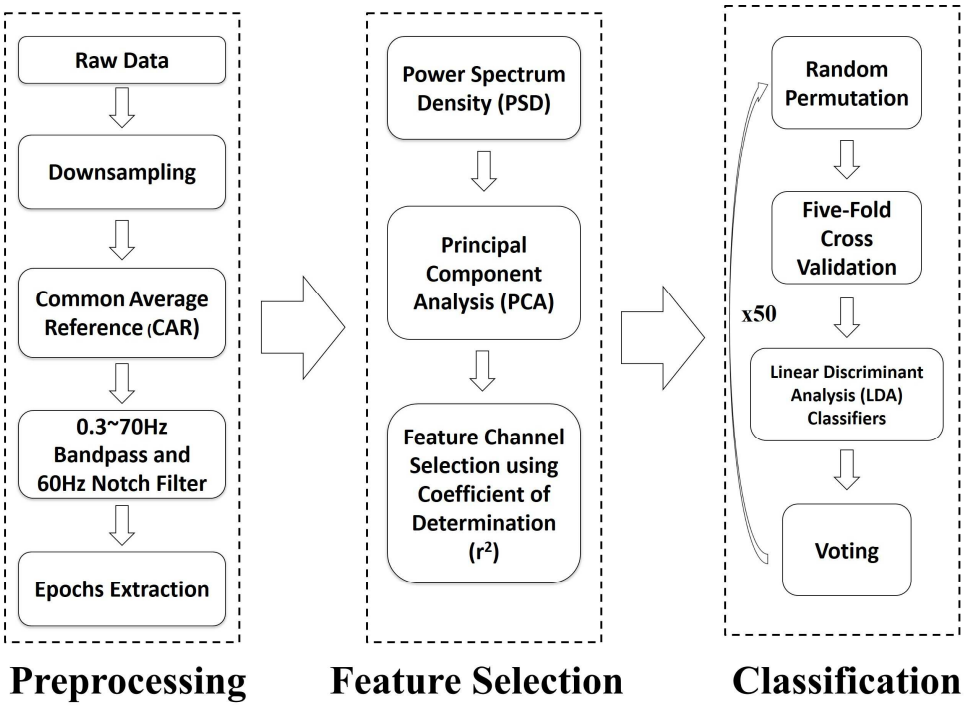

Figure 5.2 Diagram of data processing

The SPCA was then applied to the preprocessed EEG. The SPCA procedures, which have been detailed the descriptions in Chapter 4, will be briefly summarized in the following, and the detailed information can be found in Section 4.3.2. Time-series EEG trial data were firstly transferred to the frequency domain by calculating the power spectrum density (PSD) using Welch's method (Welch, 1967). Secondly, at each channel, PCA was performed on EEG spectral data pooled from trials related to four MI conditions and the resting condition to extract useful spectral features (Miller et al., 2009b). PCA rotated the original coordinate system to maximize variance of each principal component (PC) in spectra and minimize covariance among PCs (Johnson and Wichern, 2007). In other words, PCA constructed a rotation matrix, which diagonalized the covariance matrix of original data. In this way, original EEG spectral data were decomposed into various PCs, and spectral features mostly related to all tasks, but indicating difference for different tasks, were identified.

The process of SPCA involved multiple steps. Firstly, covariance matrix of EEG spectral data was constructed, revealing inter-frequency correlations and inner-frequency variances produced by trials from all conditions. Secondly, eigenvectors of the covariance matrix were computed, which decomposed EEG spectral data into spectral PCs that reflect spectral features related to MIs. Spectral PCs were sorted by corresponding eigenvalues in a descending order. Finally, EEG spectral data from trials of different MIs were projected onto identified spectral PCs on each channel and their projection weights and associated spatial distributions of these weights were calculated for different MIs. Only projection weights of the first five PCs were selected for consideration, since they already accounted for the most variation within the EEG

spectral data (e.g. 99.97% from Session 1 of Subject 1). Based on projection weights and their spatial patterns, the PC indicating the most distinguishable features among different MIs was identified.

5.1.4 Selection of Feature Channels and Classification

Coefficient of determination (r^2) evaluated the proportion of variance accounted by inter-condition trials to the total variance (Shenoy et al., 2006). It was adopted to reveal spatial differences related to different tasks. Four MI conditions (LT, LF, RT, and RF) in the present study suggested six MI pairs. For each pair, r^2 value was calculated on each channel using data of projection weights of both conditions on the most distinguishable PC, using Equation 4.6 in Chapter 4. The r^2 values from all channels were then mapped onto corresponding channel locations on the scalp. Channels were rearranged based on their corresponding R^2 values for each MI pair. Only the channels located above cortical areas associated with motor functions and with large R^2 values were selected as feature channels.

In order to evaluate whether identified spatio-spectral features (i.e., spectral PC over feature channels) provided indicative information in decoding different MIs, the linear discriminant analysis (LDA) classifier was used to simultaneously classify four different types of MIs (LT, LF, RT, and RF) using a five-fold cross validation. Eighty percent of trials were used to train LDA classifiers, and the rest were used for test. Each test trial went through six binary LDA classifiers, which were for each pair of conditions. Each LDA classifier voted for one condition and the one with most votes was the final label for the test trial, which was compared to the true label for the calculation of decoding accuracy in each MI. Average accuracy was calculated by

averaging decoding accuracies from four MIs. Trials were randomly permuted 50 times for training and testing to yield mean accuracy for each condition. The guess level of four-class problems (i.e., 25%) and its 95% confidence interval (CI) were calculated (Muller-Putz et al., 2008), which served as references for the significance of classification results.

5.2 Spectral Structures from Different Motor Imageries

Figure 5.3(a) presents the average elements (magnitudes of eigenvectors) of the first five principal components in spectral domain. Results from C3 (on the left motor cortex) and C4 (on the right motor cortex) were chosen to display since the motor

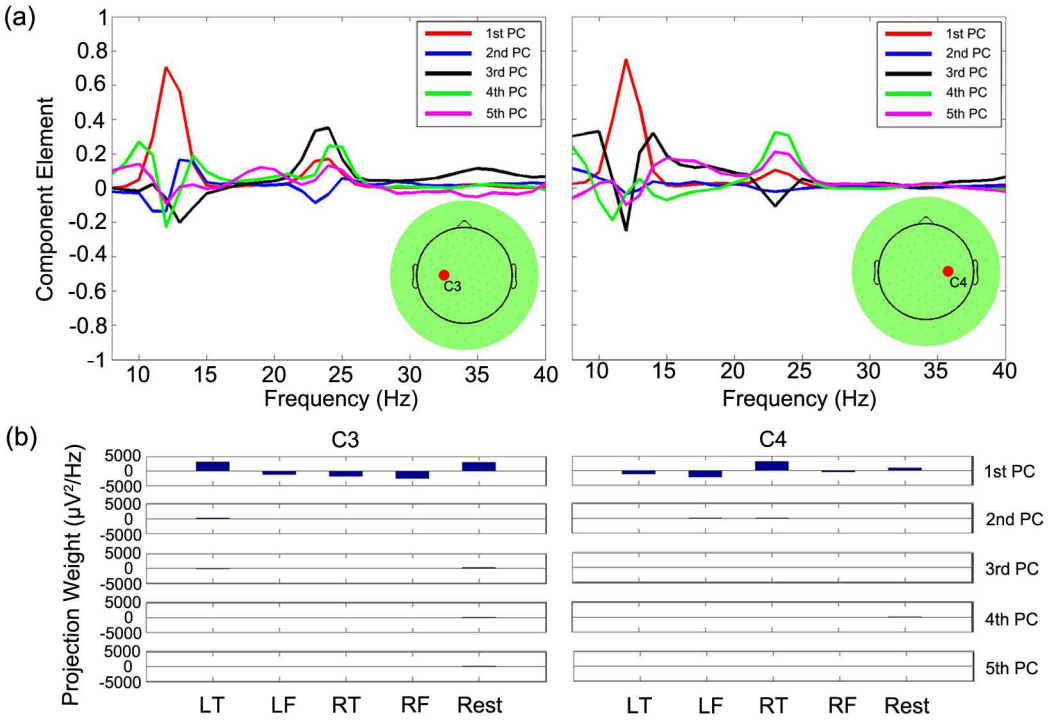

Figure 5.3 Spectral structures and projection weights
(a) Average elements of the first five PCs from Subject 1; (b) Average projection weights of four MIs and resting condition on the first five PCs from the same subject.

cortex is one of the most important brain areas in MI (Miller et al., 2010). Different PCs suggest distinct spectral patterns, revealing different underlying physiological information in the spectral domain. Comparing PC elements on C3 and C4, general structures in elements of same PCs are similar, while they show variations in magnitudes, especially for the second, third and fifth PCs. The first spectral PC accounts for the largest portion of variance in EEG spectral data (Johnson and Wichern, 2007), which suggests spectral peaks at 12 Hz and 24 Hz of mu and beta rhythms.

Figure 5.3(b) visualizes the average projection weights of EEG data from four MIs and the resting condition on the first five PCs. The projection weights on the first PC indicate the most distinguishable patterns among different MIs, as well as between MIs and the resting condition. While there are some variations on other PCs as well, the difference is relatively small. This might suggest that the most useful information for discriminating different MIs resides in the first PC. Comparing projection weights on the first PC at different channels, it also shows distinct patterns, which indicates distinguishable spectral patterns in different MIs exist in multiple channels. It facilitates the idea to explore spatio-spectral patterns for decoding different MIs.

5.3 Topography of r^2 Values and Classification Results

Figure 5.4 presents r^2 topographies for each MI pair. It is notable that the magnitudes of r^2 vary across different pairs, with largest r^2 between LF and RT, and smallest r^2 between LT and LF. Most observable differences in spatio-spectral patterns related to the first PC show on the scalp over brain areas related to motor functions in

all MI pairs. It further indicates the different spatial patterns among different MI pairs, which suggests distinguishable patterns among four types of MIs.

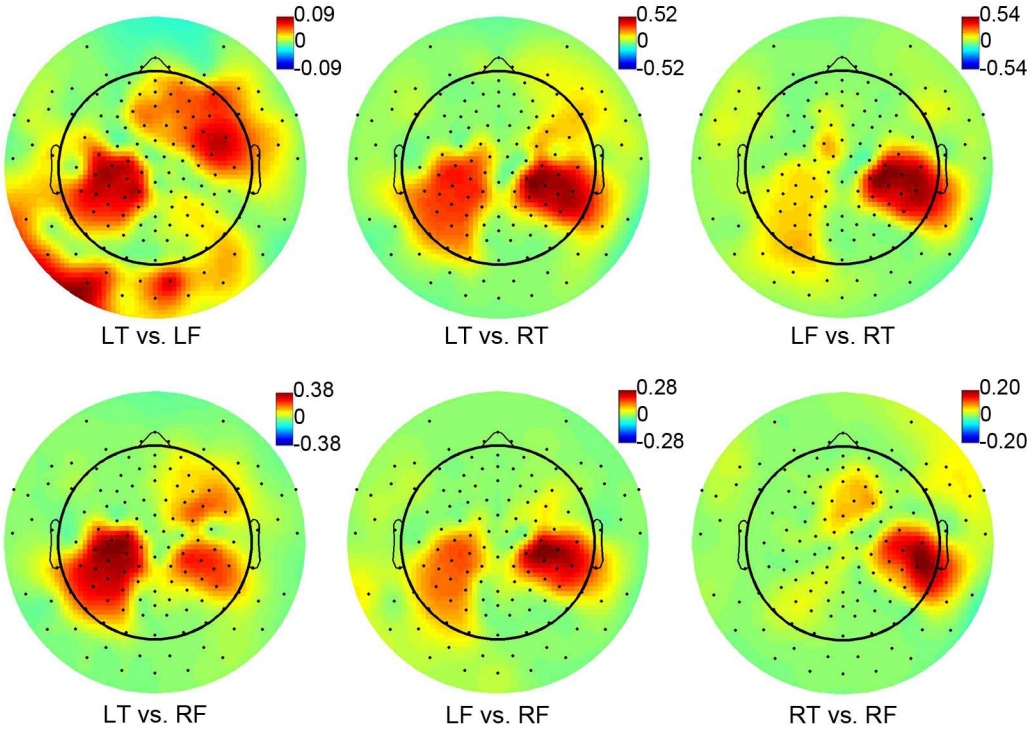

Figure 5.4 r^2 topographies of six MI pairs
Black dots indicate channel locations. Colorbar represents r^2 values.

Figure 5.5 shows the classification results for each MI and their average in a four-class MI decoding problem with the use of the identified spatio-spectral pattern. The results show the mean decoding accuracies of each condition, obtained from 50 random permutations of all trials. The decoding accuracies vary across different MIs, i.e., LT: 49.4%, LF: 50%, RT: 52.4%, and RF: 40.1%. The decoding accuracies for all conditions are significantly higher than the guess level (25%) and the upper boundary at the 95% CI (32%). The average decoding accuracy reaches up to 48%, which is also significantly higher than the guess level and the upper boundary of 95% CI.

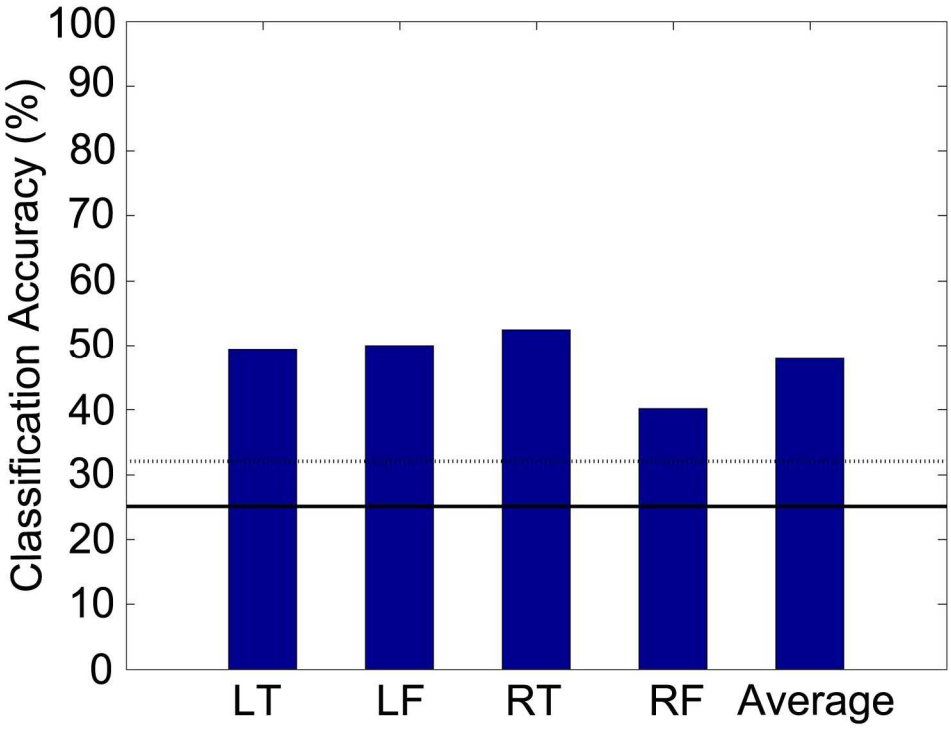

Figure 5.5 Average decoding accuracy for each MI
Black solid line indicates 4-class guess level. Dashed line indicates upper boundary of 95% CI of the guess level.

5.4 Discussion and Summary

In the chapter, the underlying spatio-spectral features related to different MIs of thumb and fist on both hands were explored using EEG. The SPCA used for decoding finger movements in studies of Chapter 4 were applied to extract corresponding spectral and spatial features of MIs, which were further validated by the LDA classifier with 50 times of random permutations. The obtained results (48%) demonstrated the existence of distinguishable features about different MIs of one hand in noninvasive EEG.

Unlike other MI-based BCI studies (Costa and Cabral, 2000; Wolpaw and McFarland, 2004), which only considered MIs from different hands, the present study aims to explore distinguishable features related to MIs of finer movements in one hand,

providing a possible mean to increase limited DOFs of control signals for MI-based BCIs. Compared to ECoG-based studies (Miller et al., 2009b), experiments using scalp EEGs are towards a non-invasive BCI, with signals much lower in SNRs and spatial resolutions. Furthermore, data in scalp EEG were from different MI types instead of real movements, which further decreased SNRs in data (Miller et al., 2010). These aspects impose difficulties in non-invasive EEG-based BCIs. In addition, MIs from both hands, rather than just from one hand, are included to increase DOFs in the present study. Despite of these difficulties, with the proposed method, extracted spatio-spectral features yield a decoding accuracy significantly higher than the guess level and 95% confidence level when evaluated by simple LDA classifiers.

It is worth to note that extracted features are only on the first PC in this preliminary study. Other PCs can also contain information useful for decoding different MIs. Spatial and spectral features from combination of different PCs may further improve the decoding accuracy, as the decoding of finger movements in Chapter 4. Moreover, since only a simple classifier is used in the present study, more advanced classifiers, such as SVM classifier (Zhou et al., 2009a) used in studies in Chapter 4, could be used to improve decoding accuracy. In addition, MI-based BCIs usually show progressive performance improvements along with training process (Wolpaw and McFarland, 2004; McFarland et al., 2005). More robust features are possible to be extracted, when including more sessions in the future.

In conclusion, I investigated the feasibility of discriminating four different MI types from both hands, with two MIs from the one hand, using non-invasive scalp EEG.

With the proposed methods, a spectral component was identified and showed different patterns and spatial distributions in different MIs. Using this new feature, an average decoding accuracy significantly higher than the guess level and 95% confidence level for four types of MIs was achieved when evaluated by a LDA classifier. The preliminary results in this chapter demonstrate the existence of discriminative information in EEG oscillations about different MI conditions about fine body parts.

Chapter 6: Conclusion and Future Directions

My research works in investigating EEG oscillations from human motor brains are summarized in this dissertation. Three studies are presented, including the capturing of neurodevelopmental changes of motor brains in infant EEG, the decoding of different individual finger movements and the decoding of motor-imagery tasks involving individual finger movements in adult EEG. All studies are carried out through the analysis of EEG oscillatory activities. The findings in these studies further the understanding about the human motor brain in both developing phase by studying the developmental changes of mu rhythm, and mature phase by identifying new discriminative information in EEG oscillations about movements/MIs of fine body parts. The first aspect expands the scanty knowledge about motor development that could potentially be used to assess treatment options of neurological disorders acquired during developmental phase of motor brains. The second aspect improves the resolution of EEG in classifying motor tasks of different fine body parts that could potentially push forward the development of advanced assistive technologies for people with severe motor impairments acquired at later ages. Both aspects have great implication to interventions for motor impairments at different stages, in an effort to promote motor skills and quality of life for people suffering from these medical conditions.

6.1 Added Resolutions in Capturing Motor Development

Among the limited number of studies about the infant mu rhythm, EEG recordings are acquired from various age resolutions, which are largely limited by the availability of resources in infant participants. Some studies focus on subjects of the

same age group, investigating functional correlates of the mu rhythm at that specific age (Stapel et al., 2010; Paulus et al., 2013). Such studies reveal age-specific neural mechanisms underlying certain behavioral tasks but don't provide information about their dynamic variations along maturation. There are also studies that are either cross sectional with different subject samples in each age group (Stroganova et al., 1999) or longitudinal with months apart between different age groups (Marshall et al., 2002). For example, Marshall et al. (2002) analyzed EEG longitudinally recorded from 29 subjects at 5, 10, 14, 24, 51 months of age. While such studies are good for discovering general development of the motor brain with developmental changes in a long age span, detailed developmental changes in fine age ranges are overlooked.

The study in Chapter 3 of this dissertation contributes to the scanty knowledge about motor development at early ages. It investigates the age-related changes in EEG mu rhythm during infancy in weekly increment between 5 and 7 months of age to further the understanding about motor development in a fine age resolution. Compared to other studies about the infant mu rhythm, the weekly age resolution of EEG recordings and carefully designed data processing procedures enable the capturing of detailed information about motor development that is not available before. Firstly, results from the present study are able to reveal the emergence of mu rhythm peaks in a weekly resolution. Moreover, the added resolutions in EEG recordings enable the evaluation of developmental changes of the mu rhythm with spectral peak distributions to reveal concrete peak shifting patterns of the mu rhythm along maturation.

The spatio-spectral analysis taking into consideration of both high spatial and spectral resolution of EEG provides even further information. This allows the

examination of mu rhythm ranges along maturation and dynamic changes of its spatial patterns at this age range. To sum up, the findings in the study of infant mu rhythm in this dissertation not only consolidate previous findings about the frequency peak formulation and shifting patterns in the infant mu rhythm during maturation, but also complement other studies with redefined frequency ranges and changes in spatial patterns, providing more insights about motor function development at this age range.

6.2 Improved Resolutions in Decoding Movements/Motor Imageries

While decoding movements/motor imageries of large body parts using features from EEG mu rhythm has been demonstrated in many studies and implemented as control signals to drive BCI applications (Yuan and He, 2014; Doud et al., 2011), decoding movements/motor imageries of fine body parts are less explored due to the doubt that not enough EEG resolution is available to capture difference of activation from fine body parts. Such limitation largely confines motor-rhythm based BCIs to simple applications.

The study in Chapter 4 investigates the resolution of EEG oscillatory activities in decoding movements of fine body parts. A novel type of spectral structures (spectral PCs) in EEG from SPCA analysis is uncovered, presenting distinct spectral and spatial characteristics from the classic mu rhythm. Three decoding tasks, i.e., detecting individual finger movements from the resting condition, pairwise decoding of individual finger movements and decoding all individual finger movements from one hand, are designed to comprehensively evaluate the decoding efficacy of spectral PCs in comparison to the classic mu rhythm in movements of fine body parts. Significant

higher decoding accuracies for all three tasks are achieved by spectral PCs comparing to the classic mu rhythm, suggesting the exceeding sensibility to movements of fine body parts from the former features. Moreover, significant decoding performance from spectral PCs features demonstrates sufficient information in EEG oscillations for decoding movements of fine body parts.

The study in Chapter 5 is an extension to the previous one by taking one step further to decode different motor imageries involving finger movements. In this preliminary study, four MIs tasks including motor imageries of thumb and fist from each hand undergo similar classification procedures as in the previous study, and decoding performance demonstrates the feasibility of EEG oscillations in discriminating motor imageries of fine body parts.

The improved resolutions in decoding movements/motor imageries from EEG oscillations enable the discrimination of different fine body parts. This would not only greatly enlarge the repertoire of control signals available for motor-rhythm based BCIs, but also facilitate the development of BCI with flexible and intuitive control paradigms, due to the feasible identifications of dexterous body parts in human.

6.3 Implications to Interventions for Motor Impairments

Motor impairments taking place during different ages require different approaches for interventions. Findings from the studies in this dissertation could have great implications to the interventions at different stages. For neurological diseases during developmental phase of motor brain, early interventions are believed to associate with positive effect on the motor development (Hadders-Algra, 2014), while direct

neurodevelopmental evidence is still not available. Study in Chapter 3 expands knowledge about the development of mu rhythm, which is indicative of the development human motor functionalities (Smith, 1941; Hagne et al., 1973). Such link makes mu rhythm a potential and promising biomarker to assess the effectiveness of early intervention, as well as a guideline for designing effective interventions.

For damages to the human motor system during mature phase, advanced assistive technologies are promising ways to promote movement abilities. BCI technology helps sufferers regain communication and mobility bypassing damaged neural pathway. Improved resolutions in decoding movements/ motor imageries of fine body parts with EEG could overcome the limitations of motor-rhythm based BCIs with added control features, and push the complexity of noninvasive BCI applications to provide more comprehensive and practical assistance to potential users.

6.4 Recommendations for Future Research

The studies in the present dissertation contribute to the further understanding about the human motor brain and can facilitate the future development and assessment of interventions for motor impairments at different stages. However, there are still some aspects worthy of future efforts for improvements. In the study of infant motor development, EEG sessions are recorded from infants from 5 to 7 months of age on a weekly basis, while information beyond this age range is not available due to the limitation of experimental design. In future studies, efforts could be extended to EEG recorded from participants outside of this age range with the proposed processing techniques to capture more complete information of motor development at early ages.

While features from new spectral structures demonstrate that EEG contains information about finger movements and motor imageries, the capability in decoding them in single-trial EEG is still suboptimal. Several factors could be culprits and are worth exploring for improvements. Although the SVM classifier implemented in the present study has been widely adopted, it has been reported that linear program machine (a sparse SVM algorithm) can outperform regular SVM in similar decoding tasks using ECoG signals (Shenoy et al., 2007). A search for more robust decoding algorithms could facilitate the thorough evaluation of new spectral structures and their decoding efficacy in these tasks. EEG signals are known to be susceptible to noises, such as, from ambient environments, motion artifacts, and many others. While spatial CAR filtering and ICA are used to improve SNR in EEG in the present studies, other advanced signal processing methods, e.g. common spatial pattern (Ramoser et al., 2000) and stochastic resonance (Lin et al., 2008), can be integrated to further improve EEG signal quality. Particularly, for decoding individual finger movements, another factor might originate from the decoding tasks.

Movements of individual fingers are usually accompanied with concurrent movements of other fingers, due to muscle connections, tendon organization, and neural control distribution in the hand (Hager-Ross and Schieber, 2000). It is still unclear whether these concurrent movements of uninstructed fingers contribute to misclassifications in the confusion matrices (Figure 4.13 and 4.14), requiring further efforts to understand the effect from behavior correlation. All of these aspects are recommended in future studies to improve decoding performance of fine body parts towards practical usage.

As for decoding motor imageries of fine body parts, the study in Chapter 5 demonstrated the EEG's feasibility with motor tasks involving thumb of each hand as an initial step towards rich control features from motor imageries for BCI. Motor imageries of ipsilateral fingers would further serve such a purpose, whereas it has not been investigated yet, requiring more efforts in future studies.

References

Arthor, D., and Vassilvitskii.S. (2007): K-means++: The Advantages of Careful Seeding. Proceedings of the Eighteenth Annual ACM-SIAM Symposium on Discrete Algorithms. 2007: 1027–1035

Bach-y-Rita, P. (1990): Brain plasticity as a basis for recovery of function in humans. Neuropsychologia. 28(6): 547-554

Ball, T., Kern, M., Mutschler, I., Aertsen, A., and Schulze-Bonhage, A. (2009): Signal quality of simultaneously recorded invasive and non-invasive EEG. Neuroimage. 46(3): 708-716

Bell, A.J., and Sejnowski, T.J. (1995): An information-maximization approach to blind separation and blind deconvolution. Neural Comput. 7(6): 1129-1159

Berchicci, M., Zhang, T., Romero, L., Peters, A., Annett, R., Teuscher, U., Bertollo, M., Okada, Y., Stephen, J., and Comani, S. (2011): Development of mu rhythm in infants and preschool children. Dev Neurosci. 33(2): 130-143

Bin, G., Gao, X., Yan, Z., Hong, B., and Gao, S. (2009): An online multi-channel SSVEP-based brain-computer interface using a canonical correlation analysis method. J Neural Eng. 6(4): 046002

Birbaumer, N. (2006): Breaking the silence: brain-computer interfaces (BCI) for communication and motor control. Psychophysiology. 43(6): 517-532

Blankertz, B., Curio, G., and Muller, K.R. (2002). Classifying single trial EEG: towards brain computer interfacing. Adv. Neural Inf. Process. Syst. 14, 157–164.

Blauw-Hospers, C.H., and Hadders-Algra, M. (2005): A systematic review of the effects of early intervention on motor development. Dev Med Child Neurol. 47(6): 421-432

Bottcher, L. (2010): Children with spastic cerebral palsy, their cognitive functioning, and social participation: a review. Child Neuropsychol. 16(3): 209-228

Bradberry, T.J., Gentili, R.J., and Contreras-Vidal, J.L. (2010): Reconstructing three-dimensional hand movements from noninvasive electroencephalographic signals. J Neurosci. 30(9): 3432-3437

Bradberry, T.J., Rong, F., and Contreras-Vidal, J.L. (2009): Decoding center-out hand velocity from MEG signals during visuomotor adaptation. Neuroimage. 47(4): 1691-1700

Canolty, R.T., Edwards, E., Dalal, S.S., Soltani, M., Nagarajan, S.S., Kirsch, H.E., Berger, M.S., Barbaro, N.M., and Knight, R.T. (2006): High gamma power is phase-locked to theta oscillations in human neocortex. Science. 313(5793): 1626-1628

Chang, C.C., and Lin, C.J. (2011): LIBSVM: A library for support vector machines. ACM T. Intel. Sys. Technol. 2: 1-27

Chestek, C.A., Gilja, V., Blabe, C.H., Foster, B.L., Shenoy, K.V., Parvizi, J., and Henderson, J.M. (2013): Hand posture classification using electrocorticography signals in the gamma band over human sensorimotor brain areas. J Neural Eng. 10(2): 026002

Christensen, D., Van Naarden Braun, K., Doernberg, N.S., Maenner, M.J., Arneson, C.L., Durkin, M.S., Benedict, R.E., Kirby, R.S., Wingate, M.S., Fitzgerald, R., and Yeargin-Allsopp, M. (2014): Prevalence of cerebral palsy, co-occurring autism spectrum disorders, and motor functioning - Autism and Developmental Disabilities Monitoring Network, USA, 2008. Dev Med Child Neurol. 56(1): 59-65

Christopher Reeve Paralysis Foundation. (2009): One Degree of Separation: Paralysis and Spinal Cord Injury in the United States. http://www.christopherreeve.org

Costa, E.J., and Cabral, E.F., Jr. (2000): EEG-based discrimination between imagination of left and right hand movements using Adaptive Gaussian Representation. Med Eng Phys. 22(5): 345-348

Davidson, R.J., and Fox, N.A. (1989): Frontal brain asymmetry predicts infants' response to maternal separation. J Abnorm Psychol. 98(2): 127-131

Delorme, A., and Makeig, S. (2004): EEGLAB: an open source toolbox for analysis of single-trial EEG dynamics including independent component analysis. J Neurosci Methods. 134(1): 9-21

Delorme, A., Palmer, J., Onton, J., Oostenveld, R., and Makeig, S. (2012): Independent EEG sources are dipolar. PLoS One. 7(2): e30135

Doud, A.J., Lucas, J.P., Pisansky, M.T., and He, B. (2011): Continuous three-dimensional control of a virtual helicopter using a motor imagery based brain-computer interface. PLoS One. 6(10): e26322

Edelman, G.M. (1993): Neural Darwinism: selection and reentrant signaling in higher brain function. Neuron. 10(2): 115-125

Ergenoglu, T., Demiralp, T., Bayraktaroglu, Z., Ergen, M., Beydagi, H., and Uresin, Y. (2004): Alpha rhythm of the EEG modulates visual detection performance in humans. Brain Res Cogn Brain Res. 20(3): 376-383

Farwell, L.A., and Donchin, E. (1988): Talking off the top of your head: toward a mental prosthesis utilizing event-related brain potentials. Electroencephalogr Clin Neurophysiol. 70(6): 510-523

Fogassi, L., and Luppino, G. (2005): Motor functions of the parietal lobe. Curr Opin Neurobiol. 15(6): 626-631

Fox, N.A., Henderson, H.A., Rubin, K.H., Calkins, S.D., and Schmidt, L.A. (2001): Continuity and discontinuity of behavioral inhibition and exuberance: psychophysiological and behavioral influences across the first four years of life. Child Dev. 72(1): 1-21

Glaser E.M., Ruchkin D.S. (1976) Principles of Neurobiological Signal Analysis. New York: Academic Press

Gu, Y., Dremstrup, K., and Farina, D. (2009): Single-trial discrimination of type and speed of wrist movements from EEG recordings. Clin Neurophysiol. 120(8): 1596-1600

Hadders-Algra, M. (2000): The neuronal group selection theory: a framework to explain variation in normal motor development. Dev Med Child Neurol. 42(8): 566-572

Hadders-Algra, M. (2001): Evaluation of motor function in young infants by means of the assessment of general movements: a review. Pediatr Phys Ther. 13(1): 27-36

Hadders-Algra, M. (2014): Early diagnosis and early intervention in cerebral palsy. Front Neurol. 5:185

Hager-Ross, C., and Schieber, M.H. (2000): Quantifying the independence of human finger movements: comparisons of digits, hands, and movement frequencies. J Neurosci. 20(22): 8542-8550

Hagne, I., Persson, J., Magnusson, R., and Petersen, I. (1973): Spectral analysis via fast fourier transform of waking EEG in normal infants. In: Kellaway, P., Petersen, I., editors. Automation of clinical EEG. New York: Raven

Han J., Kamber M., Pei J. (2012) Data Mining: Concepts and Techniques. MA, USA: Morgan Kaufmann.

Hashimoto, Y., and Ushiba, J. (2013): EEG-based classification of imaginary left and right foot movements using beta rebound. Clin Neurophysiol. 124(11): 2153-2160

Hassanien, A.E., and Azar, A.T. (2014): Brain-computer interfaces: current trends and applications. New York: Springer

Hoshi, E., and Tanji, J. (2000): Integration of target and body-part information in the premotor cortex when planning action. Nature. 408(6811): 466-470

Hsu, C.W., Chang, C.C., and Lin, C.J. (2010): A practical guide to support vector classication. Technical report National Taiwan University.

Hsu, C.W., and Lin, C. J. (2002): A comparison of methods for multiclass support vector machines. IEEE Tran. Neural Networ. 13: 415-425

Hustad, K.C., Allison, K., McFadd, E., and Riehle, K. (2014): Speech and language development in 2-year-old children with cerebral palsy. Dev Neurorehabil. 17(3): 167-175

Hyvarinen, A., and Oja, E. (2000): Independent component analysis: algorithms and applications. Neural Netw. 13(4-5): 411-430

Imamura, H., Matsumoto, R., Inouchi, M., Matsuhashi, M., Mikuni, N., Takahashi, R., and Ikeda, A. (2011): Ictal wideband ECoG: direct comparison between ictal slow shifts and high frequency oscillations. Clin Neurophysiol. 122(8): 1500-1504

Johnson R. A. and Wichern D. W. (2007): Applied Multivariate Statisitical Analysis. Upper Saddle River: Pearson Education Inc.

Jones, M.W., Morgan, E., Shelton, J.E., and Thorogood, C. (2007): Cerebral palsy: introduction and diagnosis (part I). J Pediatr Health Care. 21(3): 146-152

Kim, S.C., Lee, M.H., Jang, C., Kwon, J.W., and Park, J.W. (2013): The effect of alpha rhythm sleep on EEG activity and individuals' attention. J Phys Ther Sci. 25(12): 1515-1518

Kirschfeld, K. (2005): The physical basis of alpha waves in the electroencephalogram and the origin of the "Berger effect". Biol Cybern. 92(3): 177-185

Kirschstein, T., and Kohling, R. (2009): What is the source of the EEG? Clin EEG Neurosci. 40(3): 146-149

Kolobe, T.H., Pidcoe, P., and Warner, M. (2013): Use of robotics to promote prone locomotion in infants with and without cerebral palsy. Pediatr Phys Ther. 25(1): 85-86

Kuhlman, W.N. (1978): Functional topography of the human mu rhythm. Electroencephalogr Clin Neurophysiol. 44(1): 83-93

Leeb, R., Friedman, D., Muller-Putz, G.R., Scherer, R., Slater, M., and Pfurtscheller, G. (2007): Self-paced (asynchronous) BCI control of a wheelchair in virtual environments: a case study with a tetraplegic. Comput Intell Neurosci. 79642

Lehtonen, J., Jylanki, P., Kauhanen, L., and Sams, M. (2008): Online classification of single EEG trials during finger movements. IEEE Trans Biomed Eng. 55(2): 713-720

Leuthardt, E.C., Schalk, G., Moran, D., and Ojemann, J.G. (2006): The emerging world of motor neuroprosthetics: a neurosurgical perspective. Neurosurgery. 59(1): 1-14

Li, Y., Gao, X., Liu, H., and Gao, S. (2004): Classification of single-trial electroencephalogram during finger movement. IEEE Trans Biomed Eng. 51(6): 1019-1025

Liao[CO], K., Xiao[CO], R., Gonzalez, J., and Ding, L. (2014): Decoding individual finger movements from one hand using human EEG signals. PLoS One. 9(1): e85192

Lin, C.C., Ju, M.S., Hsu, C.W., and Sun, Y.N. (2008): Applying stochastic resonance to magnify mu and beta wave suppression. Comput Biol Med. 38(10): 1068-1075

Lin, C.T., Wu, R.C., Liang, S.F., Chao, W.H., Chen, Y.J., and Jung T.P. (2005): EEG-based drowsiness estimation for safety driving using independent component analysis. IEEE Trans. on Circuits Syst. 52: 2726-2738

Lindsley D.B. (1939): A Longitudinal Study of the Occipital Alpha Rhythm in Normal Children: Frequency and Amplitude Standards. Pedagog Semin J Genet Psychol. 55(1): 197-213

Magnani, G., Cursi, M., Leocani, L., Volonte, M.A., Locatelli, T., Elia, A., et al. (1998): Event-related desynchronization to contingent negative variation and self-paced movement paradigms in Parkinson's disease. Mov. Disord. 13: 653–660

Mak, J.N., Arbel, Y., Minett, J.W., McCane, L.M., Yuksel, B., Ryan, D., Thompson, D., Bianchi, L., and Erdogmus, D. (2011): Optimizing the P300-based brain-computer interface: current status, limitations and future directions. J Neural Eng. 8(2): 025003

Marshall, P.J., Bar-Haim, Y., and Fox, N.A. (2002): Development of the EEG from 5 months to 4 years of age. Clin Neurophysiol. 113(8): 1199-1208

Marshall, P.J., and Meltzoff, A.N. (2011): Neural mirroring systems: exploring the EEG mu rhythm in human infancy. Dev Cogn Neurosci. 1(2): 110-123

Marshall, P.J., Saby, J.N., and Meltzoff, A.N. (2013): Infant Brain Responses to Object Weight: Exploring Goal-Directed Actions and Self-Experience. Infancy. 18(6)

Marshall, P.J., Young, T., and Meltzoff, A.N. (2011): Neural correlates of action observation and execution in 14-month-old infants: an event-related EEG desynchronization study. Dev Sci. 14(3): 474-480

Márton, L.F., Brassai, S.T., Bakó, L., and Losonczi, L. (2014): Detrended Fluctuation Analysis of EEG Signals. Procedia Technology. 12(125-132

McFarland, D.J., McCane, L.M., David, S.V., and Wolpaw, J.R. (1997): Spatial filter selection for EEG-based communication. Electroencephalogr Clin Neurophysiol. 103(3): 386-394

McFarland, D.J., Miner, L.A., Vaughan, T.M., and Wolpaw, J.R. (2000): Mu and beta rhythm topographies during motor imagery and actual movements. Brain Topogr. 12(3): 177-186

McFarland, D.J., Sarnacki, W.A., Vaughan, T.M., and Wolpaw, J.R. (2005): Brain-computer interface (BCI) operation: signal and noise during early training sessions. Clin Neurophysiol. 116(1): 56-62

McKinney, S.M., Dang-Vu, T.T., Buxton, O.M., Solet, J.M., and Ellenbogen, J.M. (2011): Covert waking brain activity reveals instantaneous sleep depth. PLoS One. 6(3): e17351

Miller, D.P., Fagg, A.H., Ding, L., Kolobe, T.H., and Ghazi, M.A. (2015): Robotic crawling assistance for infants with cerebral palsy. Workshops at the Twenty-Ninth AAAI Conference on Artificial Intelligence

Miller, K.J., Schalk, G., Fetz, E.E., den Nijs, M., Ojemann, J.G., and Rao, R.P. (2010): Cortical activity during motor execution, motor imagery, and imagery-based online feedback. Proc Natl Acad Sci U S A. 107(9): 4430-4435

Miller, K.J., Sorensen, L.B., Ojemann, J.G., and den Nijs, M. (2009a): Power-law scaling in the brain surface electric potential. PLoS Comput Biol. 5(12): e1000609

Miller, K.J., Zanos, S., Fetz, E.E., den Nijs, M., and Ojemann, J.G. (2009b): Decoupling the cortical power spectrum reveals real-time representation of individual finger movements in humans. J Neurosci. 29(10): 3132-3137

Mognon, A., Jovicich, J., Bruzzone, L., and Buiatti, M. (2011): ADJUST: An automatic EEG artifact detector based on the joint use of spatial and temporal features. Psychophysiology. 48(2): 229-240

Morash, V., Bai, O., Furlani, S., Lin, P., and Hallett, M. (2008): Classifying EEG signals preceding right hand, left hand, tongue, and right foot movements and motor imageries. Clin Neurophysiol. 119(11): 2570-2578

Müller-Putz G.R., Scherer R., Brunner C., Leeb R., Pfurtscheller G. (2008) Better than random: a closer look on BCI results. Int J Bioelectromagn. 10: 52-55.

Muller-Putz, G.R., Scherer, R., Pfurtscheller, G., and Rupp, R. (2005). EEG-based neuroprosthesis control: a step towards clinical practice. Neurosci. Lett. 382, 169-174

Neuper, C., and Pfurtscheller, G. (1996): Post-movement synchronization of beta rhythms in the EEG over the cortical foot area in man. Neurosci Lett. 216(1): 17-20

Neuper, C., Wortz, M., and Pfurtscheller, G. (2006): ERD/ERS patterns reflecting sensorimotor activation and deactivation. Prog Brain Res. 159: 211-222

Niedermeyer, E. (1997): Alpha rhythms as physiological and abnormal phenomena. Int J Psychophysiol. 26(1-3): 31-49

Orekhova, E.V., Stroganova, T.A., Posikera, I.N., and Elam, M. (2006): EEG theta rhythm in infants and preschool children. Clin Neurophysiol. 117(5): 1047-1062

Paulus, M., Hunnius, S., and Bekkering, H. (2013): Neurocognitive mechanisms underlying social learning in infancy: infants' neural processing of the effects of others' actions. Soc Cogn Affect Neurosci. 8(7): 774-779

Paulus, M., Hunnius, S., van Elk, M., and Bekkering, H. (2012): How learning to shake a rattle affects 8-month-old infants' perception of the rattle's sound: electrophysiological evidence for action-effect binding in infancy. Dev Cogn Neurosci. 2(1): 90-96

Pfurtscheller, G. (1989): Functional topography during sensorimotor activation studied with event-related desynchronization mapping. J. Clin. Neurophysiol. 6: 75–84.

Pfurtscheller, G., and Aranibar, A. (1977): Event-related cortical desynchronization detected by power measurements of scalp EEG. Electroencephalogr Clin Neurophysiol. 42(6): 817-826

Pfurtscheller, G., Brunner, C., Schlogl, A., and Lopes da Silva, F.H. (2006): Mu rhythm (de)synchronization and EEG single-trial classification of different motor imagery tasks. Neuroimage. 31(1): 153-159

Pfurtscheller, G., and Lopes da Silva, F.H. (1999): Event-related EEG/MEG synchronization and desynchronization: basic principles. Clin Neurophysiol. 110(11): 1842-1857

Pfurtscheller, G., Müller-Putz, G.R., Pfurtscheller, J., and Rupp, R. (2005): EEG-based asynchronous BCI controls functional electrical stimulation in a tetraplegic patient. EURASIP J. Appl. Si. Pr. 3152–3155

Pfurtscheller, G., Stancak, A., Jr., and Edlinger, G. (1997): On the existence of different types of central beta rhythms below 30 Hz. Electroencephalogr Clin Neurophysiol. 102(4): 316-325

Pistohl, T., Schulze-Bonhage, A., Aertsen, A., Mehring, C., and Ball, T. (2012): Decoding natural grasp types from human ECoG. Neuroimage. 59(1): 248-260

Purves D., Augustine G.J., Fitzpatrick D., Hall W.C., LaMantia A.-S., McNamara J.O., and Williams S.M. (2004): Neuroscience, 3rd Edition. Sunderland, MA: Sinauer Associates, Inc

Ramoser, H., Muller-Gerking, J., and Pfurtscheller, G. (2000): Optimal spatial filtering of single trial EEG during imagined hand movement. IEEE Trans Rehabil Eng. 8(4): 441-446

Rosenbaum, P., Paneth, N., Leviton, A., Goldstein, M., Bax, M., Damiano, D., Dan, B., and Jacobsson, B. (2007): A report: the definition and classification of cerebral palsy April 2006. Dev Med Child Neurol Suppl. 109: 8-14

Saby, J.N., and Marshall, P.J. (2012): The utility of EEG band power analysis in the study of infancy and early childhood. Dev Neuropsychol. 37(3): 253-273

Saby, J.N., Marshall, P.J., and Meltzoff, A.N. (2012): Neural correlates of being imitated: an EEG study in preverbal infants. Soc Neurosci. 7(6): 650-661

Schalk, G., Kubanek, J., Miller, K.J., Anderson, N.R., Leuthardt, E.C., Ojemann, J.G., Limbrick, D., Moran, D., Gerhardt, L.A., and Wolpaw, J.R. (2007): Decoding two-dimensional movement trajectories using electrocorticographic signals in humans. J Neural Eng. 4(3): 264-275

Schalk, G., McFarland, D.J., Hinterberger, T., Birbaumer, N., and Wolpaw, J.R. (2004): BCI2000: a general-purpose brain-computer interface (BCI) system. IEEE Trans Biomed Eng. 51(6): 1034-1043

Schwartz, A.B., Cui, X.T., Weber, D.J., and Moran, D.W. (2006): Brain-controlled interfaces: movement restoration with neural prosthetics. Neuron. 52(1): 205-220

Sellers, E.W., Krusienski, D.J., McFarland, D.J., Vaughan, T.M., and Wolpaw, J.R. (2006): A P300 event-related potential brain-computer interface (BCI): the effects of matrix size and inter stimulus interval on performance. Biol Psychol. 73(3): 242-252

Shenoy, P., Krauledat, M., Blankertz, B., Rao, R.P., and Muller, K.R. (2006): Towards adaptive classification for BCI. J Neural Eng. 3(1): R13-23

Shenoy, P., Miller, K.J., Ojemann, J.G., and Rao, R.P. (2007): Finger movement classification for an electrocorticographic BCI. Int IEEE EMBS Conf Neural Eng. 2007: 192-195

Sitaram, R., Caria, A., Veit, R., Gaber, T., Rota, G., Kuebler, A., and Birbaumer, N. (2007): FMRI brain-computer interface: a tool for neuroscientific research and treatment. Comput Intell Neurosci. 25487

Smith J.R. (1938): The Electroencephalogram During Normal Infancy and Childhood: I. Rhythmic Activities Present in the Neonate and Their Subsequent Development, Pedagog Semin J Genet Psychol. 53(2): 431-453

Smith J.R. (1939): The occipital and precentral alpha rhythms during the first two years. J Psychol. 7:223–226

Smith J.R. (1941): The frequency growth of the human alpha rhythms during normal infancy and childhood. J Psychol. 11: 177–198

Snider, J., Plank, M., Lynch, G., Halgren, E., and Poizner, H. (2013): Human cortical theta during free exploration encodes space and predicts subsequent memory. J Neurosci. 33(38): 15056-15068

Stapel, J.C., Hunnius, S., van Elk, M., and Bekkering, H. (2010): Motor activation during observation of unusual versus ordinary actions in infancy. Soc Neurosci. 5(5-6): 451-460

Stippich, C., Ochmann, H., and Sartor, K. (2002): Somatotopic mapping of the human primary sensorimotor cortex during motor imagery and motor execution by functional magnetic resonance imaging. Neurosci Lett. 331(1): 50-54

Stroganova, T.A., Orekhova, E.V., and Posikera, I.N. (1999): EEG alpha rhythm in infants. Clin Neurophysiol. 110(6): 997-1012

Szurhaj, W., Labyt, E., Bourriez, J.L., Cassim, F., Defebvre, L., Hauser, J.J., Guieu, J.D., et al. (2001): Event-related variations in the activity of EEG-rhythms. Application to the physiology and the pathology of movements. Epileptic. Disord. 59–66.

Urgen, B.A., Plank, M., Ishiguro, H., Poizner, H., and Saygin, A.P. (2013): EEG theta and Mu oscillations during perception of human and robot actions. Front Neurorobot. 7: 19

van den Broek, S.P., Reinders, F., Donderwinkel, M., and Peters, M.J. (1998): Volume conduction effects in EEG and MEG. Electroencephalogr Clin Neurophysiol. 106(6): 522-534

Vanni, S., Revonsuo, A., and Hari, R. (1997): Modulation of the parieto-occipital alpha rhythm during object detection. J Neurosci. 17(18): 7141-7147

Vapnik, V.N. (1998). Statistical learning theory. New York: Wiley-Interscience.

Vapnik, V.N. (1999). The nature of statistical learning theory. New York: Springer.

Wang, Y., Gao, X., Hong, B., Jia, C., and Gao, S. (2008): Brain-computer interfaces based on visual evoked potentials. IEEE Eng Med Biol Mag. 27(5): 64-71

Welch P. (1967): The use of fast Fourier transform for the estimation of power spectra: A method based on time averaging over short, modified periodograms. IEEE Trans Audio Electroacoust. 15: 70-73

Welford A.T. (1980) Reaction Times. New York: Academic Press.

Wendel, K., Narra, N.G., Hannula, M., Kauppinen, P., and Malmivuo, J. (2008): The influence of CSF on EEG sensitivity distributions of multilayered head models. IEEE Trans Biomed Eng. 55(4): 1454-1456

Wilson, J.A., Schalk, G., Walton, L.M., and Williams, J.C. (2009): Using an EEG-based brain-computer interface for virtual cursor movement with BCI2000. J Vis Exp. (29)

Wolpaw, J.R., Birbaumer, N., McFarland, D.J., Pfurtscheller, G., and Vaughan, T.M. (2002): Brain-computer interfaces for communication and control. Clin Neurophysiol. 113(6): 767-791

Wolpaw, J.R., and McFarland, D.J. (2004): Control of a two-dimensional movement signal by a noninvasive brain-computer interface in humans. Proc Natl Acad Sci U S A. 101(51): 17849-17854

Xiao, R., and Ding, L. (2013): Evaluation of EEG features in decoding individual finger movements from one hand. Comput Math Methods Med. 2013: 243257

Xiao, R., and Ding, L. (2015): EEG resolutions in detecting and decoding finger movements from spectral analysis. Front Neurosci. 9: 308

Xiao, R., Liao, K., and Ding, L. (2012): Discriminating multiple motor imageries of human hands using EEG. Conf Proc IEEE Eng Med Biol Soc. 2012: 1773-1776

Xiao, R., Qi, X., Fagg, A., Kolobe, T., Miller, D., and Ding, L (2015): Spectra of Infant EEG within the First Year of Life: A Pilot Study. Int. IEEE EMBS Conf. 2015: 4753-4756.

Yoo, S.S., Fairneny, T., Chen, N.K., Choo, S.E., Panych, L.P., Park, H., Lee, S.Y., and Jolesz, F.A. (2004): Brain-computer interface using fMRI: spatial navigation by thoughts. Neuroreport. 15(10): 1591-1595

Yuan, H., and He, B. (2014): Brain-computer interfaces using sensorimotor rhythms: current state and future perspectives. IEEE Trans Biomed Eng. 61(5): 1425-1435

Zhou H., Xu Q., Wang Y., Huang J., and Wu J. (2009a): An Improved Support Vector Machine Classifier for EEG-Based Motor Imagery Classification. Lect Notes Comput Sc. 5553: 267-275

Zhou, J., Yao, J., Deng, J., and Dewald, J.P. (2009b): EEG-based classification for elbow versus shoulder torque intentions involving stroke subjects. Comput Biol Med. 39(5): 443-452

Appendix

WOLTERS KLUWER HEALTH, INC. LICENSE TERMS AND CONDITIONS

Oct 06, 2015

This Agreement between Ran Xiao ("You") and Wolters Kluwer Health, Inc. ("Wolters Kluwer Health, Inc.") consists of your license details and the terms and conditions provided by Wolters Kluwer Health, Inc. and Copyright Clearance Center.

License Number	3723260731792
License date	Oct 06, 2015
Licensed Content Publisher	Wolters Kluwer Health, Inc.
Licensed Content Publication	Neurosurgery
Licensed Content Title	THE EMERGING WORLD OF MOTOR NEUROPROSTHETICS: A NEUROSURGICAL PERSPECTIVE
Licensed Content Author	Eric Leuthardt, Gerwin Schalk, Daniel Moran, et al
Licensed Content Date	Jan 1, 2006
Licensed Content Volume Number	59
Licensed Content Issue Number	1
Type of Use	Dissertation/Thesis
Requestor type	Individual
Portion	Figures/table/illustration
Number of figures/tables/illustrations	1
Figures/tables/illustrations used	1
Author of this Wolters Kluwer article	No
Title of your thesis / dissertation	EEG OSCILLATORY ACTIVITIES FROM HUMAN MOTOR BRAIN
Expected completion date	Dec 2015
Estimated size(pages)	100
Requestor Location	Ran Xiao 1415 George Ave Apt 222 NORMAN, OK 73072 United States Attn: Ran Xiao
Billing Type	Invoice
Billing Address	Ran Xiao 1415 George Ave Apt 222

NORMAN, OK 73072
United States
Attn: Ran Xiao

Total 0.00 USD

Terms and Conditions

Terms and conditions Wolters Kluwer Health

1. **Transfer of License:** Wolters Kluwer hereby grants you a non-exclusive license to reproduce this material for this purpose, and for no other use, subject to the conditions herein
2. **Credit Line:** A credit line will be prominently placed, wherever the material is reused and include: the author(s), title of article, title of journal, volume number, issue number and inclusive pages.
   Where a journal is being published by a learned society, the details of that society must be included in the credit line.
   i. **for Open access journals:**The following statement needs to be added when reprinting the material in Open Access journals only: 'promotional and commercial use of the material in print, digital or mobile device format is prohibited without the permission from the publisher Wolters Kluwer Health. Please contact healthpermissions@wolterskluwer.com for further information
3. **Exceptions:** In case of ***Disease Colon Rectum, Plastic Reconstructive Surgery, The Green Journal, Critical care Medicine, Pediatric Critical Care Medicine, the American Heart Publications, the American Academy of Neurology*** the following guideline applies: no drug/ trade name or logo can be included in the same page as the material re-used.
4. **Translations:** When requesting a permission to translate a full text article, Wolters Kluwer/ Lippincott Williams & Wilkins request to receive the pdf of the translated document. This disclaimer should be added at all times:
   Wolters Kluwer Health and its Societies take no responsibility for the accuracy of the translation from the published English original and are not liable for any errors which may occur.
5. **Warranties** The requestor warrants that the material shall not be used in any manner which may be considered derogatory to the title, content, or authors of the material, or to Wolters Kluwer
6. **Indemnity:** You hereby indemnify and hold harmless Wolters Kluwer and their respective officers, directors, employees and agents, from and against any and all claims, costs, proceeding or demands arising out of your unauthorised use of the Licensed Material.
7. **Geographical Scope:** Permission granted is valid worldwide in the English language and the languages specified in your original request
8. Wolters Kluwer cannot supply the requestor with the original artwork or a "clean copy."
9. Permission is valid if the borrowed material is original to a Wolters Kluwer imprint (Lippincott-Raven Publishers, Williams &Wilkins, Lea & Febiger, Harwal, Rapid Science, Little Brown & Company, Harper & Row Medical, American Journal of Nursing Co, and Urban & Schwarzenberg)
10. **Termination of contract:** If you opt not to use the material requested above please notify RightsLink or Wolters Kluwer Health/ Lippincott Williams & Wilkins within 90 days of the original invoice date.
11. This permission does not apply to **images** that are credited to publications other than Wolters Kluwer journals. For images credited to non-Wolters Kluwer Health journal publications, you will need to obtain permission from the journal referenced in the figure or table legend or credit line before making any use of image(s) or table(s)
12. **Third party material:** Adaptations are protected by copyright, so if you would like to reuse material that we have adapted from another source, you will need not only our permission, but the permission of the rights holder of the original material. Similarly, if you want to reuse an adaptation of original LWW content that appears in another publishers work, you will need our permission and that of the next publisher. The adaptation should be credited as follows: Adapted with permission from Wolters Kluwer Health: Book author, title, year of publication or Journal name, article author, title, reference citation, year of publication.

13. **Altering or modifying material:** Please note that modification of text within figures or full-text article is strictly forbidden.
14. Please note that articles in the **ahead-of–print stage** of publication can be cited and the content may be re-used by including the date of access and the unique DOI number. Any final changes in manuscripts will be made at the time of print publication and will be reflected in the final electronic issue. Disclaimer: Articles appearing in the Published Ahead-of–Print section have been peer-reviewed and accepted for publication in the relevant journal and posted online before print publication. Articles appearing as publish ahead–of-print may contain statements, opinions, and information that have errors in facts, figures, or interpretation. Accordingly, Lippincott Williams & Wilkins, the editors and authors and their respective employees are not responsible or liable for the use of any such inaccurate or misleading data, opinion or information contained in the articles in this section.
15. **Duration of the license:**
    i. Permission is granted for a one-time use only within 12 months from the date of this invoice. Rights herein do not apply to future reproductions, editors, revisions, or other derivative works. Once the 12- month term has expired, permission to renew must be submitted in writing.
    ii. For content reused in another journal or book, in print or electronic format, the license is one-time use and lasts for the 1st edition of a book or for the life of the edition in case of journals.
    iii. If your Permission Request is for use on a website (which is not a journal or a book), internet, intranet, or any publicly accessible site, you agree to remove the material from such site after 12 months or else renew your permission request.
16. **Contingent on payment:** *While you may exercise the rights licensed immediately upon issuance of the license at the end of the licensing process for the transaction, provided that you have disclosed complete and accurate details of your proposed use, no license is finally effective unless and until full payment is received from you (either by publisher or by CCC) as provided in CCC's Billing and Payment terms and conditions. If full payment is not received on a timely basis, then any license preliminarily granted shall be deemed automatically revoked and shall be void as if never granted. Further, in the event that you breach any of these terms and conditions or any of CCC's Billing and Payment terms and conditions, the license is automatically revoked and shall be void as if never granted. Use of materials as described in a revoked license, as well as any use of the materials beyond the scope of an unrevoked license, may constitute copyright infringement and publisher reserves the right to take any and all action to protect its copyright in the materials.*
17. **Waived permission fee:** If the permission fee for the requested use of our material has been waived in this instance, please be advised that your future requests for Wolters Kluwer materials may attract a fee on another occasion. Please always check with the Wolters Kluwer Permissions Team if in doubt healthpermissions@wolterskluwer.com

For Books only:

18. Permission is granted for a one time use only. Rights herein do not apply to future reproductions, editions, revisions, or other derivative works.

Service Description for Content Services

Subject to these terms of use, any terms set forth on the particular order, and payment of the applicable fee, you may make the following uses of the ordered materials:

• Content Rental: You may access and view a single electronic copy of the materials ordered for the time period designated at the time the order is placed. Access to the materials will be provided through a dedicated content viewer or other portal, and access will be discontinued upon expiration of the designated time period. An order for Content Rental does not include any rights to print, download, save, create additional copies, to distribute or to reuse in any way the full text or parts of the materials.

• Content Purchase: You may access and download a single electronic copy of the materials

ordered. Copies will be provided by email or by such other means as publisher may make available from time to time. An order for Content Purchase does not include any rights to create additional copies or to distribute copies of the materials.

The materials may be accessed and used only by the person who placed the Order or the person on whose behalf the order was placed and only in accordance with the terms included in the particular order.

SPECIAL CASES:

1. **For STM Signatories only, as agreed as part of the STM Guidelines**

Any permission granted for a particular edition will apply also to subsequent editions and for editions in other languages, provided such editions are for the work as a whole in situ and does not involve the separate exploitation of the permitted illustrations or excerpts.

Please click here to view the STM guidelines.

Other Terms and Conditions:
v1.13

Questions? customercare@copyright.com or +1-855-239-3415 (toll free in the US) or +1-978-646-2777.